Montanuniversität Leoben

Evolution of Microstructure and Mechanical Properties of a High Co-Ni Steel

Doctoral Thesis

Dipl. Ing. Marina Gruber

Materials Center Leoben in cooperation with
Böhler Edelstahl GmbH & Co KG

Leoben, April 2016

Affidavit

I declare in lieu of oath, that I wrote this thesis and performed the associated research myself, using only literature cited in this volume.

Acknowledgments

At first, I like to thank my supervisor Prof. Reinhold Ebner for giving me the possibility to conduct this thesis at the Materials Center Leoben (MCL), and for his expertise, the fruitful discussions and for finding time to help and guide me in the last three years.
I am also grateful to my supervisor Prof. Otmar Kolednik for the advices and knowledge regarding fracture mechanics.

I would also like to thank Dr. Stefan Marsoner for his scientific and technological aid and his help in all aspects. I am also thankful to Dr. Gerald Ressel, who supported me mentally and for his huge courage for my PhD project within the last one and a half year.

My thank is also expressed to Dr. Harald Leitner and DI Sarah Ploberger for their engagement and for the constructive discussions especially at the beginning of the thesis.

As the present thesis was founded by the Materials Center Leoben and by Böhler Edelstahl GmbH & Co KG, the companies are also thankfully acknowledged.

My thank is as well expressed to Dr. Francisca Mendez Martin for the support regarding atom probe tomography and to Dr. Krystina Spiradek-Hahn for the conduction of transmission electron microscopy investigations and her expertise.
I would also like to thank the colleagues from the laboratories at MCL for supporting some of the investigations over the last three years and the nice time during coffee breaks. Furthermore, I would like to thank all colleagues, which were involved in my project at the Materials Center Leoben, at Böhler Edelstahl, at the Department Metallkunde und Werkstoffprüfung and at the Erich Schmid Institute.

I am also thankful for the great community of PhD students at MCL for the entertainment during and the fun with them at work.

Finally, as my family and friends supported me unconditionally during the time of my thesis, I would also like to express my deepest gratitude to them.

Die besten Entscheidungen sind meistens diejenigen,
die auch getroffen wurden.

Contents

1 Introduction and scope of this work

Generally, materials, which combine high hardness and strength values as well as excellent toughness properties are attractive for heavily loaded constructions and tooling applications. Among these steel grades, which present such an exceptional combination of properties are high Co-Ni secondary hardening steels. The most prominent representatives of this steel class are the alloys HY180, AF1410, Aermet® 100, Aermet® 310, and Aermet® 340. Their composition is characterized by high contents of cobalt and nickel and by the addition of chromium, molybdenum and carbon for carbide precipitation. Additionally, these steels form reverted austenite on martensite laths during tempering. As a consequence, these alloys connect properties of maraging steels, such as the high Ni contents and reverted austenite formation, with features predominately found in tool steels, e.g. carbide precipitation for hardening.
High Co-Ni steels are widely used in the field of aerospace and military as landing gears or ballistic tolerant components. Since the mechanical properties are crucial in this field of application, they have been excessively investigated for many decades for these alloys. However, the focus of the investigations was laid on the high toughness values, which are, despite the complex microstructure of these materials, predominately ascribed to the presence of thin reverted austenite layers.
Nevertheless, the affect of austenite on toughness in martensitic steels is still controversial, as it was found in prior investigations that austenite may improve or deteriorate toughness properties. However, it is principally asserted that the higher the stability, i.e. the resistance against transformation of austenite to martensite, the higher the toughness increment is.
Many heat treatments and thermodynamic calculations regarding the austenite stability have been performed for enhancing the toughness properties in high Co-Ni steels. Nevertheless, for these steels a detailed analysis of the microstructure, including the nucleation and evolution of reverted austenite is missing.

As a result, the aim of this work was to evaluate the effect of heat treatment and resulting microstructure on the mechanical properties of a 11 wt.% Ni, 13.5 wt.% Co, 2.9 wt.% Cr, 1.2 wt.% Mo and 0.22 wt.% C high Co-Ni steel. Thus, the phase arrangement of martensite, reverted and retained austenite was analyzed and the evolution of reverted austenite during tempering and its influence on element redistribution in martensite and retained austenite was studied. Furthermore, the influence of cryogenic treatment on the formation

behavior of carbides and on the stability of retained and reverted austenite was characterized. Thereby, the effect of microstructure, retrieved from various heat and cryogenic treatments, on the mechanical properties could be analyzed.
As a consequence of these findings fundamental information about formation process and stability of retained and reverted austenite were obtained, which can be used for further improving the material's properties.

This work is divided in five sections. In Section 2 "Austenite in martensitic steels and its influence on toughness properties" an introduction is given about the stability, the formation and transformation process of retained and reverted austenite in martensitic steels. It also comprises an overview about high Co-Ni and maraging steels and the affect of austenite on mechanical properties in these steel grades. Section 3 ("Setup of experiments and kinetic calculations") deals with the experimental methodology of this work. In this section the applied heat treatments as well as the setup of experiments and thermodynamic and kinetic calculations are described. The findings of the characterization of the investigated high Co-Ni steel are presented in Section 4 "Results and discussion". In 4.1 ("Characterization of microstructure and fundamental properties") the results from microstructural characterization, including the analyses of reverted austenite evolution and element redistribution during tempering, are shown. Furthermore, the formation principles of reverted austenite are discussed by the aid kinetic calculations. The effect of cryogenic treatment on the evolution of carbides, austenite and martensite is evaluated in Section 4.2 ("Influence of cryogenic treatment on the microstructural evolution during tempering"). In this section also the stability of retained and reverted austenite is analyzed. The results from analyzing the mechanical properties are presented in Section 4.3 "Characterization of the mechanical properties at different heat treatment conditions". Finally, in Section 5 the central statements of this work are summarized and an outlook on further objectives and activities in this field of research is given.

2 Austenite in martensitic steels and its influence on toughness properties

2.1 Effects of alloying elements on the austenite phase field

The phase in iron alloys or steels, which presents a face-centered-cubic (FCC) structure, is generally denoted as austenite or γ-iron. In pure iron this FCC phase is stable between 910°C and 1390°C. Alloying elements are affecting the region of stable γ-iron and the transition temperature to the body-centered-cubic (BCC) α-ferrite. Elements, which extend the equilibrium FCC phase field, are attributed to austenite stabilizing elements. Conversely, elements, which enlarge the ferrite phase field, are denoted as ferrite stabilizing elements. Austenite stabilizers are elements such as carbon, manganese, nickel and nitrogen. These elements have a higher solubility in austenite than in ferrite. Regarding the effect on the austenite phase field, these elements can be divided in two groups. Carbon and nitrogen cause an expansion of the austenite phase field, which is restricted as shown in Fig. 2.1 (a) [1–3].

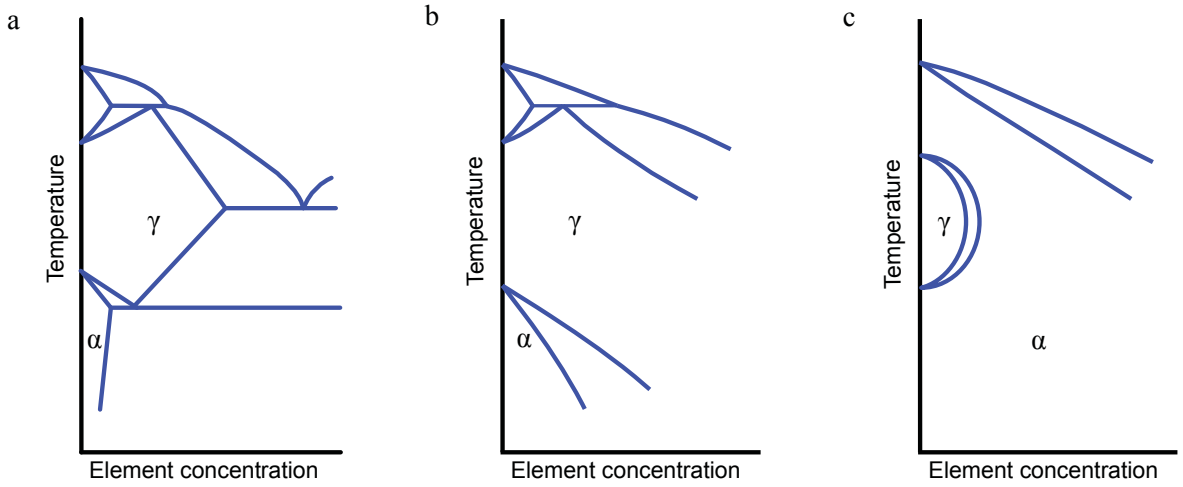

Figure 2.1: Influence of alloying elements on the austenite phase field. (a) Carbon and nitrogen. (b) Nickel and manganese. (c) Cr, Si, Al, Mo, W, Nb, V and Ti [2].

Elements such as nickel and manganese cause an open austenite phase field, as indicated by Fig. 2.1 (b). Thus, by a sufficient addition of Ni or Mn, the region of α-iron can be suppressed down to room temperature.

Basically, cobalt is an austenite stabilizer. Nevertheless, an enlargement of the austenite phase field occurs only for Co concentrations higher 50 at.%. For lower cobalt contents no distinct influence on the transition temperature from γ-iron to α-iron can be identified,

as shown in Fig. 2.2 [2, 4].

Ferrite stabilizers, such as Cr, Si, Al, Mo, W, Nb, V and Ti, are mainly carbide forming elements. These elements restrict the FCC phase as illustrated in Fig. 2.1 (c) [1, 2].

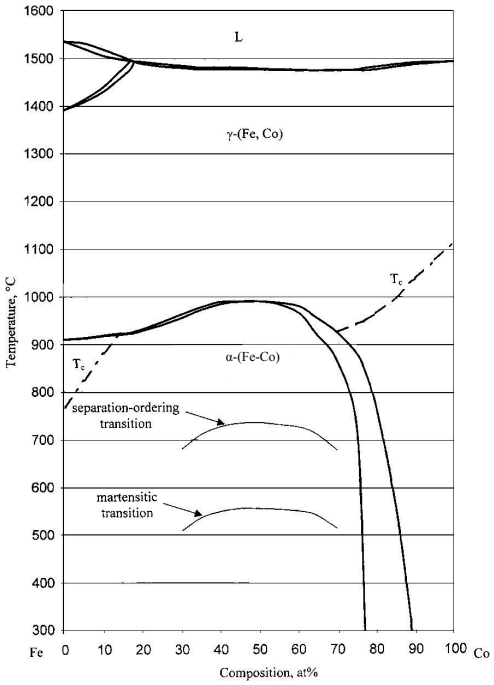

Figure 2.2: Influence of cobalt on the region of the austenite phase field [4].

2.2 Effects of alloying elements on the martensite start temperature

The most prominent element, which causes a martensitic transformation upon quenching from the austenite phase field, is carbon. As carbon atoms remain in the octahedron interstitial sites during the transformation, the body-centered lattice becomes tetragonal distorted [1].
A martensitic transformation can also be evoked by other alloying elements. In contrast to the Fe-C martensite, the Fe-Ni martensite presents lower hardness values but a higher toughness. Nickel-martensite does not exhibit a tetragonal distorted lattice and can be created even at low cooling rates, since this phase transformation generally occurs at temperatures (<400°C) at which the diffusion of substitutional elements is hindered [1]. Also, a martensitic transformation could occur in Fe-Co alloys with 30-70 at.% cobalt (Fig. 2.2). Iron and cobalt atoms may also form an ordered BCC phase. The formation of either martensite or an ordered Fe-Co phase depends on the conditions of heat treatment, e.g. the annealing temperature [5, 6].

The temperature upon cooling, at which the transformation austenite to martensite starts is denoted as martensite start (M_s) temperature. Most of the typical alloying elements in steel reduce the M_s-temperature. Exceptions are made by aluminum and cobalt, as they clearly enhance this transition temperature [7, 8]. Austenite stabilizing elements, as well as chromium, show a massive reduction of the M_s-temperature.
The decrease of the M_s-temperature is accompanied with the decrease of martensite finish temperature (M_f), the temperature at which the martensitic transformation is finished. If the M_f-temperature is situated below room temperature, untransformed austenite will remain in the material. This austenite is termed as retained austenite. If both, the M_s- and the M_f-temperature, are below room temperature the material is austenitic, as depicted in Fig. 2.3. It is indicated by Bergmann [1] that alloys with more than 30 % Ni are metastable austenitic.

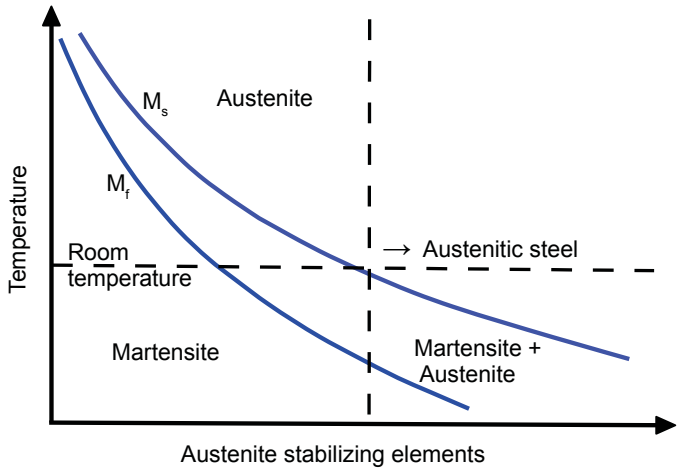

Figure 2.3: Influence of alloying elements on the M_s- and M_f-temperature [1].

The M_s-temperature (°C, wt.%) in dependence of the composition of the steel can be evaluated with Eq. 1 or 2. Furthermore, these equations give a hint of the influence of each alloying element on the transformation temperature.

$$Ms = 545 - 330C + 2Al + 7Co - 14Cr - 13Cu - 23Mn - 5Mo - 4Nb - 13Ni - 7Si + 3Ti + 4V \quad [7] \tag{1}$$

$$Ms = 525 - 350 * (C - 0.005) - 45Mn - 35V * (Nb + Zr + Ti) - 30Cr - 20Ni - 16Mo - 8W - 5Si + 6Co + 15Al \quad [8] \tag{2}$$

2.3 Retained and reverted austenite

2.3.1 Formation process and properties of retained and reverted austenite

Commonly, the austenite present e.g. in tool steels, bainitic and QTP steels, TRIP (transformation induced plasticity) or in general in martensitic (bainitic) steels is denoted as retained austenite [3, 9–14].
Another type of austenite, present within martensite, is reverted austenite. This one is also termed as precipitated or dispersed austenite [15, 16]. Compared to retained austenite, reverted austenite is formed during tempering (after quenching from austenitizing) above temperatures of 450°C-500°C [17–20]. Fig. 2.4 indicates the regions of retained and reverted austenite formation during heat treatment.

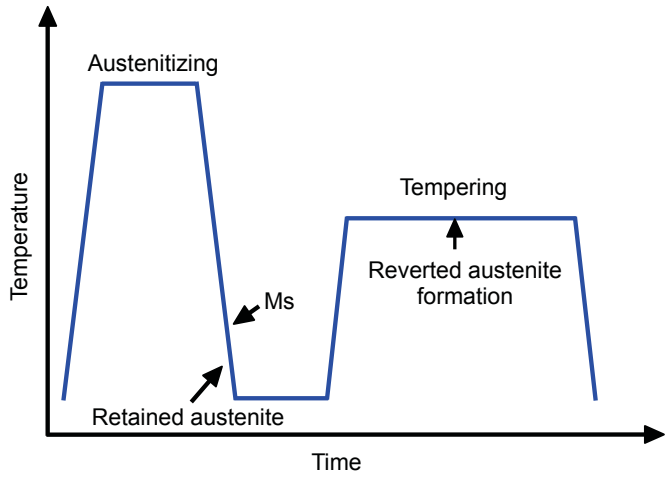

Figure 2.4: Formation of retained and reverted austenite during heat treatment.

Reverted austenite can be found in maraging steels [20, 21], cryogenic or 9Ni steels [22–24] and high Co-Ni steels [15, 18, 25]. Additionally, metastable austenitic steels or in general steels with a duplex-like microstructure also present austenitic regions with comparable chemical compositions or transformation properties, even though heat treatments and the formation processes might be different [16, 26, 27].
These types of steels forming reverted austenite during tempering exhibit relatively high Ni or Mn contents, as these elements cause an enlargement of the FCC phase field. Van Genderen et al. [19] demonstrated that the formation of reverted austenite is evoked by the addition of Ni, as it forms in Fe-Ni-C steels, whereas in Fe-C steels no formation occurs during annealing.
Nonetheless, the growth mechanism of reverted austenite is controversial. It is described

by Sinha et al. [28] that the nucleation sites for reverted austenite are grain and lath boundaries, dislocations or other lattice imperfections. Due to segregation of nickel at these locations the transformation temperatures, such as the austenite start temperature, are locally lowered. As a result, reverted austenite forms at these sites. Schnitzer et al. [20] argued that the formation process of austenite in a PH13-8Mo maraging steel is controlled by the diffusion of Ni to existing austenite nuclei. Consequently, the nickel concentration in reverted austenite is much higher than in martensite. Conversely, it was proposed for a precipitation-hardened maraging-TRIP steel that reverted austenite forms along existing retained austenite films. Additionally, it is described that the formation of reverted austenite on boundaries is promoted by the diffusion of Mn to interfaces. As a result, reverted austenite is enriched in manganese [29, 30]. Conversely, Shiang, Farooque and Li et al. [21, 31, 32] described that the formation of reverted austenite in maraging steels is dominated by a shear process but as reverted austenite exhibits compositional differences to the matrix, also diffusional processes may occur.

Originated by their formation processes, retained and reverted austenite exhibit distinct differences. The composition of retained austenite can be predominately varied by the carbon content due to a tempering or partitioning treatment [10, 33, 34]. Conversely, the composition of reverted austenite presents chemical differences to martensite regarding substitutional elements, e.g. manganese and nickel [15, 25, 29]. It is reported by Haidemenopoulos and Le et al. [18, 32] that the composition of reverted austenite can be varied by the tempering conditions. Higher tempering temperatures cause a lower nickel content in austenite because the driving force for austenite formation is higher and less nickel for formation is necessary. Furthermore, reverted austenite can be easily turned in size, i.e. thickness, by altering tempering temperature and time [18, 25].

2.3.2 Transformation behavior of austenite and toughness properties

Retained and reverted austenite can transform into martensite as a result of external conditions, e.g. varying temperature, applied strains or stresses.

Generally, a martensitic transformation of reverted or retained austenite occurs as a result of cooling below the martensite start temperature. Accordingly, sub-zero treatments can also cause a reduction of retained austenite phase fraction [35, 36]. Additionally, a transformation of austenite can also proceed during tempering processes. Retained austenite of low alloyed steels might transform into ferrite and cementite or bainite as a

result of tempering in the range between 200°C and 350°C. However, retained austenite in higher alloyed steels (e.g. high speed steels) is more stable and transforms during cooling after tempering into martensite. Hence, tempering of higher alloyed tool steels is done multiple times to reduce the retained austenite content and to temper the martensite formed upon cooling. In most cases, the transformation of austenite due to tempering in ferrite and carbides (bainite) or in martensite upon cooling results in an embrittlement [3].

Retained and reverted austenite can also be transformed into martensite due to mechanical loading. An overview about the influence of mechanical loading and temperature on the phase transition is given in Fig. 2.5. Below the M_s-temperature, a spontaneous martensitic transformation proceeds. By raising the temperature above M_s, the transition of austenite has to be assisted by external loading. The $M_{s\sigma}$-temperature describes the transition from the stress-assisted into the strain-induced mode of transformation. Up to this temperature the austenite transforms before reaching its yield strength and the transformation of austenite proceeds stress-assisted. However, beyond the $M_{s\sigma}$-temperature the austenite gets plastically deformed before it transforms. As a result, new nucleation sites, which enable and promote a strain-induced transformation, are created. Beyond the M_d-temperature, the austenite is too stable to transform [15, 16].

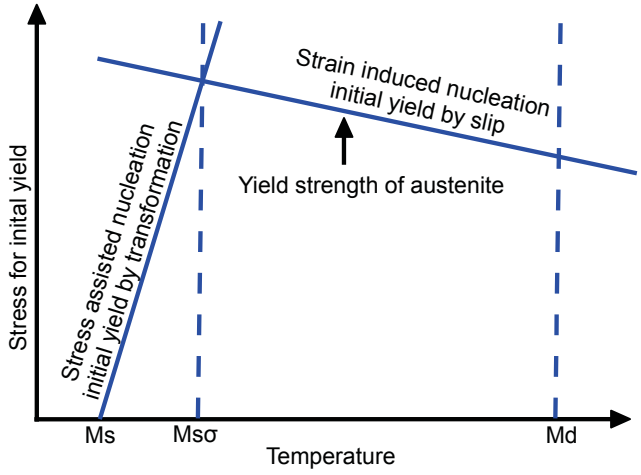

Figure 2.5: Influence of external loading and temperature on the austenite to martensite transformation behavior [16].

The mechanical induced transformation of austenite can evoke a transformation induced plasticity (TRIP) effect or a transformation toughening effect. Materials bearing a TRIP effect principally present high fracture strains, uniform elongations and a high strain hardening. These materials are commonly ductile materials, such as low alloyed steels for plates [5]. In contrast to the TRIP mechanism, the transformation toughening effect

is rather based on a toughness enhancement than on a raise of ductility. This effect is mainly found in brittle materials, such as ceramics with transforming zirconium oxide particles [37, 38]. Additionally, transformation toughening is also reported in the field of high Co-Ni steels, since the high fracture toughness values are partially ascribed to the transformation of austenite upon loading [15, 39, 40].

It is described by Geberich et al. [41] that the TRIP effect is a product of the strain energy absorption. Since the strain-induced transformation of austenite into martensite consumes energy, the energy available for crack propagation is reduced [42]. Others argue that the transformation present in TRIP steels is controlled by the applied strain and is thus stress-assisted [43, 44].
Additionally, the transition of austenite into martensite causes an increase of hardness. This yields to a localized deformation in the remaining austenite until this austenite transforms. Thus, necking is delayed and a high uniform elongation is produced by this mechanism [42, 45, 46]. Furthermore, it is assumed by Antolovich et al. [42] that the TRIP effect leads also to a toughness enhancement of the material.

The transformation toughening effect considers the raise of volume due to the martensitic transformation. For a toughness enhancement, the transformation accompanied with the volumetric increase must proceed ahead of the crack tip to generate compression stresses. These compression stresses in the region of crack tip, shield the tensile stresses produced by the external loading. As a result, the effective stress intensity at crack tip is lowered. This leads to an enhancement of toughness as described by Eq. 3. The toughness of the material K_0 can be enhanced by ΔK_C due to stress shielding of the transforming particles and thus, the critical stress intensity factor K_{IC} and the fracture toughness of the material is raised [15, 16, 37, 39, 40].

$$K_{IC} = K_0 + \Delta K_C \tag{3}$$

The raise of toughness is proportional to the volume change during transformation, which can be calculated by Eq. 4. The change of volume due to transformation is ΔV, V is the initial volume and a_{fcc} and a_{bcc} are the lattice constants of austenite and martensite [15, 16, 39, 40].

$$\frac{\Delta V}{V} \propto \left(\frac{a_{bcc}}{a_{fcc}}\right)^3 - 1 \tag{4}$$

The volume change as a result of an austenite to martensite transformation is dependent on the chemical composition of austenite and martensite, since the composition influences the lattice parameters [8, 39, 47–52].
A raise of the carbon content in general causes an enhancement of the transformational volume change. In unalloyed steels the volume change due to martensitic transformation is about 3-4 % [53]. In Fe-Ni alloys the change of volume is influenced by the INVAR effect, as this effect is accompanied with high lattice parameter values for the FCC-phase. Generally, the INVAR effect is present in iron alloys with about 36 % Ni below the Curie temperature [50]. It was also determined by Shibata et al. [54] that the transformational volume change in Fe-Ni-Co alloys is reduced by the increase of the Co and Ni content and thus, in these steels an austenite to martensite transformation without a significant change of volume can occur.

Austenite may also enhance the toughness properties without generating a TRIP or transformation toughening effect. Sato [35] suggested that austenite enhances toughness properties by blunting or grain boundary sliding. Conversely, it is reported by Kim and Scheartz [55] that the toughness of martensite can be increased by the diffusion of interstitial elements such as carbon into austenite, because of the higher solubility [24, 56]. Syn and Kim et al. [24, 56] claimed that austenite present at grain boundaries would enhance the toughness by interrupting the crystallographic alignment of martensite packets. However, also a martensite formed upon mechanical loading would interrupt cleavage planes and thus impede cleavage fracture.

2.4 Stability of austenite

The toughness increment of austenite containing alloys is determined by the stability of austenite. Leal and Haidemenopoulos [15, 16] found that the largest toughness (or strain of fracture) enhancement for an operation temperature in the range or slightly above the $M_{s\sigma}$ temperature. This $M_{s\sigma}$ temperature is an inherent property of the austenite coupled to its stability. The stability of austenite can also be described by the resistance against transformation [57] and is influenced by [18]:

- The size and form of the austenite phase
- The composition of austenite
- The strength of the material and the stress state

2.4.1 Influence of size and morphology

The stability of austenite increases with decreasing grain size [9, 33, 58]. Haidemenopoulos and Grujicic et al. [15, 59] reported that in thicker austenite films more nucleation sites for martensitic transformation are available. Thus, the probability for transformation is higher in thicker films compared to thin ones, causing a lower resistance against transformation. A different approach was done by Waitz et al. [58]. They predicted that the energy barrier for transformation is higher for smaller grains (due to a higher fraction of interfaces compared to the volume of the grain) resulting again in a higher stability for smaller grains. Additionally, it was demonstrated by Bhadeshia at al. [9] that austenite films are more susceptible to transformation than blocky austenite. This suggests again that film-shaped austenite in general exhibits a higher stability.

2.4.2 Influence of chemical composition

The composition of austenite has a major influence on its stability. As described in the Section 2.3.1 the concentration of substitutional elements in reverted austenite can be turned by heat treatment parameters. Thus, its stability can be varied. Commonly, high contents of Ni or Mn are used to stabilize the reverted austenite [15, 18, 20, 30, 40]. It is reported by Ayer, Haidemenopoulos and Li et al. [18, 25, 32] that the nickel content in reverted austenite decreases by increasing the tempering temperature, since at higher

temperatures less nickel is required for creating reverted austenite. This is shown by the experimental results of a high Co-Ni steel in Fig. 2.6. Hence, the reverted austenite formed at higher temperatures has a lower stability.
In contrast, retained austenite is generally stabilized with high C contents by quenching and partitioning processes [11, 33, 60, 61]. In these quenched and partitioned steels the formation of carbides is weak or suppressed by alloying and hence, less carbon is consumed for carbide precipitation [9, 60].

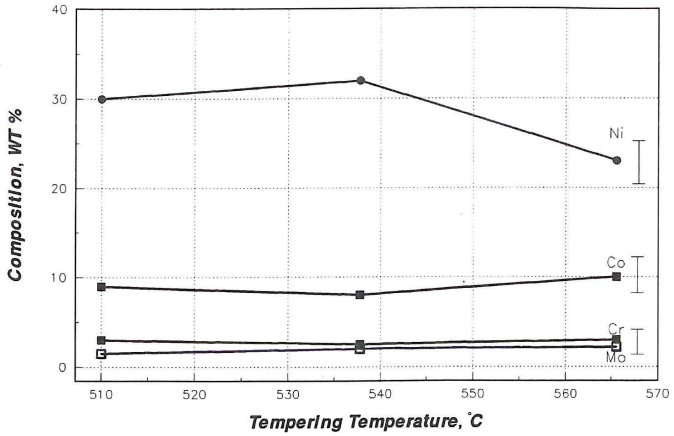

Figure 2.6: Chemical composition of reverted austenite in Aermet® 100 due to tempering for 5 h at different temperatures [25].

2.4.3 Influence of the strength of the matrix and the stress state

For transforming austenite into martensite by external mechanical loading distinct stresses or strains are necessary. As the strength of the material affects the contribution of the mechanical driving force to the total driving force for the transformation of austenite, the stability of austenite is influenced. Also, the stress state influences the stability of austenite. It is described in the works of Leal, Haidemenopoulos and Olson et al. [15, 16, 18, 62] that the stress triaxiality (tension) at crack tip favor the transformation of austenite in martensite, as this transformation is accompanied with an volume increase.

2.5 Alloying systems using the toughening effect of reverted austenite

Generally, retained and reverted austenite may influence toughness properties. Since the main interest of this work is put on alloying systems with reverted austenite, they are treated in detail in the following.

2.5.1 High Co-Ni steels

The steel class of high Co-Ni steels is characterized by high concentrations of cobalt and nickel. These steels exhibit a Fe-Ni-C-martensitic matrix and form secondary hardening carbides and reverted austenite during tempering. Representatives of this steel class are the alloys HY180, AF1410, Aermet® 100, Aermet® 310 and Aermet® 340 [63–65]. In the Table 2.1 the chemical compositions of these materials are listed.

	C	**Ni**	**Co**	**Cr**	**Mo**	**Fe**
	wt%	**wt%**	**wt%**	**wt%**	**wt%**	**wt%**
HY180	0.13	10.0	8.0	2.0	1.0	Bal.
AF1410	0.15	10.0	14.0	2.0	1.0	Bal.
Aermet® 100	0.23	11.1	13.4	3.1	1.2	Bal.
Aermet® 310	0.25	11.0	15.0	2.4	1.4	Bal.
Aermet® 340	0.33	12.0	15.6	2.25	1.85	Bal.

Table 2.1: Nominal composition of high Co-Ni steels [66–70].

Additionally, these steels provide an excellent combination of toughness properties on one side and high hardness and strength levels on the other side [63, 65, 66]. A summary of their mechanical properties is given in Table 2.2.

	Tensile strength MPa	**Yield strength MPa**	**Fracture toughness MPa$\sqrt{m}$**	**Impact toughness J**	**Hardness HRC**
HY180	1410	1240	203	81	43
AF1410	1725	1550	165	88	49
Aermet® 100	1956	1724	126	41	53-54
Aermet® 310	2172	1896	65	27	-
Aermet® 340	2379	2068	37	15	57

Table 2.2: Mechanical properties of high Co-Ni steels [65–69].

2.5.2 The alloy Aermet® 100

Evolution of austenite and its influence on toughness

The most prominent material of the class of high Co-Ni steels is the alloy Aermet® 100. In Aermet® 100 retained as well as reverted austenite are present. Due quenching to room temperature from austenitizing at 885°C for 1 h (standard austenitizing treatment), approx. 5-7 % retained austenite remain untransformed [35, 71]. To reduce this retained austenite phase fraction, the alloy is cryogenically treated at -73°C. Ayer and Machmeier [25] described that the content of austenite after cryogenic treatment is below the detection limit, whereas Gruber [71] and Sato [35] found approx. 1-3 % austenite left.

Tempering of this alloy at temperatures above 450°C causes a formation of reverted austenite [17, 25]. This is also shown in Fig. 2.7, which illustrates the increase of austenite phase fraction as a function of tempering temperature. The standard tempering treatment of Aermet® 100 is performed at 482°C for 5 h. Due to this tempering treatment reverted austenite is predominately created at the martensite lath boundaries in form of thin, nm-sized films (interlath austenite), as depicted in Fig. 2.8. Moreover, austenite precipitates were also found inside the martensite laths (intralath austenite) by Lippard [40]. It was also determined for this alloy that the reverted austenite formed upon tempering is enriched in nickel and depleted in cobalt [25]. However, the carbon concentration in austenite, and by that the influence of carbon on the microstructural evolution was not evaluated in any of these studies [25, 39, 40].

Tempering at 482°C for 5 h causes also the precipitation of $(Mo,Cr)_2C$ secondary hardening carbides. These carbides have a length of approx. 9 nm and a diameter of 3 nm and exhibit a hexagonal-close-packed (HCP) crystal structure [25, 72, 73]. Additionally, no cementite should be present after this tempering treatment [25].

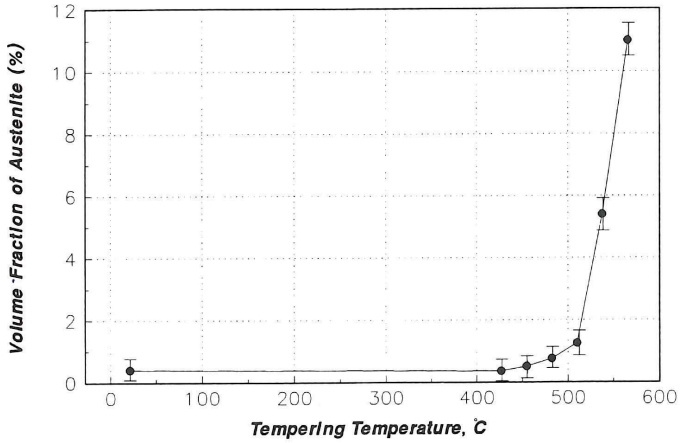

Figure 2.7: Increase of the reverted austenite phase fraction in Aermet® 100 due to tempering for 5 h at different temperatures [25].

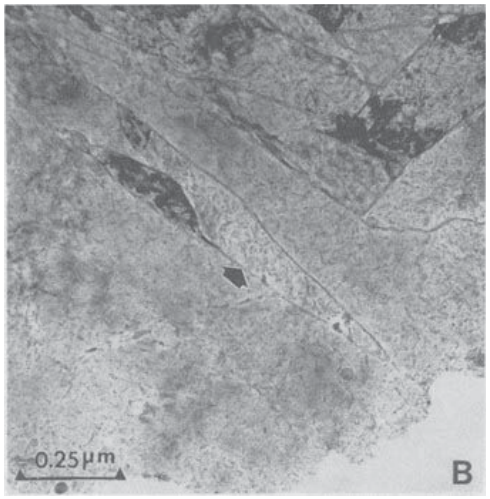

Figure 2.8: Microstructure of Aermet® 100 after tempering at 482°C for 5 h. The arrow indicates reverted austenite [25].

The mechanical properties of this alloy are strongly influenced by cryogenic treatment. Sato and Gruber [35, 71] demonstrated that fracture toughness values of tempered samples are higher, if a preceding cryogenic treatment is conducted. This is shown in Table 2.3, which summarizes the influence of cryogenic treatment on the mechanical properties of Aermet® 100. Additionally, the cryogenically treated conditions exhibit lower tensile strengths but higher yield strengths compared to the samples without cryogenic treat-

ment. This behavior of non-cryogenically treated conditions might be a result of an early transformation of austenite into martensite [16, 35, 71].

		Cryogenically treated samples	**Non-cryogenically treated samples**
Tensile strength	[MPa]	2032	2106
Yield strength	[MPa]	1785	1645
Fracture toughness K_Q	[MPa$\sqrt{m}$]	165	89

Table 2.3: Influence of cryogenic treatment on mechanical properties of the alloy Aermet® 100 [71].

Although Aermet® 100 exhibits excellent fracture toughness values, the toughening mechanism of austenite in this alloy is controversial. It is described by Ayer [25] and Sato [35] that a non-transforming austenite enhances toughness due to grain boundary sliding. Conversely, Lippard [40] and Kuehmann [39] argue that a transformation toughing effect occurs.

In prior investigations concerning the toughness properties of Aermet® 100, many additional heat treatments were tried for enhancing toughness properties [35, 39, 40]. Most of them comprise a two step heat treatment with the intention to produce a higher volume fraction of reverted austenite with a higher nickel content. As a consequence, lots of stable austenite precipitates should be created and the toughness values should increase. However, a significant toughness increase without a decrease of hardness was not found for Aermet® 100 by any of these heat treatments [35, 39, 40].

In the works of Haidemenopoulos [15], Lippard [40] and Kuehmann [39] lots of thermodynamic calculations were performed for high Co-Ni steels to determine the austenite stability at different heat treatment conditions for predicting fracture toughness properties. However, there is a lack of experimental results regarding microstructure and the transformation behavior of austenite for these steels for confirming the findings from thermodynamic calculations.

Additional factors affecting the toughness of Aermet® 100

Since toughness properties of high Co-Ni steels are of major interest, a modification of non-metallic inclusion is conducted for improving the toughness-strength relationship. Non-metallic inclusions, such as MnS or CrS, present in high Co-Ni steels lead to a reduction of toughness values, as voids can be nucleated. Hence, rare earth elements such as lanthanum and cerium are added, which form oxides or oxisulfides [74]. It is described by Handerhan and Garrison et al. [74, 75] that due to these additions larger inclusion with larger inclusion spacings are produced. Since the fracture initiation toughness is dependent on inclusion spacing as described by Eq. 5, higher toughness values are obtained by this modification.

$$\delta_{IC} \approx \ X_0(R_V/R_I) \ [74, \ 75] \tag{5}$$

The crack opening displacement at fracture initiation is δ_{IC}, $\mathrm{X_0}$ is the inclusion spacing, $\mathrm{R_V}$ the average size of the voids and $\mathrm{R_I}$ the radius of inclusions. As shown in Fig. 2.9, the crack opening displacement at fracture initiation exhibits a linear relationship with $\mathrm{X_0(R_V/R_I)}$. Thus, larger inclusion spacings result in higher fracture toughness values. As a result, Heat#1 of Aermet® 100, which exhibits the lowest inclusion content and the largest spacing, has the highest fracture toughness value [35].

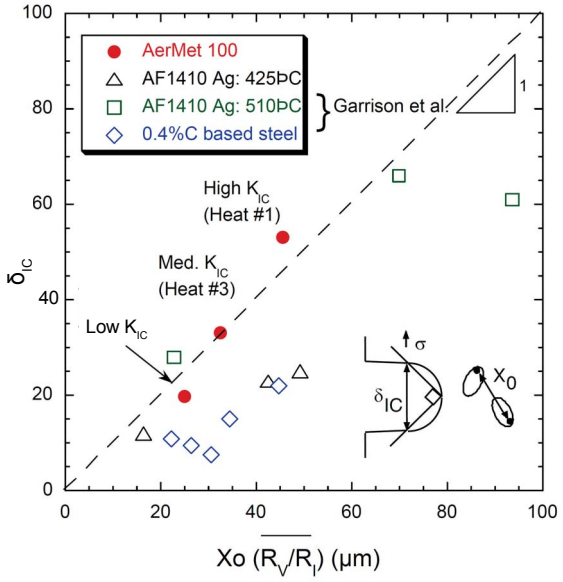

Figure 2.9: Correlation of crack opening displacement at fracture initiation δ_{IC} with $X_0(R_V/R_I)$. A linear relationship is found for the steel AF1410, Aermet 100 and a 0.4 C steel. The Heat#1 of Aermet® 100 exhibits the lowest inclusion content and the largest spacing. The δ_{IC} were calculated from J_{IC} values [35].

.

Furthermore, also secondary particles, such as carbides precipitated during tempering, influence toughness properties as they promote the coalescence of voids [75, 76]. This is depicted in Fig. 2.10.

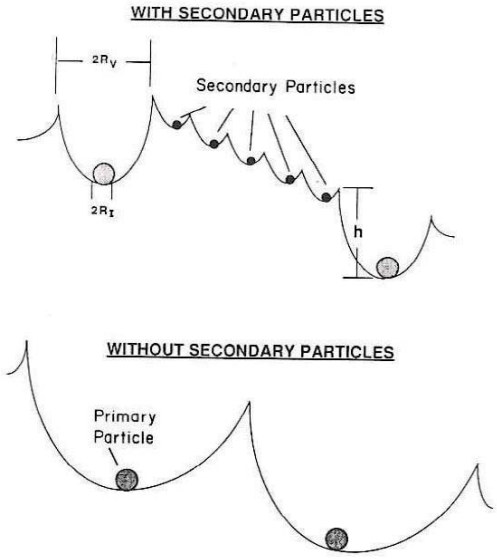

Figure 2.10: Influence of secondary particles on the fracture process [76].

2.5.3 Maraging steels

Austenite reversion during aging arises also in maraging or precipitation hardening steels. High strength levels as well as good toughness and ductility properties are typical properties of these steels. In contrast to the most other steel types, maraging steels present very low carbon concentrations. Furthermore, they form fine dispersed intermetallic precipitates during aging instead of carbides. Additionally, maraging steels exhibit relatively high contents of nickel, chromium, manganese or cobalt and also smaller amounts of molybdenum, titanium or aluminum [77].

Compared to high Co-Ni steels much more experimental work was done concerning the properties of reverted austenite in maraging steels.
Reverted austenite in maraging steels was found to be present in different types regarding its form and position, as depicted in Fig. 2.11. This austenite can have a granular or an elongated form. Furthermore, three different types of austenite regarding the formation or position are described by Shiang et al. [21]. Matrix austenite, which is formed by diffusional processes, is located at retained austenite or at prior austenite grain boundaries. At austenite grain and at martensite lath boundaries as well as inside the martensite laths lath-like austenite is created. By the formation of this austenite a structure with alternating martensite and austenite films is produced. Recrystallized austenite is present along martensite packet boundaries or within martensite laths. This austenite is free of dislocations and is formed at higher aging temperatures and longer aging times [20, 21, 78, 79].

The reverted austenite in maraging steel grades is highly enriched in Ni or Mn. In steel grades with Ni-rich intermetallic precipitates, the formation of reverted austenite is promoted by the dissolution of them during overaging. As a result of this, the reverted austenite is free of these precipitates [20, 29].

In most cases, the reverted austenite in maraging steels enhances toughness and ductility properties but lowers strength and hardness values. Nevertheless, there are various effects of reverted austenite on mechanical properties, which might be dependent on the type of steel and its heat treatment, as also indicated by the findings from literature.
It was observed by Schnitzer et al. [80] that reverted austenite in a PH13-8Mo steel, which is formed at 575°C, is not stable during tensile tests and transforms strain induced into martensite. A higher reverted austenite phase fraction leads to a higher ductility and strain hardening but to a lower strength of the material.

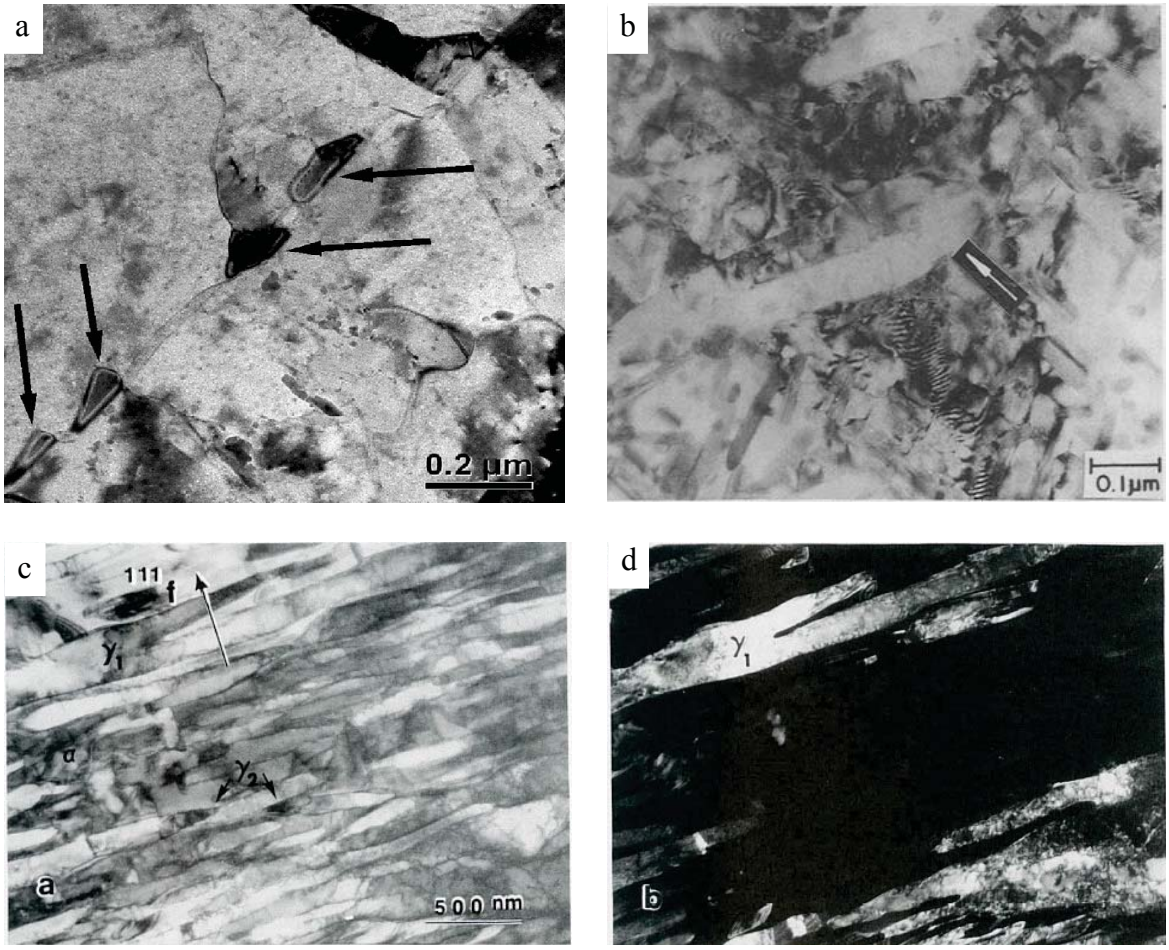

Figure 2.11: Different austenite morphologies in maraging steels. (a) Matrix austenite in a PH13-8Mo steel [20]. (b) Recrystallized austenite in a 350 grade maraging steel. (c) Bright-field image of lath-like austenite in an Fe-19.5Ni-5Mn steel [78]. (d) Dark-field image of the lath-like austenite [21].

Conversely, austenite, which was formed during aging at 580°C for 3 h (overaged), in an 18 % Ni (300) maraging steel is stable during tensile tests down to −100°C. It is described, that higher aging temperatures lead to a transformation of austenite during tensile tests. This is a result of the lower Ni content of austenite formed at higher temperatures. Due to the transformation, a TRIP effect is produced and fracture strains of 20 % are reached [81]. Furthermore, Visvanathan et al. [79] reported that at peak hardness in a 18 % Ni (350) maraging steel no reverted austenite is present. In the overaged condition, a reduction of strength but an enhancement of ductility and toughness was observed. This enhancement of toughness and ductility was attributed to reverted austenite.

3 Setup of experiments and kinetic calculations

3.1 Material and heat treatment

The investigated material was a high Co-Ni steel. Its actual composition was determined by X-ray fluorescence (XRF) spectroscopy and is listed in Table 3.1. The alloy was commercially produced and forged into round bars with a diameter of 100 or 200 mm.

C	**Ni**	**Co**	**Cr**	**Mo**	**Fe**	**Si**	**Mn**	**P**	**S**	**O**
0.22	11.0	13.5	2.9	1.2	Bal.	<0.05	<0.02	$<5*10^{-3}$	$5*10^{-4}$	$4*10^{-4}$

Table 3.1: The actual composition of the investigated alloy in weight percent (wt.%).

The heat treatments of the alloy comprised austenitization in a vacuum furnace and tempering in batch furnaces. The cooling rate after austenitization was 10°C/ min. Furthermore, half of the conditions were cryogenically treated (CT) in a freezing chamber at −73°C for 1 h. The heat treatments are summarized in Table 3.2.

Austenitizing	**Cryogenic treatment**	**Tempering** 1st step	**Tempering** 2nd step
	−73°C/ 1 h	-	
	-	-	
	−73°C/ 1 h	482°C from 10 min to 50 h	-
885°C/ 1 h,	-	482°C from 10 min to 10 h	-
cooling with	−73°C/ 1 h	540°C from 10 min to 10 h	-
10°C/ min	-	540°C from 10 min to 10 h	-
	−73°C/ 1 h	600°C from 10 min to 10 h	-
	-	600°C from 10 min to 10 h	-
	−73°C/ 1 h	482°C for 1 h	482°C for 4 h
	-	482°C for 1 h	482°C for 4 h

Table 3.2: Heat treatments of the investigated alloy.

3.2 Imaging methods

Scanning electron microscopy (SEM) measurements were conducted on a EVO MA 5 microscope from Zeiss with a LaB_6 cathode and a large chamber for analyzing samples from fracture toughness tests. Stereophotogrammetric measurements were also conducted on a LEO 440 SEM.

Transmission electron microscopy (TEM) analyses were carried out on a Philips CM12 microscope with 120 kV operation voltage as well as on a FEI Tecnai F20 and a Philips CM20 STEM microscope with 200 kV operation voltage. The chemical composition of microstructural elements during TEM and SEM measurements was analyzed by energy-dispersive X-ray spectroscopy (EDS). The sample preparation for TEM analyses was conventional. Disc-shaped samples with a diameter of 3 mm were ground to a thickness of approx. 80 μm and subsequently electro polished.

A Cameca Local Electrode Atom Probe (LEAP) 3000X HR in laser mode was used for atom probe tomography (APT) measurements. The measurements were carried out at 60 K with a puls rate of 200 kHz and a laser energy of 200 nJ. For sample preparation rods were cut from the bulk material with side lengths of about 0.3 mm. Thereafter, these rods were electro polished for obtaining a sharp tip with a radius of approx. 50 nm [82]. The software package IVAS version 3.6.8 was used for reconstruction of the data.

3.3 Hardness measurements

A QNess Q10 A+ testing machine was used for hardness measurements at room temperature (RT) according to the standard for Vickers hardness tests of metallic materials EN ISO 6507-1 [83]. The hardness values presented in this work are the mean values of five single measurements. The applied load during testing was 10 kg (HV10).

3.4 X-ray diffraction analyses

X-ray diffraction measurements at RT were carried out on a D8 Discover diffractometer from Brucker AXS. For a precise determination of the crystallographic properties of austenite and martensite, Cr-K_α radiation with a relatively high wavelength of 2.29 Å was used. The data obtained from measurements was evaluated with software package Topas 4-2.

For analyzing the austenite phase fraction the Rietveld method [84] was used. The lattice parameters and the lattice distortions of austenite and martensite were determined by Whole Powder Decomposition analysis [85–87]. The absolute measuring inaccuracy for austenite phase fraction measurements was approx. 1 % for 1 - 10 % and 3 % for up to 30 % austenite phase fraction. The detection limit was about 1 %. The inaccuracy for martensite lattice parameter determination was 0.0005 Å and the inaccuracy for austenite lattice parameter determination was 0.001 Å.

Additionally, austenite phase fraction measurements at defined stress levels during tensile testing were performed on a Xstress 3000 G2 diffractometer from Stresstech with Cr radiation. The phase fraction of austenite was evaluated by comparing the areas within the 200- and 220-γ peaks with the areas within 200- and 211-α peaks.
The XRD measurements were conducted in the middle of the tensile test specimens, i.e. the region at which the specimens fractured. To exclude a preceding transformation of austenite due to residual stresses on the sample surface, the region for XRD analyses on the tensile test specimens was ground and electrolytically eroded.

3.5 Dilatometry and differential scanning calorimetry analyses

Dilatometer investigations were carried out on a DIL 805A dilatometer from TA Instruments (formerly BAEHR).
In Table 3.3 the tempering treatments of CT and non-CT samples, which were performed in the dilatometer, are summarized. The dilatometer samples were tubular and had a length of 10 mm, a diameter of 4 m and a wall thickness of about 1 mm. Cooling to -100°C was performed with a freezing unit from TA Instruments, which was attached to the dilatometer. This freezing unit refrigerates helium with liquid nitrogen and subsequently conducts the helium through the hollow samples. Martensitic transformations during the dilatometer experiments were also analyzed. Thereto, the M_s-temperatures were evaluated by determining the first deviation from the linear behavior of the relative length change curves upon cooling. The measuring accuracy of the M_s-temperatures was in the range of ± 10°C.

Heat	**Hold**	**Cool**	**Heat**	**Hold**	**Cool**
100°C/min	482°C/1 h	100°C/min to -100°C	-	-	
100°C/min	482°C/5 h	100°C/min to -100°C	-	-	
20°C/min	482°C/1 h	20°C/min to 20°C	20°C/min	482°C/4 h	20°C/min to -100°C
100°C/min	540°C/1 h	100°C/min to -100°C	-	-	
100°C/min	540°C/5 h	100°C/min to -100°C	-	-	
100°C/min	600°C/1 h	100°C/min to -100°C	-	-	
100°C/min	600°C/5 h	100°C/min to -100°C	-	-	

Table 3.3: Tempering treatments of CT and non-CT samples, which were performed in the dilatometer.

Furthermore, dilatometer experiments in combination with differential scanning calorimetry (DSC) measurements were conducted.
The DSC measurements were performed on a STA 449 C Jupiter from Netzsch. For an accurate determination of the tempering processes in the DSC, the heat capacity changes during heating were evaluated. Hence, additional measurements were carried out without samples for the baseline correction and with sapphire samples for determining the heat capacity.
CT and non-CT specimens were heated in the dilatometer and in the DSC to 620°C (1st run) and cooled to room temperature and again heated with the same parameters (2nd run) to 900°C. Additionally, CT and non-CT samples were heated to 900°C in a single step. The heating and cooling rates were 20°C/ min. The temperature profiles of the performed heat treatments in the DSC and in the dilatometer are shown in Fig. 3.1.
For a precise evaluation of the processes during heating, the signals obtained from the 2nd run were subtracted from the signals obtained from the 1st run. As a result, the net signals of irreversible processes, i.e. the tempering processes, can be evaluated [88].
The samples for these dilatometer analyses had a diameter of 4 mm and a length of 10 mm and the samples for DSC measurements had the same diameter but a thickness of approximately 1 mm.

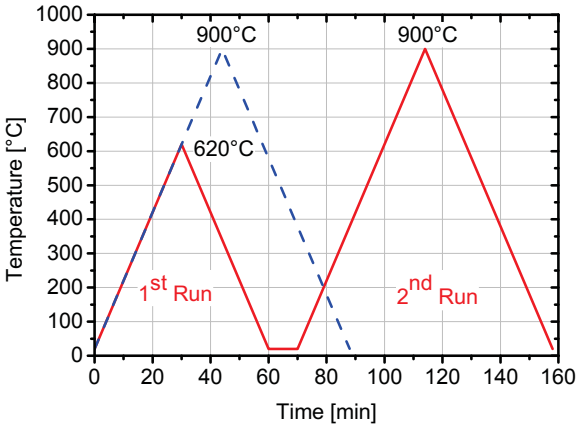

Figure 3.1: Temperature profile of the performed heat treatments in the DSC and dilatometer.

Additionally, larger samples with a length of 15 mm and a diameter of 10 mm were tempered in the dilatometer but further analyzed by austenite phase fraction and hardness measurements. These CT and non-CT samples were heated to various temperatures up to 620°C and subsequently (without holding) cooled to room temperature. The heating rate was 20°C/ min and the cooling rate was 100°C/ min.

3.6 Tensile tests

Uniaxial tensile tests were carried out by using a Z250 universal testing machine from Zwick. The tests were performed according to the standard EN ISO 6892-1 [89] for tensile tests at room temperature. The elongation was analyzed with a contact-type extensometer and for measuring the applied force a 250 KN load cell was employed. The specimens had a gage length l_0 of 40 mm, a length of the reduced section l_C of 48 mm and an initial diameter S_0 of 8 or 6 mm. The used sample geometry is shown in Fig. 3.2.

3.7 Fracture toughness measurements

Fracture toughness tests were performed according to the standard ASTM E399-09 [90] by three point bending tests. For the measurements single edge-notched bend (SENB) specimens with side grooves for enhancing the constraint were used. Due to the limited availability of the investigated material, the sample size was restricted. The thickness B was 10 mm, the minimum thickness B_n was 8 mm and the width W was 20 mm. The

Figure 3.2: Used sample geometry for tensile tests.

used sample geometry without side grooves is depicted in Fig. 3.3. The specimens were taken from a L-C orientation. Fatigue precracking was performed on a RUMUL resonance testing machine from Russenberger Pruefmaschinen with a minimum to maximum stress ratio of 10 in compression and 0.1 in tension. The maximum stress intensity factors during precracking were 50 MPa$\sqrt{m}$ in compression and 21 MPa$\sqrt{m}$ in tension. The number of cycles was in the range between 10^5 to 10^6. The fracture toughness tests were conducted on a Zwick Z250 universal testing machine.

Figure 3.3: Dimensions of the used SENB samples for fracture toughness measurements.

Due to the restricted sample size, valid K_{IC} values according to the standard ASTM E399-09 [90] were only obtained for non-CT samples tempered at 482°C for 5 h. As a result, K_Q and K_{max} (K values at force maximum) values were used for comparison of the heat treatment conditions.

Additionally, the crack tip opening displacement at crack initiation (COD_i) and at a crack extension Δa of 160 μm ($COD_{\Delta a=160\ \mu m}$) were analyzed as criterion for toughness properties for different heat treatment conditions. The COD values were determined according

to Kolednik and Stampfl [91, 92] by stereophotogrammetric analyses on fractured SENB specimens. To determine the height profiles of both sides of the fracture surfaces, SEM images from the fracture surfaces photographed with tilt angels of 0°, 5° and 10° were made. The software Mex 5.1 from Alicona was used for determining these height profiles. Line profiles were created at exactly the same positions on both fracture surfaces with a minimum distance to the sample edge of 2.5 mm. These profile pairs were adjusted in the way that they touch in the point of the first void coalescence after the blunting zone for the COD_i value and at distinct points during crack extension for evaluating the $COD_{\Delta a=160\ \mu m}$ value, which is the COD value after 160 μm crack extension. After the adjustment of the profiles, the distance between the fatigue crack surfaces was taken as COD value. For every heat treatment condition three positions were analyzed and for each position three different line profile pairs were drawn and the values were averaged.

The fracture toughness K_{COD} was calculated from the COD values according to Kolednik [93] by using the Eq. 6 and 7:

$$K_{COD} = \sqrt{2 * \sigma_f * E * COD} \tag{6}$$

$$\sigma_f = \frac{e^n}{(1+n) * n^n} * R_m \tag{7}$$

where σ_f is the flow stress, n the work hardening exponent, R_m the tensile strength and E is the Young's modulus. The work hardening exponent was estimated according to Fig. 3.4. The evaluated values of n were 0.143 for the sample tempered 482°C for 5 h, 0.129 for the CT sample tempered at 482°C for 5 h, 0.133 for the sample tempered at 482°C for 1+4 h and 0.096 for the CT sample tempered at 482°C for 1+4 h.

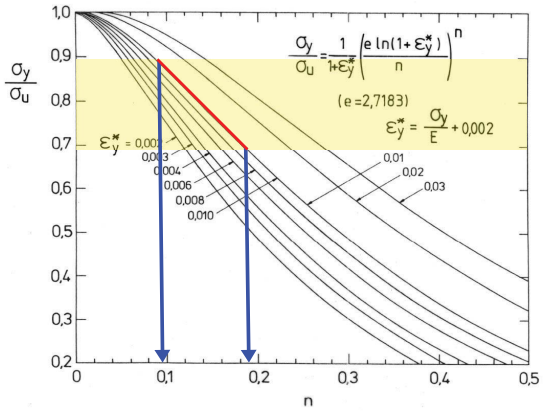

Figure 3.4: Estimation of the work hardening exponent according to ESIS P2-92 [94]. The tensile strength is σ_u and the yield strength is σ_y. The region of the ratio of the the yield strength and tensile strength as well as the value of ϵ^* for the investigated heat treatment conditions is marked. The values of the work hardening exponent were between 0.096 and 0.143.

3.8 Thermo-Calc, DICTRA and MatCalc calculations

Equilibrium calculations were preformed by using the Thermo-Calc version 3.0.1 in combination with the thermodynamic database TCFE7 [95].

Kinetic calculations were carried out with the software package DICTRA version 24. For these calculations the mobility database MOB2 [96] and the thermodynamic database TCFE3 [97] were used. The setup for DICTRA calculations comprised a planar system geometry with two phase regions. For the region of martensite a BCC phase and for the region of austenite a FCC phase was created. The austenitic region for the calculations at 482°C had a width of 4 nm and the martensitic region had a width of 32 nm. For the simulations at 600°C, the regions had a width of 10 nm and 320 nm, respectively. The grid points in austenite and martensite were geometrically distributed with a higher density near the interface. Both phases exhibited a linear initial element distribution.

Diffusional calculations were carried out with MatCalc version 5.61 [98] by using the thermodynamic database for iron alloys mc_fe_V2.040 [99] and the diffusion database mc_fe_V2.006 [100].

4 Results and discussion

4.1 Characterization of microstructure and fundamental properties

High Co-Ni steels exhibit a complex microstructure consisting of a martensitic matrix, carbides and retained and reverted austenite [25, 35]. Since the microstructure is strongly influenced by cryogenic and tempering treatments, it was analyzed for the present steel grade regarding:

- the phase arrangement and the size of austenite films and carbides after austenitizing and after tempering,
- the influence of tempering and cryogenic treatment on the austenite phase fraction and
- the influence of tempering on the element distribution in martensite and austenite.

Thereto, SEM, TEM, APT investigations as well as austenite phase fraction and hardness measurements were carried out. Furthermore, the results were correlated with thermodynamic and kinetic calculations.

Some contents of this section are also subject of the Publication V [101].

4.1.1 Austenite phase fraction and hardness evolution upon tempering

Austenite phase fraction measurements at room temperature were conducted on austenitized (= non-CT) and cryogenically treated (CT) samples as well as on CT and on non-CT samples tempered at 482°C, 540°C or 600°C between 10 min and 50 h. The results are presented in Fig. 4.1. The austenite phase fraction after austenitizing and quenching to room temperature is approx. 6.5 %. Due to performing a cryogenic treatment at −73°C for 1 h, the austenite content is reduced by about 3 % to 3.5 %.
Tempering of high Co-Ni steels leads in general to a raise of austenite content due to the formation of reverted austenite [25]. This is also observed for the investigated material. Tempering of CT samples at 482°C for 50 h causes a raise of austenite phase fraction to approx. 10.5 %. Nevertheless, the formation of reverted austenite is more pronounced at elevated temperatures, since tempering of CT and non-CT specimens at 540°C or 600°C

for 10 h leads to an increase of austenite phase fractions to about 15 % and 30 %, respectively.

The results in Fig. 4.1 indicate that the austenite phase fraction increases gradually due to tempering of CT samples at 482°C and 540°C as well as for CT and non-CT at 600°C. Conversely, tempering of non-CT samples at 482°C or 540°C causes a reduction of austenite phase fraction within the first hour of tempering and the followed cooling to room temperature (RT). Due to tempering of non-CT specimens at 482°C for 1 h a minimum austenite phase fraction of approx. 2 % is reached. Tempering at 540°C leads to a minimum austenite phase fraction of approx. 3 wt.% after a holding time of 10 min. However, the austenite phase fraction of non-CT samples tempered at 482°C and 540°C increases again gradually when tempering is continued. Nevertheless, it is expected that also for tempering of non-CT samples at 600°C a reduction of austenite phase fraction occurs within the first minutes of tempering and the followed cooling to RT. Since for this condition the formation of austenite is more intense, a reduction of austenite content within the first minutes might not be detectable by this testing setup.

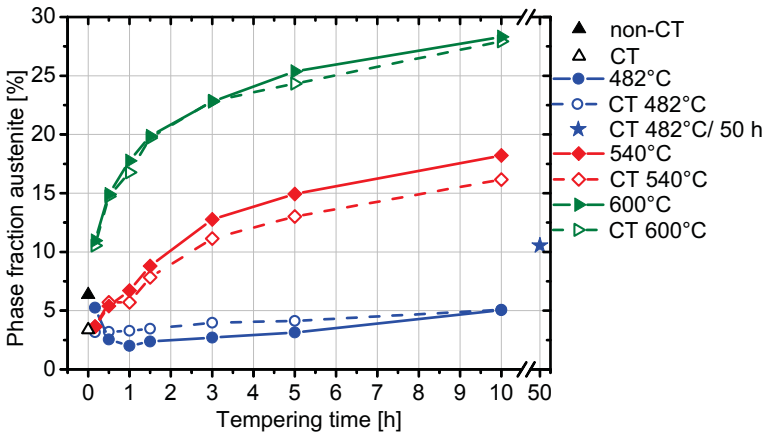

Figure 4.1: Results of austenite phase fraction measurements of austenitized and cryogenically treated samples as well as of CT and non-CT samples tempered at 482°C, 540°C or 600°C for times between 10 min and 50 h. The measurements were conducted after the heat treatment at room temperature.

The results in Fig. 4.1 demonstrate that the reduction of austenite phase fraction during tempering of non-CT samples at 482°C for 1 h leads to austenite contents, which are comparable to them of the CT conditions before tempering. Thus, for analyzing the evolution of austenite phase fraction more precisely a two step tempering treatment is performed, which comprises a tempering step at 482°C for 1 h, subsequent cooling to room temperature and another tempering step at 482°C for 4 h (482°C 1+4 h). The results

are listed in Table 4.1. Again, for the non-CT conditions the austenite phase fraction is decreased after the first tempering step of 1 h. However, by continuing the tempering process at 482°C for 4 h, the austenite phase fraction increases for both, CT and non-CT conditions. Therefore, it is suggested that the reverted austenite formation occurs for both conditions in the same manner. Accordingly, also the reverted austenite phase fraction formed during tempering for 4 h at 482°C are comparable for CT and non-CT conditions. Furthermore, the overall austenite contents in the samples tempered for 1+4 h are in the same range than the contents in the samples tempered for 5 h. Based on these findings it is suggested that a two-step tempering treatment has no influence on the overall austenite content but probably on the transformation properties of austenite during tempering. Hence, this tempering treatment will be further analyzed in Section 4.2.2.

	Before tempering	**482°C/ 1 h**	**482°C/ 1+4 h**
CT	3.5	3.5	4.0
non-CT	6.5	2.0	4.0

Table 4.1: Austenite phase fraction (%) measurements of CT and non-CT samples before and after tempering at 482°C for 1 h and for 1+4 h and cooling down to room temperature.

The results from hardness measurements are shown in Fig. 4.2. The hardness of the austenitized and subsequently cooled sample was determined with 530 HV and is slightly lower than the hardness of the cryogenically treated sample. Tempering of CT and non-CT specimens at 482°C for 5 h causes an increase of hardness to approx. 580 HV. For CT samples the peak hardness is reached after approx. 1.5 h, whereas for the non-CT samples the peak hardness is reached after approx. 3 h holding time at 482°C. The hardness due to tempering CT and non-CT samples at 482°C for 1+4 h was determined with 590 and 591 HV, respectively. Hence, the hardness for the conditions tempered at 482°C for 1+4 h is in the same range than the hardness of the samples tempered at 482°C for 5 h. However, tempering at 540°C and 600°C leads to a strong reduction of hardness to about 450 HV and 400 HV, respectively.

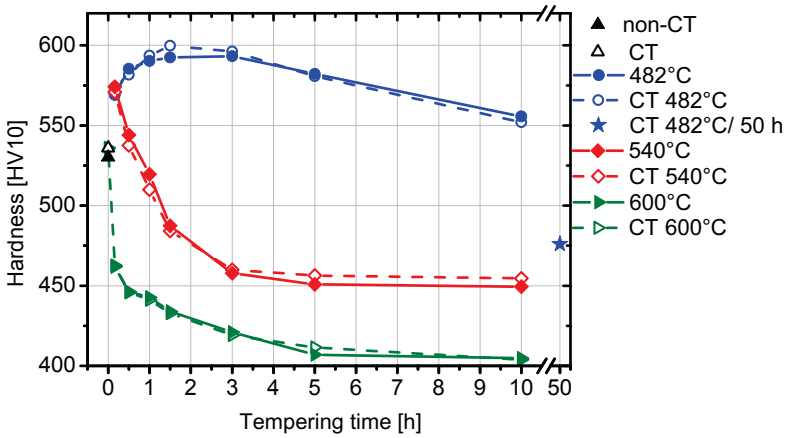

Figure 4.2: Results of hardness measurements at RT for austenitized and cryogenically treated samples as well as for CT and non-CT samples tempered at 482°C, 540°C or 600°C for times between 10 min and 50 h.

4.1.2 Microstructure of austenitized and cryogenically treated conditions

SEM analyses

The microstructure of austenitized and cryogenically treated samples was characterized by SEM experiments. The results, which are depicted in Fig. 4.3, reveal that the steel grade exhibits a fine martensitic microstructure. The prior austenite grain size is approx. 10 μm and the thickness of martensite laths is approx. 500 nm. However, no significant microstructural differences are observable between the CT and the non-CT specimen.

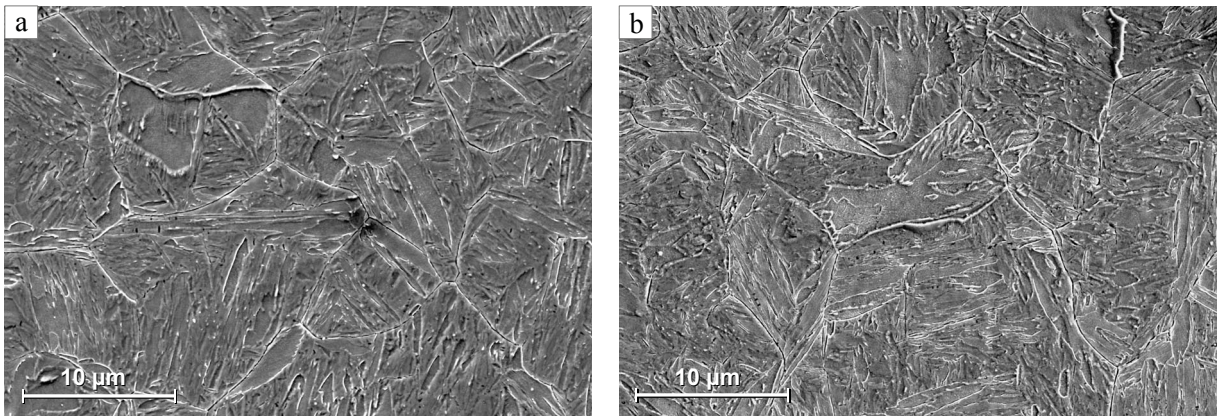

Figure 4.3: SEM images of the CT (a) and of the non-CT (b) sample. A fine martensitic structure is found for both conditions.

TEM analyses

For a more detailed analysis of the microstructure and for characterizing the retained austenite present in the CT and in the non-CT conditions, TEM investigations were performed. The bright-field (BF) image of the microstructure of the CT sample is presented in Fig. 4.4 (a). The accompanying dark-field (DF) image, which uses a 200-γ diffraction peak for evaluating the retained austenite is illustrated in Fig. 4.4 (b). It was determined that retained austenite is present in form of thin films along martensite lath boundaries. The thickness of these films is in the range from 3 nm (detection limit) to about 40 nm. As the austenite films might not always be perpendicular orientated to the sample surface, an exact determination of the film thickness is difficult. The BF and the DF images of the non-CT specimen are presented in Fig. 4.5. Again, no distinct differences, regarding the phase arrangement of retained austenite and martensite and the thickness of the films are found between the CT and the non-CT specimens.

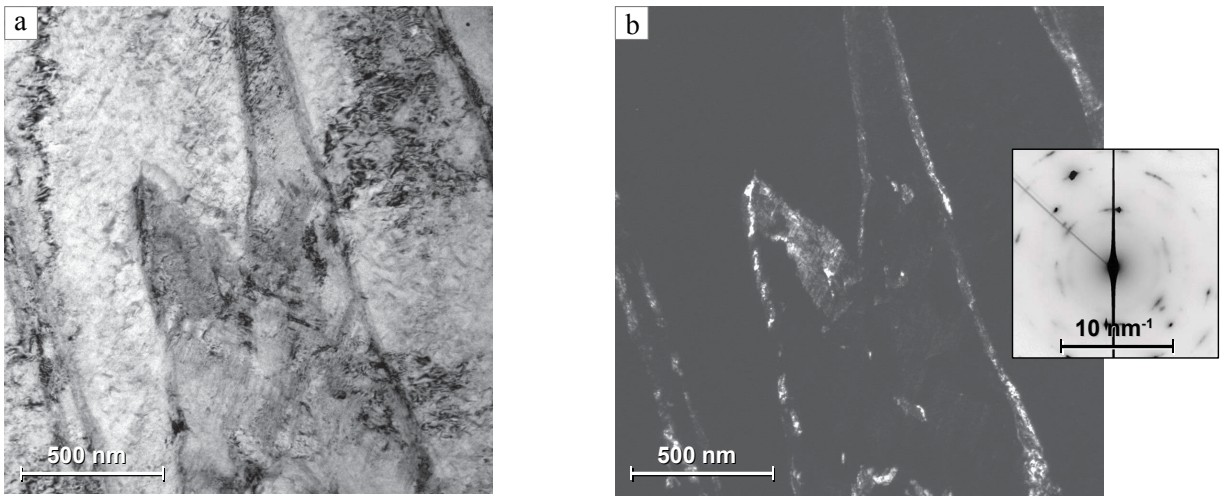

Figure 4.4: (a) TEM BF image of the CT condition. (b) Related TEM DF image, which uses a 200-γ diffraction peak for determining the thin retained austenite films present on martensite lath boundaries.

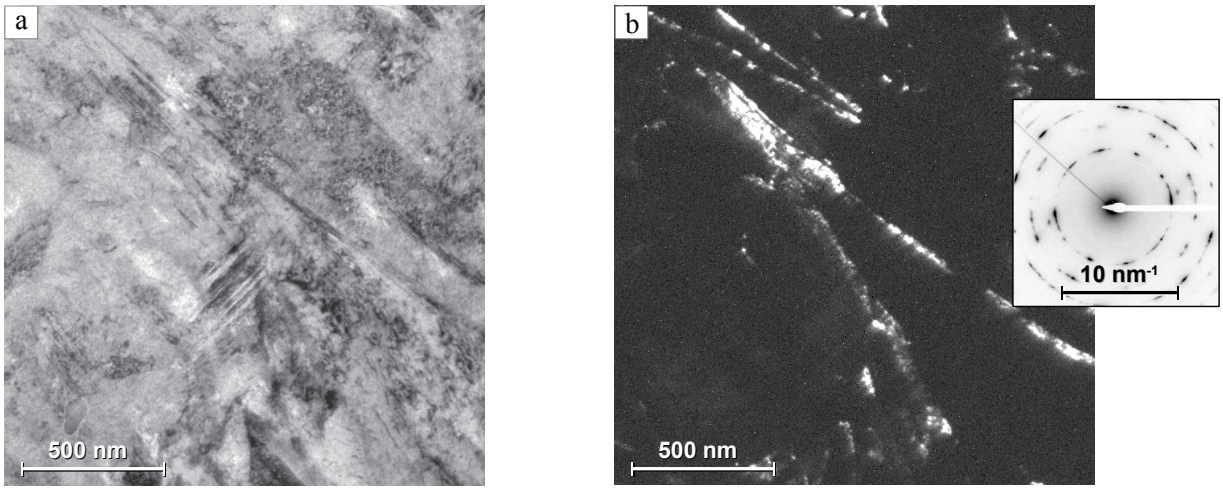

Figure 4.5: (a) TEM BF image of the non-CT condition. (b) Related TEM DF image, which uses a 200-γ diffraction peak for determining the thin retained austenite films present on martensite lath boundaries.

4.1.3 Microstructure of the conditions tempered at 482°C

TEM analyses

The microstructure of specimens tempered at 482°C was analyzed by TEM. As there were again no microstructural differences observable between CT and non-CT conditions, only the micrographs from CT samples are illustrated. The TEM BF image of the sample tempered for 5 h is pictured in Fig. 4.6 (a) and the related DF image by using a 200-γ diffraction peak is shown in Fig. 4.6 (b). It was found that in this condition the microstructure consists of martensite, austenite, which is mainly present at martensite lath boundaries, and small carbides (about 6 nm) within the martensite laths. An increase of the thickness or number of austenite films compared to the cryogenically treated specimen without tempering is not observed. It is suggested that this is caused by the less pronounced formation reverted austenite due to tempering at 482°C for 5 h. As both, reverted and retained austenite, are probably present within the samples tempered at 482°C for 5 h, the FCC phase found by TEM is termed as austenite and no differentiation between retained and reverted is conducted.

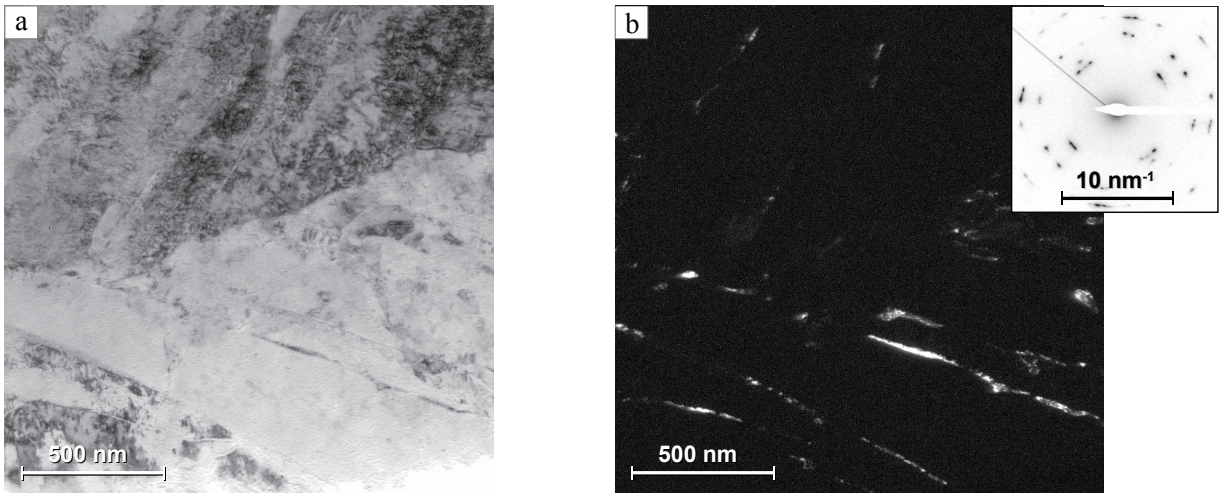

Figure 4.6: (a) TEM BF image of the CT sample tempered at 482°C for 5 h. It shows thin austenite films on martensite lath boundaries. (b) Related TEM DF image, which uses a 200-γ diffraction peak for illustrating the austenite.

TEM analyses were also carried out on the CT sample tempered at 482°C for 50 h. The results are presented by the BF images in Fig. 4.7 (a) and Fig. 4.8 (a) as well as by the DF images in Fig. 4.7 (b) and Fig. 4.8 (b). For both analyses, it is identified that the austenite films, present at martensite lath boundaries, have significantly grown in thickness to about 20-80 nm.

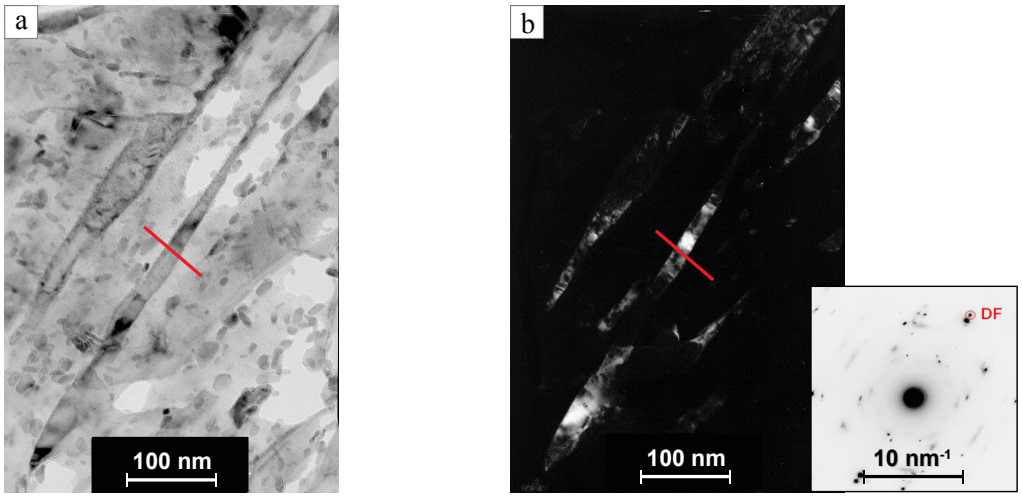

Figure 4.7: (a) TEM BF image of the CT sample tempered at 482°C for 50 h. (b) TEM DF image by using a 311-γ diffraction peak for illustrating the austenitic regions. The position for the EDS line scan is marked by the red line [101].

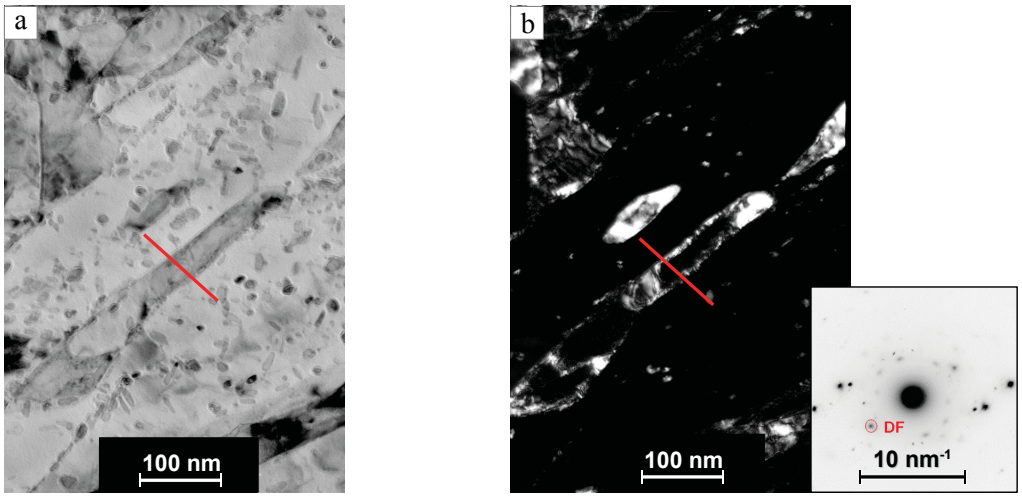

Figure 4.8: (a) TEM BF image of the CT sample tempered at 482°C for 50 h. (b) TEM DF image by using a 111-γ diffraction peak for illustrating the austenitic regions. The position for the EDS line scan is marked by the red line.

EDS line scans were created across the austenitic zones on the positions marked in Fig. 4.7 and Fig. 4.8 for analyzing the element distribution near the austenite - martensite interface. The results are shown by the line profiles in Fig. 4.9 (a) and (b). Both profiles exhibit regions with FCC crystal structures, which are enriched in Ni and depleted in Co. These regions are ascribed to reverted austenite, as reverted austenite presents such a composition this steel grades [15, 25]. In the middle of both analyzed positions, zones with lower Ni and slightly higher Co intensities (similar to the martensite outside) occur. These zones are termed in the following as “interaustenitic layers”. The interaustenitic layer of the first position (Fig. 4.7) exhibits a FCC structure and is therefore austenitic. Conversely, the interaustenitic layer on the other position (Fig. 4.8) is probably martensitic, as the ongoing investigations in Section 4.2.2 will demonstrate. For characterizing the structure of this interaustenitic layer, a more detailed diffraction analyses would be necessary, which was not subject of this work.
Nevertheless, these TEM investigations demonstrate that within the reverted austenite an interaustenitic layer is located, which is either austenitic or probably martensitic and exhibits a concentration of Ni and Co similar to martensite.

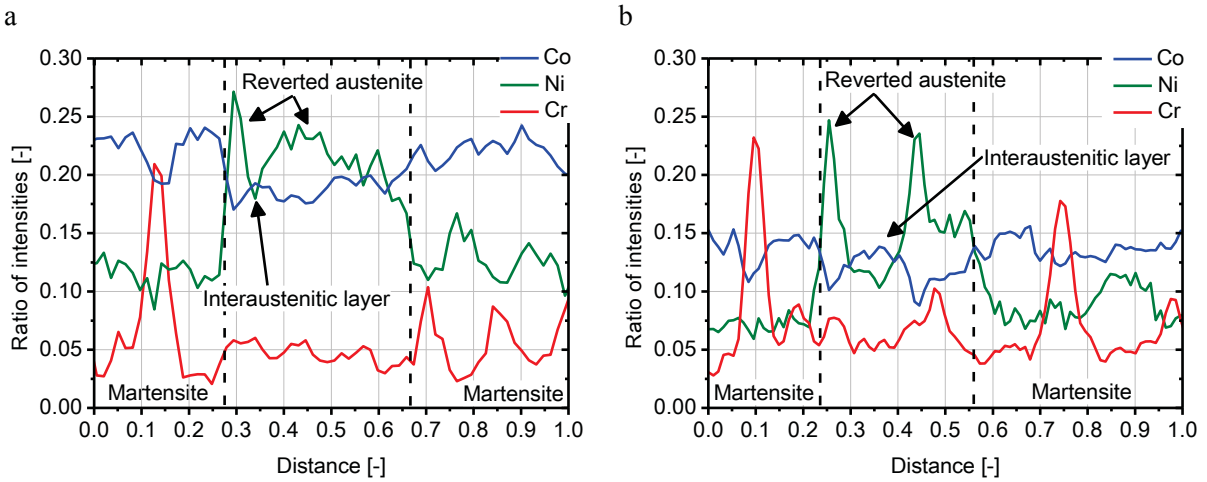

Figure 4.9: EDS line profiles across reverted austenite films with interaustenitic layers. The vertical dashed lines mark roughly the zones of the reverted austenite films with the enclosed interaustenitic layers. Outside these zones, martensite and carbides (high Cr intensities) are present. (a) Austenite film with an interaustenitic layer with a FCC structure as marked in Fig. 4.7 [101]. (b) Austenite film with an interaustenitic layer, which is marked in Fig. 4.8. This layer is probably martensitic as indicated in Section 4.2.2.

Additionally, the structure and size of carbides was analyzed. The TEM image in Fig. 4.10 shows carbides, which are located within martensite laths. These carbides are suggested to be rod-shaped as also indicated in literature [25] and have a mean length of approx. 30 nm and a mean width of approx. 10 nm. The diffraction image of the carbides suggests that they might have a M_2C structure.

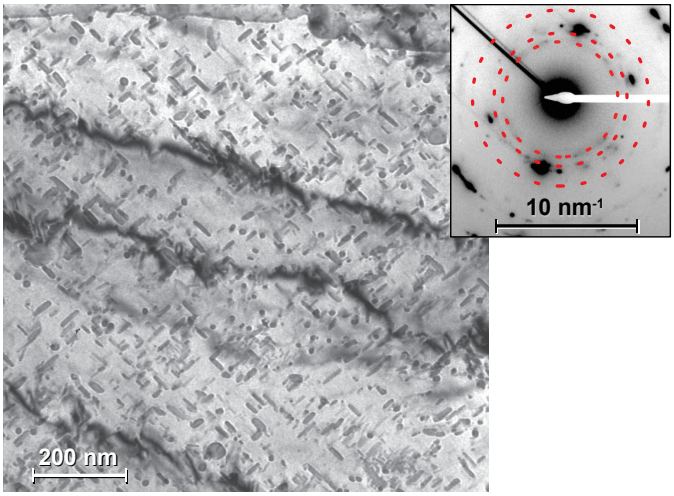

Figure 4.10: TEM BF image of the carbides in the CT sample tempered at 482°C for 50 h. The small insert shows the diffraction image. The reflections of the carbides are indicated by the circles.

APT analyses

The microstructural evolution and element redistribution during tempering was also studied by APT measurements for CT samples tempered at 482°C for 1 h , 5 h, and 50 h.

The three-dimensional reconstruction of the Ni atoms (green) of the sample tempered for 1 h is depicted in Fig. 4.11. Since it was determined by TEM and EDS measurements that reverted austenite exhibits high nickel contents, isoconcentration surfaces with 20 at.% Ni (green) were created for illustrating the austenite present in the sample. Due to an inhomogeneous nickel concentration in this sample, only the larger isosurfaces are expected to be austenitic areas. Furthermore, the sites enriched in carbon, chromium and molybdenum are attributed to carbides. For representing these carbides, isoconcentration surfaces (violet) were created at which the summed concentration of carbon and chromium atoms exceeds 11 at.%. The carbides found in this condition are finely distributed and have a mean size of about 3 nm.
Fig. 4.11 (b) shows a magnified image of the austenite film marked in Fig. 4.11 (a). It demonstrates that the reverted austenite consists of many small Ni-enriched particles (regardless of appropriate values for the isoconcentration surface). Additionally, carbides are present in the region of reverted austenite.
A one-dimensional concentration profile was created through this austenite film on a position without carbides. The profile is plotted in Fig. 4.12 (a) and the volume used for the profile is indicated in Fig. 4.12 (b) by the cylinder. The concentration profile exhibits zones of nickel enrichment, which are ascribed to reverted austenite. On the position of reverted austenite, also a slight decrease of the cobalt and a slight increase of the chromium concentration appears. In the middle between the reverted austenite films, a region with a composition similar to martensite (= outside the reverted austenite films) occurs. Thus, this region is again attributed to an interaustenitic layer.

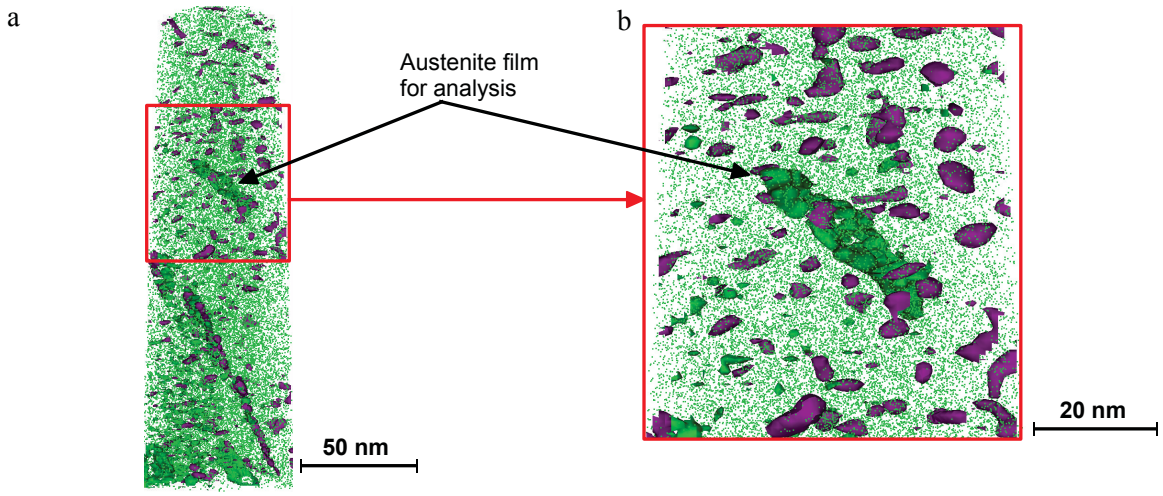

Figure 4.11: (a) Three-dimensional reconstruction of the Ni atoms (green) of the CT sample tempered at 482°C for 1 h. Carbides are represented by violet isoconcentration surfaces at which the summed concentration of Cr and C atoms is 11 at.%. The austenite is illustrated by 20 at.% Ni isoconcentration surfaces (green) and the austenite film for further analysis is marked by arrows. (b) Magnified image of the investigated austenite film inside the red box in (a) [101].

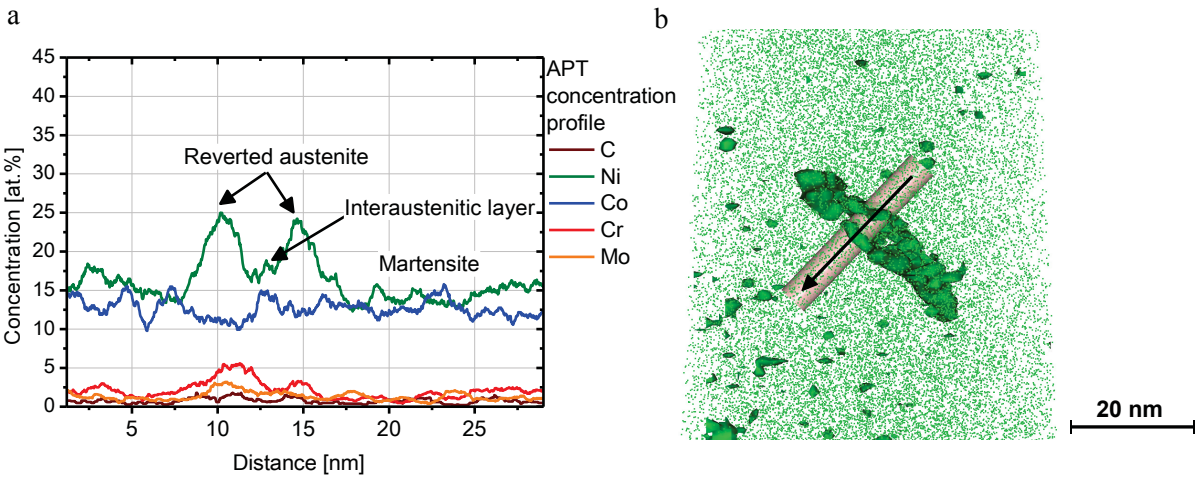

Figure 4.12: (a) One-dimensional concentration profile across the reverted austenite film of the sample tempered at 482°C for 1 h. The volume for analyzing the chemical composition is indicated in (b) by the cylinder. The zones with high nickel concentrations are ascribed to reverted austenite. An interaustenitic layer is located within the reverted austenite films.

The results of APT measurements of the sample tempered for 5 h are pictured in Fig. 4.13 (a). Again, Cr, Mo and C rich regions, illustrated by 11 at.% carbon-chromium isoconcentration surfaces (violet), are attributed to carbides. Reverted austenite is represented by a 15 at.% Ni isoconcentration surface (green). The value for the Ni isoconcentration surface was adjusted, due to different chemical compositions and element distributions in the samples, from 20 at.% to 15 at.% for a better representation of the reverted austen-

ite films.

The austenite film, which is marked in Fig. 4.13 (a) was used for further analyses. This film exhibits a closed isoconcentration surface of 15 at.% Ni. In Fig. 4.13 (b) a 12 nm thick vertical segment of the atom probe data is shown, which intersects the investigated austenite film. Thereby, it is identified that within this austenite film an interaustenitic layer with a typical elemental concentration is present. The one-dimensional concentration profile trough this austenite film is depicted in Fig. 4.14. It shows reverted austenite, indicated by the nickel enrichment and the cobalt depletion. Furthermore, also the chromium and carbon concentrations are higher in reverted austenite than in martensite, as also indicated in Table 4.2. In contrast, the interaustenitic layer exhibits similar Ni and Co contents than the martensite but also sightly higher chromium, molybdenum and carbon concentrations.

It was found that in this condition the reverted austenite films have a thickness of 1-3 nm and the carbides have a mean size of 4-5 nm.

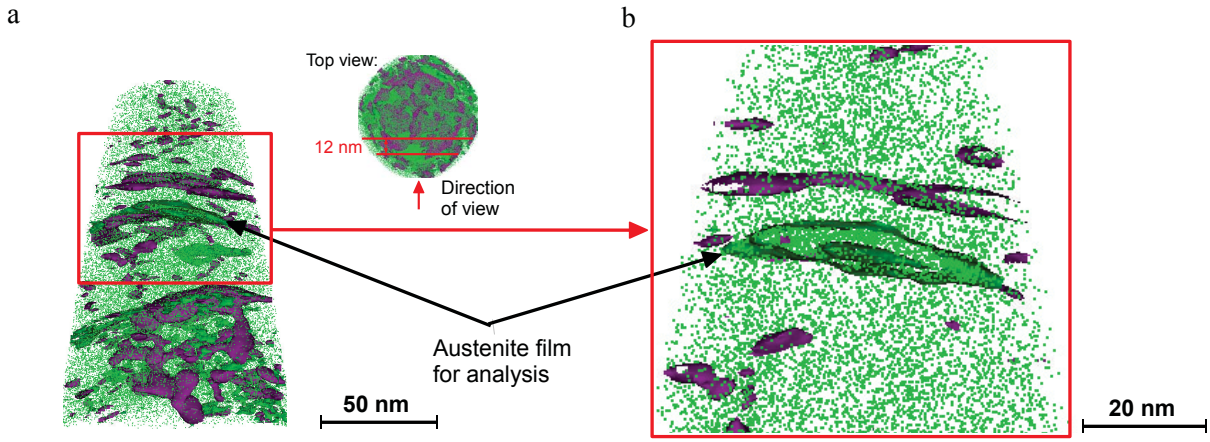

Figure 4.13: (a) Three-dimensional reconstruction of the Ni atoms (green) of the sample tempered at 482°C for 5 h. Carbides are represented by violet isoconcentration surfaces at which the summed concentration of Cr and C atoms is 11 at.%. Austenite is illustrated by 15 at.% Ni isoconcentration surfaces (green). The austenite film for further analysis is marked by arrows. The small insert shows the top view of the atom probe data and indicates the direction of view for (b). (b) A magnified, 12 nm thick, vertical segment of the entire atom probe data in (a). This vertical segment intersects the investigated austenite film [101].

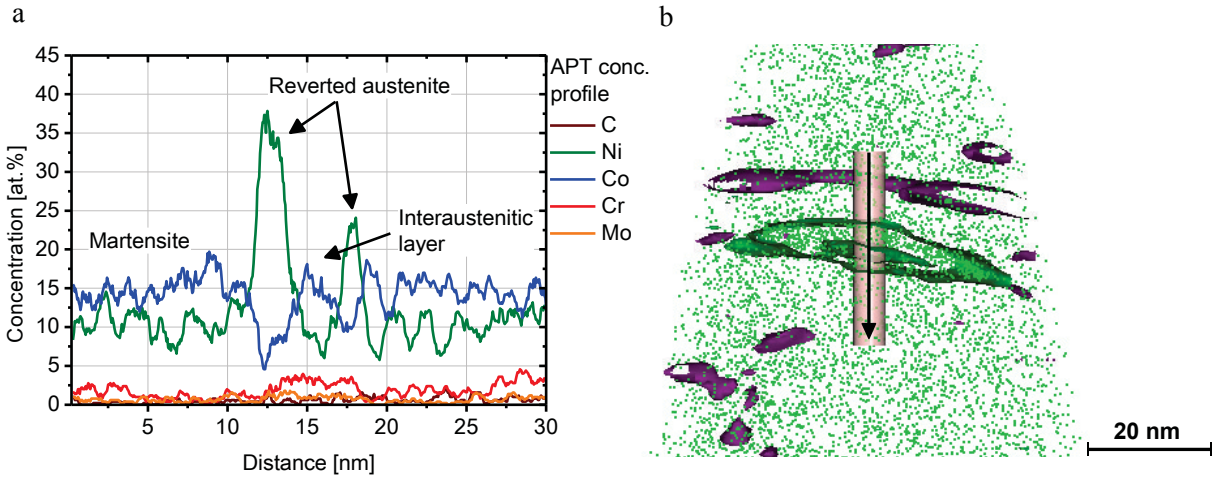

Figure 4.14: (a) One-dimensional concentration profile across the reverted austenite film of the sample tempered at 482°C for 5 h. The reverted austenite film encloses an interaustenitic layer. The volume for analyzing the chemical concentration is indicated in (b) by the cylinder [101].

	C at.%	Ni at.%	Co at.%	Cr at.%	Mo at.%	Fe at.%
Martensite	0.72	9.4	13.5	2.2	0.9	73.6
Reverted austenite	1.52	21.0	10.2	3.6	0.9	62.6
Carbides	11.85	7.3	5.7	23.0	3.1	48.9

Table 4.2: Analysis of the composition of martensite, reverted austenite and carbides in the sample tempered at 482°C for 5 h. For determining the compositions 15 at.% Ni and 11 at.% Cr+C isoconcentration surfaces were created.

Also, the microstructure after tempering at 482°C for 50 h was studied by APT. The three-dimensional reconstruction of the nickel atoms (green) is presented in Fig. 4.15. The specimen shows reverted austenite (20 at.% Ni isoconcentration surface, green) and carbides (11 at.% Cr+C isoconcentration surface, violet). The reverted austenite film extends from the bottom to the top of the specimen. The zones, where carbides are located and no nickel enrichment occurs, are attributed to martensite. Nevertheless, carbides are also identified in reverted austenite. Furthermore, an interaustenitic layer with a typical composition is found in the carbide-free region within the reverted austenite film. The elemental concentrations of the phases present in this condition are listed in Table 4.3.

The one-dimensional concentration profile trough the region of reverted austenite and the interaustenitic layer is depicted in Fig. 4.16. In this condition the reverted austenite films have a thickness of approx. 3-10 nm and are clearly enriched in Ni, Cr and Mo but

depleted in Co. As obvious by the chemical analyses, carbon is preferentially bound in carbides. Thus, no significant enrichment of the carbon is identified in reverted austenite compared to martensite. The interaustenitic layer within the reverted austenite exhibits a composition, which is rather comparable to the overall composition of the material than to the composition of martensite or reverted austenite, as shown in Table 4.3.

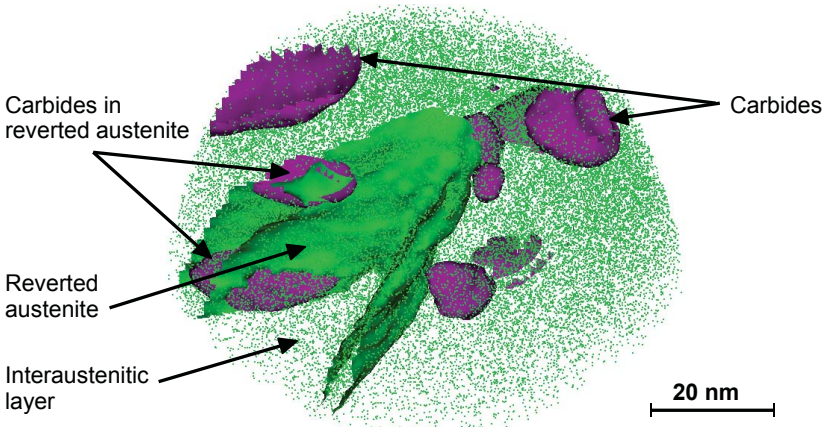

Figure 4.15: Three-dimensional reconstruction of the Ni atoms (green) of the sample tempered at 482°C for 50 h. Carbides are represented by violet isoconcentration surfaces at which the summed concentration of Cr and C atoms is 11 at.%. Reverted austenite is illustrated by a 20 at.% Ni isoconcentration surface (green). An interaustenitic layer is located within the reverted austenite film [101].

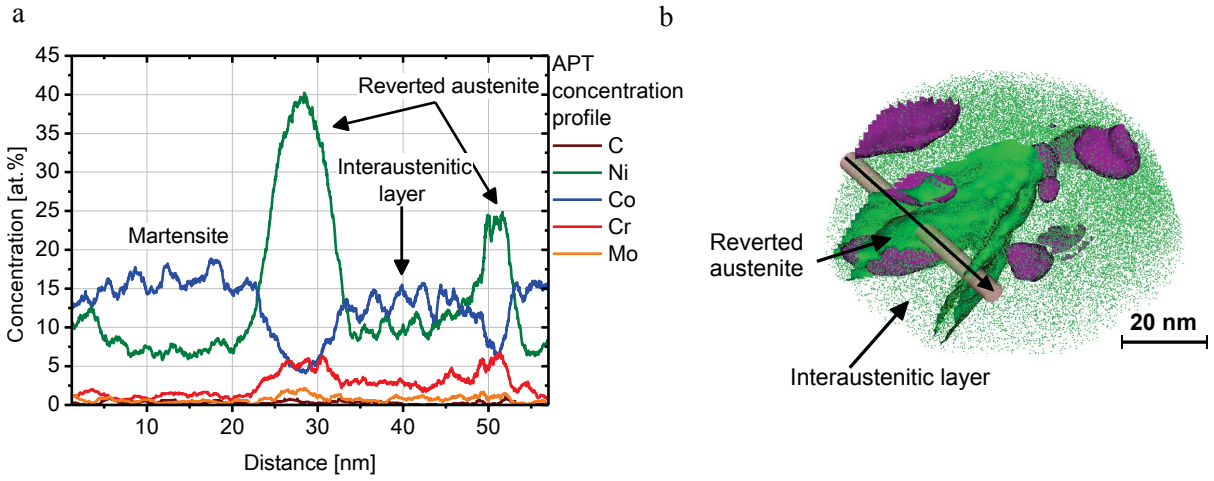

Figure 4.16: (a) One-dimensional concentration profile across the reverted austenite film with an interaustenitic layer of the sample tempered at 482°C for 50 h. The volume for analyzing the chemical concentration is indicated in (b) by the cylinder [101].

	C at.%	Ni at.%	Co at.%	Cr at.%	Mo at.%	Fe at.%
Overall composition	1.03	10.5	12.9	3.1	0.7	71.8
Martensite	0.36	8.8	13.6	1.9	0.2	75.2
Reverted austenite	0.52	29.7	7.3	5.9	1.0	55.6
Interaustenitic layer	0.35	10.7	13.0	3.4	0.8	71.7
Carbides	13.17	6.4	6.0	24.3	9.4	40.6

Table 4.3: Analyses of the composition of martensite, reverted austenite, the interaustenitic layer and carbides in the sample tempered at 482°C for 50 h. For determining the compositions, 20 at.% Ni and 11 at.% Cr+C isoconcentration surfaces were created. The overall composition of the steel was determined with XRF [101].

The element distribution in austenite, martensite and the interaustenitic layer due to tempering at 482°C for 50 h was also evaluated by proximity histograms [102]. Thereto, a 20 at.% Ni isoconcentration surface was used and and the data set of carbides (isoconcentration surface of 11 at.% Cr+C) was cut out of the volume before analyzing. In Fig. 4.17 (a) the volume for studying the element distribution near the reverted austenite-martensite interface and in Fig. 4.17 (b) the volume for analyzing the element distribution near the reverted austenite-interaustenitic layer interface is depicted. The proximity histogram for analyzing the region near the reverted austenite-martensite interface is shown in Fig. 4.18 (a) and the histogram for analyzing the region near the reverted austenite-interaustenitic layer interface is plotted in Fig. 4.18 (b).

These proximity histograms show that Ni is enriched in reverted austenite to a maximum value of 38-41 at.%, Cr is enriched to a maximum value of 6 at.% and cobalt is depleted to a minimum value of 5 at.%. In martensite, near the reverted austenite, a depletion of nickel and chromium and an enrichment of cobalt occurs. The region of nickel depletion has a width of 22 nm. The nickel content is about 8 at.% in martensite adjacent to the reverted austenite but increases gradually to 11 at.% (22 mn away from the reverted austenite), which is the overall nickel content of the material. The cobalt content in martensite near the reverted austenite is approx. 16 at.%. The region of cobalt accumulation is significantly smaller than the zone of nickel depletion and has a width of approx. 6 nm.

Conversely, in the interaustenitic layer, no distinct element enrichment or depletion zones can be observed. The composition of the interaustenitic layer is comparable to the overall composition of the material, except for the carbon concentration.

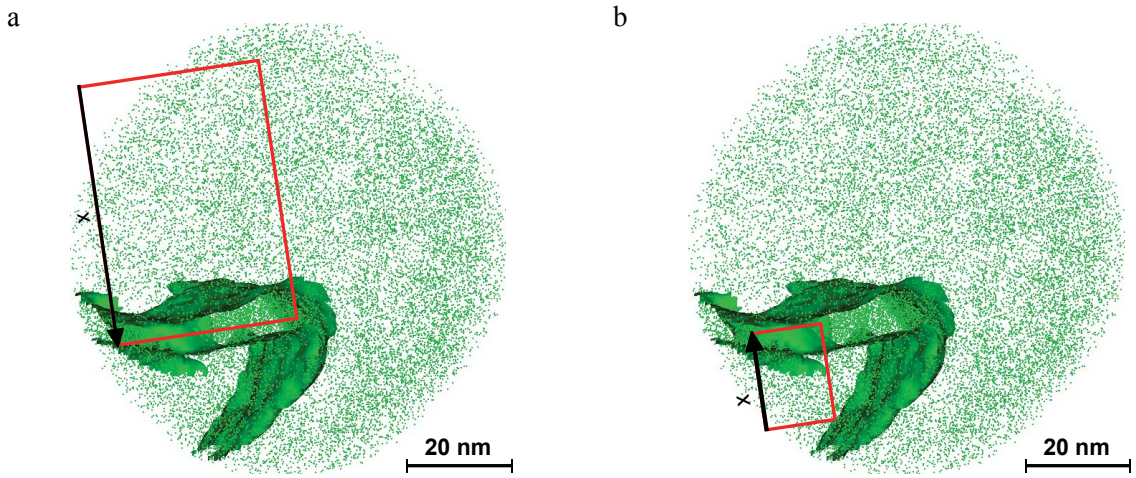

Figure 4.17: Three-dimensional reconstruction of Ni atoms of a sample tempered at 482°C for 50 h. The 20 at.% Ni isoconcentration surface (green) indicates the position of reverted austenite. The volume, which was used for analyzing the element distribution by proximity histograms near the martensite - reverted austenite interface (a) and near the interaustenitic layer - reverted austenite interface (b) is indicated by the red boxes [101].

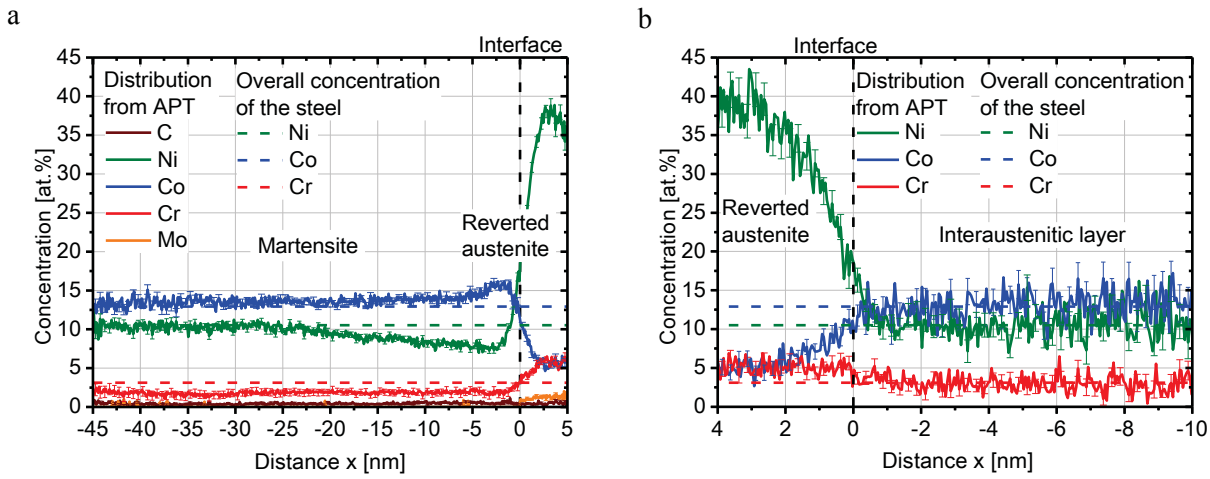

Figure 4.18: (a) Distribution of elements near the reverted austenite - martensite interface. (b) Distribution of elements near the reverted austenite - interaustenitic layer interface. The distribution was calculated by proximity histograms by averaging the elemental concentrations for equal distances x from the 20 at.% Ni isoconcentration surface. The volumes for the evaluation and the isoconcentration surfaces are indicated in Fig. 4.17 [101].

4.1.4 Microstructure of the conditions tempered at 600°C

The austenite phase fraction measurements in Section 4.1.1 reveal that due to tempering at 600°C for 5 h a massive formation of reverted austenite occurs. For analyzing the conditions present after this tempering treatment, TEM analyses of the microstructure were conducted. The results of the cryogenic treated (CT) sample tempered at 600°C for 5 h are shown in Fig. 4.19. The austenite films on the lath boundaries, which may consist of reverted and retained austenite have a thickness in the range between 60 nm and 140 nm. EDS measurements were conducted on austenitic and martensitic regions. The results are shown in Table 4.4. Also for this tempering condition an enhancement of Ni and a depletion of Co in austenite was found, whereas in martensite a reduction of nickel content is present. The carbides found in this samples have a mean length of about 30 nm and a mean width of 10 nm.

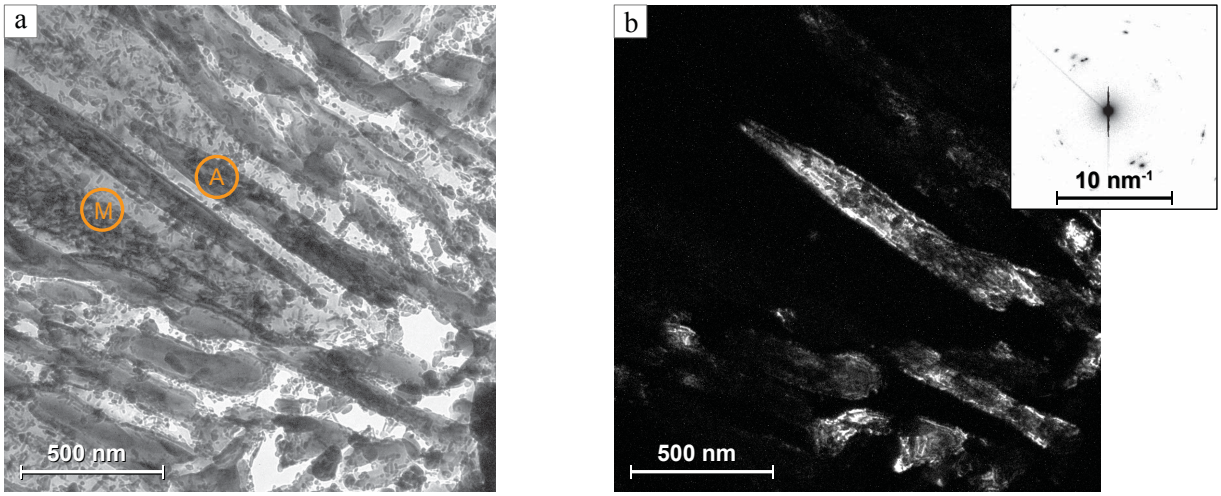

Figure 4.19: (a) TEM BF image of a CT sample, which was tempered at 600°C for 5 h. The austenite on the lath boundaries has remarkably grown in thickness compared to the CT condition. (b) Related TEM DF image, which uses a 200-γ diffraction peak for illustrating the austenite films.

		Ni	Co
Austenite	[wt.%]	18.2	9.8
Austenite	[at.%]	17.6	9.4
Martensite + carbides	[wt.%]	6.2	11.1
Martensite + carbides	[at.%]	6.0	10.6
Sample, averaged	[wt.%]	13.6	10.4
Sample, averaged	[at.%]	13.2	10.0

Table 4.4: EDS analyses of austenite (A) and martensite plus carbides (M) of the sample tempered at 600°C for 5 h. The positions for analyzing the compositions the are roughly indicated in Fig. 4.19 by the orange circles.

4.1.5 Calculation of element redistribution in austenite and martensite due to tempering

The element redistribution behavior during tempering was also studied by kinetic and thermodynamic calculations. Equilibrium calculations were conducted with Thermo-Calc at 482°C and 600°C. Since this steel grade is almost completely austenitic at 885°C, the starting composition used for calculating was the overall composition of the steel (Table 3.1). The results are presented in Table 4.5 and 4.6. It was found that approx. 18 mol.% of austenite are stable at 482°C. This austenite is enriched in nickel and depleted in cobalt, whereas the BCC phase (martensite) shows high cobalt and low nickel contents. Also, about 4.6 vol.% carbides are present in equilibrium at 482°C. At 600°C the phase fraction of stable austenite has increased to approx. 29 vol.%. However, this austenite is less enriched in Ni and depleted in Co than the austenite in equilibrium at 482°C.

Additionally, DICTRA calculations were carried out to simulate the chemical evolution and the spatial distribution of austenite and martensite during tempering at 482°C and 600°C. The microstructure before tempering would predominately consist of martensite and retained austenite. Thus, a BCC phase was created for martensite and a FCC phase was used for retained austenite. Since carbides are not considered in the calculations, the starting composition for the FCC and BCC phase was obtained from the APT sample tempered at 482°C for 50 h without taking carbides into account. This composition is listed in Table 4.7.

		BCC	FCC	$M_{23}C_6$	M_6C
Phase fraction	**mol.%**	76.9	18.1	4.8	0.3
Composition	**at.%**				
C		$1*10^{-6}$	$1*10^{-5}$	5.1	2.4
Ni		4.3	41.3	1.9	0.02
Co		16.6	3.6	0.2	2.4
Cr		0.7	1.1	52.3	1.4
Mo		0.06	0.4	20.1	70.7
Fe		Bal.	Bal.	Bal.	Bal.

Table 4.5: Equilibrium calculations with Thermo-Calc (TCFE7) at 482°C by using the actual composition of the steel. Approx. 18 mol.% austenite are stable at 482°C. The austenite is enriched in nickel and depleted in cobalt, whereas the BCC phase shows high Co and low Ni contents.

		BCC	FCC	$M_{23}C_6$	M_6C
Phase fraction	**mol.%**	66.2	28.8	4.9	0.04
Composition	**at.%**				
C		$9*10^{-5}$	$5*10^{-3}$	5.0	2.5
Ni		4.6	26.8	2.8	0.04
Co		17.1	7.2	0.7	5.6
Cr		0.8	1.6	43.2	2.2
Mo		0.2	0.8	19.5	64.8
Fe		Bal.	Bal.	Bal.	Bal.

Table 4.6: Equilibrium calculations with Thermo-Calc (TCFE7) at 600°C by using the actual composition of the steel. The phase fraction of stable austenite has increased to approx. 29 mol.% austenite at 600°C. The austenite is less enriched in nickel and depleted in cobalt than the austenite calculated at 482°C.

In Fig. 4.20 the results of the calculations at 482°C are presented. Before calculating the tempering step, the distribution of C, Ni and Co atoms in retained austenite and martensite is homogenous. By simulating a heat treatment at 482°C for 5 h or 50 h, the phase boundary between retained austenite and martensite moves in the direction of martensite. As a result, a new FCC phase is formed. This FCC phase is denoted as reverted austenite as it evolves during tempering. The reverted austenite has a thickness of about 0.7 nm due to holding for 5 h and about 2 nm for 50 h. Furthermore, it is enriched for both tempering conditions in Ni (43 at.%) and C and depleted in Co (4 at.%). Additionally, a zone of Ni depletion and of Co accumulation evolves in martensite adjacent to the reverted austenite. The zone of nickel depletion has a width of 11 nm due to

Ni	Co	C	Fe
wt.%	wt.%	wt.%	wt.%
11.5	13.5	0.1	Bal.

Table 4.7: Ni, Co and C concentrations in the APT specimen tempered at 482°C for 50 h without considering carbides.

tempering for 5 h and increases to a width of more than 30 nm after 50 h. For both conditions, the nickel content in martensite near to the reverted austenite film is about 4 at.% but increases with increasing distance from the reverted austenite film continuously to 11 at.%, i.e. the nickel concentration of the FCC and BCC phase before calculating. The zone of cobalt accumulation in martensite is significantly smaller and exhibits a width of about 7 nm after 50 h of tempering. Conversely, in retained austenite only small (<1.5 nm) depletion or accumulation zones of Ni and Co occur. However, the zones in retained austenite, which are enriched in nickel, might be also attributed to reverted austenite due to compositional similarities. Nevertheless, carbon is also enriched in retained austenite.

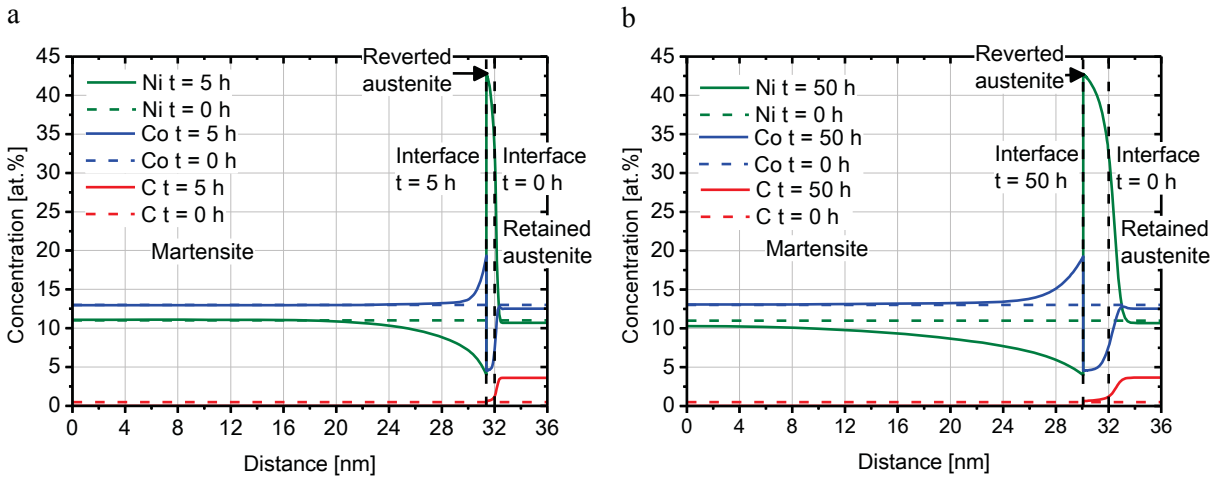

Figure 4.20: DICTRA calculations of the phase evolution and elemental redistribution processes during tempering near the martensite-retained austenite interface. (a) Tempering for 5 h at 482°C. (b) Tempering for 50 h at 482°C.

Fig. 4.21 presents the results from the DICTRA calculations for tempering at 600°C. It shows a more pronounced formation of reverted austenite in contrast to the simulation at 482°C. After 5 h at 600°C the formed austenite has a thickness of approx. 35 nm and is again enriched in Ni and depleted in Co. Also by DICTRA simulations at 600°C it is observed that the enrichment of Ni and depletion of Co in reverted austenite is less than after tempering at 482°C.

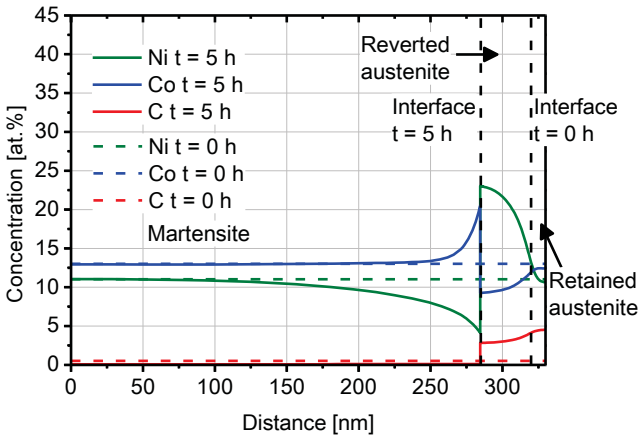

Figure 4.21: DICTRA calculation of the phase evolution and elemental redistribution processes near the martensite-retained austenite interface during tempering for 5 h at 600°C.

4.1.6 Discussion of the results from the microstructural characterization

After quenching from austenitizing treatment, the investigated steel grade exhibits a fine martensitic microstructure with approx. 6.5 % retained austenite. Due to cryogenic treatment (CT) the retained austenite phase fraction is reduced to 3.5 %. As a result of tempering at 482°C, 540°C or 600°C reverted austenite is formed. The austenite phase fraction increases continuously with increasing tempering time for CT samples. However, for non-CT samples tempered at 482°C and 540°C a reduction of austenite phase fraction occurs within the first hour of tempering. As austenite phase fraction measurements do not give any information about the type and temperature region of austenite transformation, dilatometry measurements were carried out, as shown hereinafter in Section 4.2.2. It was found by TEM analyses that retained austenite is present on martensite lath boundaries in form of thin films with a thickness of approx. 3 nm to 40 nm. As a result of tempering, reverted austenite films are predominately precipitated along martensite lath boundaries and secondary hardening carbides are formed mainly within martensite laths. The austenitic films found in CT samples after tempering at 482°C for 50 h or after tempering at 600°C for 5 h have significantly grown in size to a thickness in the range of 20 nm-140 nm.

It was detected by APT and TEM investigations that a phase, termed as interaustenitic layer, is also present along martensite lath boundaries in the tempered samples at 482°C. This phase is enclosed by reverted austenite films and exhibits a concentration of substitutional elements, which is comparable to the overall composition of the steel (Table 4.3). Such a composition might also be found in an as-quenched martensite. It is assumed that also the retained austenite present after tempering at 482°C exhibits a similar composition except for its C content due to the less pronounced diffusion of substitutional elements at relatively low temperatures in austenite [36]. Since it was determined by TEM investigations that the interaustenitic layer and the retained austenite are both present on lath boundaries and may exhibit a similar composition, it is suggested that the interaustenitic layer is basically retained austenite. Starting from that, reverted austenite is supposed to grow by nucleating at retained austenite layers and thus, producing the phase arrangement of martensite, reverted and retained austenite observed by APT and TEM measurements. Also, the results from DICTRA investigations lead to the suggestion that reverted austenite is formed by nucleating at the martensite-retained austenite interface. Dmitrieva and Raabe et al. [29, 30] also found reverted austenite, which is formed on retained austenite. However, these authors investigated a maraging steel, which contains

Mn for austenite formation and low contents of other elements. Conversely, the present steel grade shows high Ni concentration for reverted austenite formation, high contents of Co as well as significant amounts of C and Cr, which may also contribute the phase evolution during tempering. This is also indicated by the APT and TEM analyses of the chemical evolution of martensite, reverted and retained austenite due to tempering. It was revealed that regardless of the tempering time at 482°C, the reverted austenite is enriched nearly to the same amounts of Ni and Cr and depleted to similar contents of Co. Also DICTRA calculations at 482°C confirmed that reverted austenite is enriched in Ni and Cr and depleted in Co and its elemental concentration does not change with tempering time. A comparable composition is also present in equilibrium austenite at 482°C (Table 4.5). The same was found for the reverted austenite in DICTRA calculations at 600°C. However, the austenite formed at higher temperatures is less enriched in Ni and depleted in Co as also the equilibrium austenite shows less elemental variation compared to the matrix. As described by Haidemenopoulos and Li et al. [18, 32] it is suggested that at higher temperatures the Ni enrichment required for reverted austenite formation is less due to a higher driving force for formation of the FCC phase at elevated temperatures. These findings lead to the suggestion that reverted austenite is precipitated at 482°C, when it is sufficiently stable to form due to its chemical composition. As Ni is a powerful austenite stabilizer, it is expected that high nickel contents in austenite are required for a sufficient stabilization of austenite at low temperatures, i.e. 482°C. Also the other elements in reverted austenite such as Cr, Mo and C, which are present in equilibrium austenite at 482°C, contribute to its stabilization. However, Co, which enhances the M_s, is not enriched in reverted austenite. Since it is described by Ustinovshikov et al. [5, 6] that Co and Fe form an intermetallic BCC FeCo phase, it is assumed that the accumulation of Co in martensite is a result of interactions of Fe and Co atoms in BCC lattice.

Schnitzer et al. [20] proposed for Ni alloyed maraging steels that the formation of reverted austenite is controlled by the diffusion of Ni, since the activation energy for austenite formation and the activation energy for the diffusion of substitutional elements are in the same range. This prediction is in good agreement with the results in this work, as the formation of reverted austenite is coupled with element redistribution and thus, diffusional processes must occur. Since the diffusion of substitutional elements in austenite at 482°C is to neglect compared to martensite, element diffusion for the formation of Ni-enriched reverted austenite is expected to occur mainly in martensite. This is in accordance with findings from DICTRA and APT investigations, as a zone of Ni and Cr depletion and a zone of Co enhancement occurs in martensite adjacent to the reverted austenite. Conse-

quently, the reverted austenite forms by detracting Ni from the surrounding martensite. Also the retained austenite films identified by ATP investigations do not show any zones of elemental redistribution, supporting the fact that diffusion of substitutional elements in austenite at 482°C is to neglect. Nevertheless, DICTRA calculations reveal that small zones of Ni enrichment and Co depletion might also occur in retained austenite adjacent to the phase boundary of reverted austenite. This indicates that the composition of the retained austenite would move towards equilibrium composition of austenite (Table 4.5) i.e. the composition of reverted austenite.
TEM investigations demonstrated that after tempering some retained austenite layers are austenitic but other layers might be martensitic. As a consequence of that, it is suggested that the retained austenite is austenitic during tempering and thus, no diffusion takes place. However, during cooling after tempering some retained austenite films may transform into martensite, resulting in a phase arrangement as shown in Fig. 4.8. This behavior of austenite will be further treated in Section 4.2.2.

As carbon is one of the most effective austenite stabilizers, it might be expected that carbon is also present in reverted and retained austenite for stabilizing. Since the evolution of carbon concentration in austenite was not within the scope of the preceding works about high Co-Ni steels [15, 25, 39, 40] it was analyzed in the present work by APT investigations. It was revealed that carbon is preferentially bound in carbides and reverted austenite has only slightly higher carbon contents than martensite. Conversely, the results of the kinetic calculations with DICTRA indicate that carbon would accumulate in retained and reverted austenite, if no formation of carbides takes place.
Furthermore, it was identified that secondary hardening carbides are located in martensite as well as in the reverted austenite but not in the retained austenite. Thus, it is suggested that during tempering, prior to the formation of reverted austenite, secondary hardening carbides are formed in martensite. Accordingly, APT investigations show that carbides are formed within 1 h at 482°C near reverted austenite layers. Due to the subsequent growth of reverted austenite, the interface between martensite and reverted austenite moves across the carbides, but the carbides are not dissolved by this process. As a result, secondary hardening carbides are also present in reverted austenite.

All in all the experimental results correlate extremely well with the findings from kinetic calculations. It is to mention that the reverted austenite, which is identified in the APT investigations by its Ni enrichment, and the Ni-enriched FCC zones (= reverted austenite) observed by with DICTRA calculations exhibit both a thickness of 5-10 nm due to tem-

pering at 482°C for 50 h. As a result, it is suggested that the microstructural evolution during tempering can be described well by using DICTRA calculations.

4.2 Influence of cryogenic treatment on the microstructural evolution during tempering

It was revealed in the previous section that cryogenic treatment (CT) causes a decrease of the retained austenite phase fraction but not a complete elimination of this phase. In literature [25], it is described that the reduction of retained austenite phase fraction in Aermet® 100 generates an enhancement of fracture toughness values. However, cryogenic treatment may also affect other microstructural properties, which influence the toughness properties. Thus, for the investigated steel grade the impact of cryogenic treatment on the evolution of microstructure during tempering was precisely analyzed.

4.2.1 Phase evolution and carbide precipitation during heating

The effect of tempering processes upon heating of CT and non-CT samples were characterized by dilatometer and DSC investigations. The combination of both methods allows to separate the overlapping precipitation processes during tempering as well as the determination of different tempering stages, since heat flow changes in combination with the length changes give a characteristic feature of each tempering process [103]. Additionally, hardness measurements and austenite phase fraction measurements were carried out. The results of dilatometer and DSC analyses are also partially treated in the Publication IV [104].

Tempering reactions during heating of steels have been studied in prior investigations [64, 88, 103, 105–111]. An overview of the impact of tempering stages on length change and heat flow is listed in the following:

- Stage I:
  The precipitation of transition carbides such as ε and η carbides occurs between temperatures of 100°C and 200°C. Transition carbide formation causes a reduction of volume and a production of heat (exothermic) [103, 105, 106].

- Stage II:
  The transition of retained austenite into ferrite and carbides (bainite) takes place in the temperature range between 200°C and 350°C. This reaction produces a volume increase and a large exothermic reaction [103, 105–108].

- Stage III:
  The transformation of transition carbides into cementite proceeds between temperatures of 250°C and 400°C. Cementite precipitation is marked with a strong reduction of volume and a weak exothermic reaction [103, 105, 106].

- Stage IV:
  The precipitation of alloy carbides in steels with W, Mo, V additions starts at about 450°C to 500°C. Due to this secondary hardening carbide precipitation the hardness values are increased. The reaction is accompanied with a production of heat and an increase of volume [64, 88, 105, 109–111].

Characterization by dilatometry

The results from dilatometry analyses are pictured in Fig. 4.22. The relative length change curves during heating of CT and non-CT conditions to 620°C (1st run) are plotted in Fig. 4.22 (a). These curves present significant differences, as CT conditions exhibit a more pronounced deviation from linear expansion during heating in the range between 200°C and 400°C. In Fig. 4.22 (b) the relative length change curves during the 2nd run are illustrated. During this rerun, no reaction between 200°C and 400°C is observable for both, CT and non-CT conditions. However, austenite formation, which is indicated by a reduction of length, starts for CT and for non-CT samples above temperatures of 620°C-650°C. The formation process comprises two peaks, which is typical for high Co-Ni and also for maraging steels [112, 113]. The split transformation is probably a result of an inhomogeneous nickel distribution. As described in [114], slow heating rates (20°C/ min) would also promote the separation into a diffusion controlled part and into a part of shear transformation.
The differences of the relative length change curves of CT and non-CT conditions above 200°C were further analyzed by studying the derivatives of the relatives length change curves of the 1st and 2nd run, as illustrated in Fig. 4.22 (c). Additionally, for a better comparability of the processes of both conditions, the curves of the 2nd run were subtracted from the curves of the 1st run, as shown Fig. 4.22 (d).
Heating for both conditions causes three main reactions, as indicated by the arrows in Fig. 4.22 (c) and (d):
The first effect generates a reduction of length, starts at 100°C and finishes at 220°C. This process is ascribed to the formation transition carbide precipitation, as temperature regime and reduction of length are typical for this precipitation reaction.

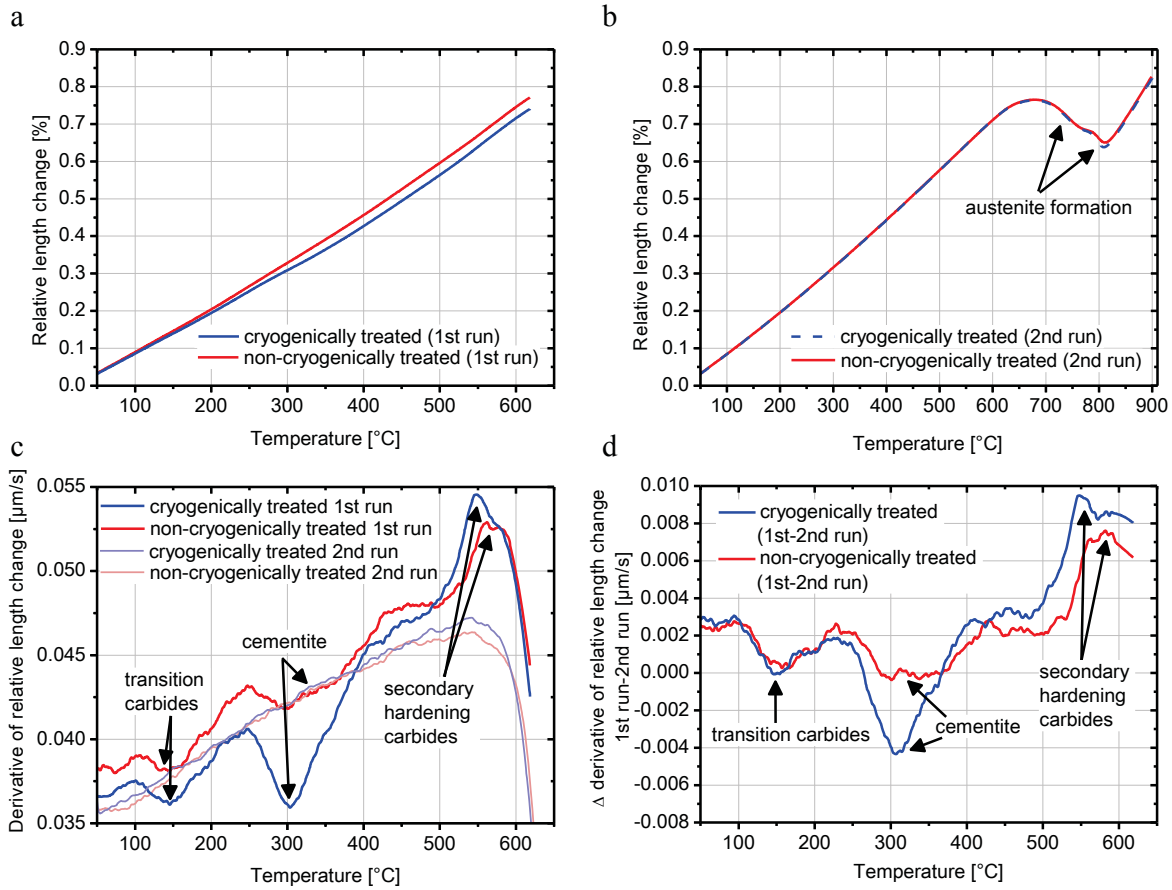

Figure 4.22: Dilatometer heating curves of CT and non-CT specimens. The heating rate was 20°C/ min. (a) Relative length change during the first heating (1st run) to 620°C. (b) Relative length change during the reheating (2nd run) to 900°C. (c) Derivatives of the length change curves of the first heating treatment (1st run) and of the rerun (2nd run). (d) The derivatives of length change curves of the 2nd run were subtracted from the ones of the 1st run [104].

The tempering process, which occurs in the temperature range between 250°C and 410°C, induces also a decrease of length. Hence, this process is attributed to cementite precipitation.

The third effect upon heating is observed beyond 450°C-500°C to the end of the investigated temperature regime. This effect causes an additional increase of relative length change of the dilatometer sample and is therefore attributed to alloy carbide precipitation, i. e. precipitation of secondary hardening carbides.

It was identified by analyzing the heating curves of CT and non-CT samples that the precipitation peak of cementite and secondary hardening carbides is sharper and thus much more intense in CT samples. Additionally, the cementite and secondary hardening carbide formation starts at somewhat lower temperatures for these conditions.

Characterization by differential scanning calorimetry

The tempering processes during heating of CT and non-CT conditions were also studied by means of DSC experiments. In Fig. 4.23 (a) the baseline corrected curves of the change of the heat capacity during the first heating (1st run) and during the rerun (2nd run) are depicted. Also by DSC experiments, it is observed that the two step austenite formation starts at about 620°C-650°C. The onset of austenite formation is characterized by the strong endothermic reaction [115]. Also, endothermic reactions due to reaching the Curie temperature [115] may overlap with the formation of austenite.
Nevertheless, the 1st run heating curves of CT and non-CT conditions exhibit distinct differences. For further studying these differences, the subtracted heating curves (2nd-1st run) were analyzed (Fig. 4.23 (b)). An exothermic reaction is observed in the temperature range between 250°C and 400°C, which can be ascribed to cementite precipitation. As cementite precipitation during DSC experiments does not produce as strong signals as dilatometer investigations [103], there are only slight difference between the signals of the CT and the non-CT samples. Another exothermic reaction is also observed starting at about 400-450°C. This reaction can be attributed to the precipitation of secondary hardening carbides [88]. Also by the DSC experiments differences between CT and non-CT samples in the regime of secondary hardening carbide precipitation are identified as shown in Fig. 4.23.

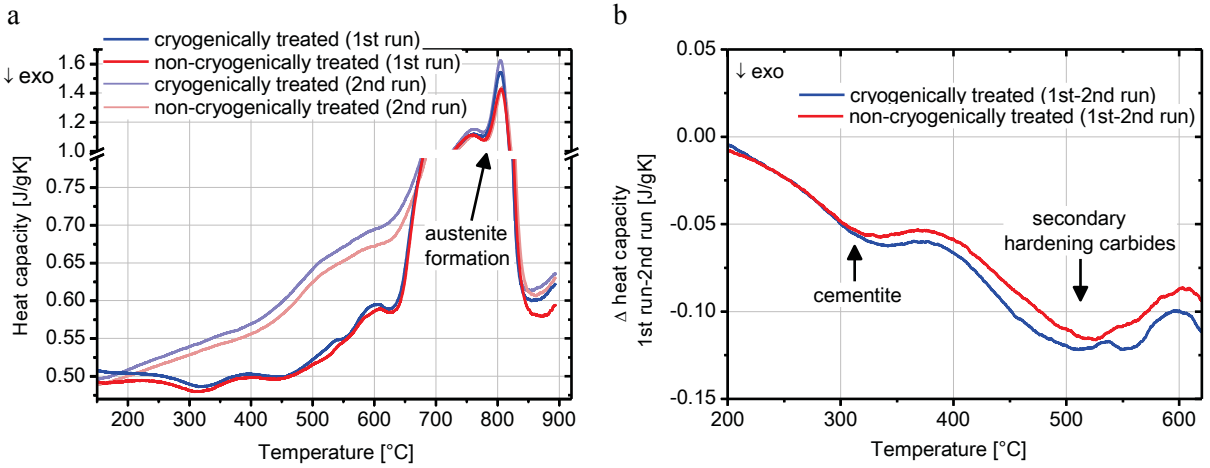

Figure 4.23: DSC heating curves of CT and non-CT samples. The heating rate was 20°C/ min. The exothermic behavior of the curves (1st run) is probably a result of tempering processes, e.g. relaxation and recovery processes of the martensite [116]. (a) Baseline corrected curves of the change of heat capacity during the first heating treatment (1st run) and during the the rerun (2nd run). The samples for the 2nd run were previously heated to 620°C. (b) Difference of heat capacity changes between the 1st and the 2nd run.

Characterization of austenite phase fraction and hardness evolution

The evolution of austenite phase fraction due to heating of CT and non-CT samples with 20°C/ min in the dilatometer to 200, 400, 500 or 580°C and followed cooling (without holding) with 100°C/ min to room temperature was characterized by XRD measurements. The findings are presented in Fig. 4.24 (a). The austenite phase fraction of the CT samples is approx. 3.5 % and remains more or less constant due to heating to various temperatures. Hence, it is suggested that due to heating no austenite transition into ferrite and carbides and no formation of reverted austenite occurs. Furthermore, it can be excluded that austenite transforms into martensite upon cooling in CT samples.
Conversely, the austenite phase fraction of the non-CT samples decreases from approx. 6.5 % as a result of annealing beyond 400°C to about 4.5 %. By analyzing the dilatometer cooling curves of non-CT samples (Fig. 4.25 (b)), it was determined that the samples, which were heated to 500°C or 580°C exhibit a slight increase of length during cooling compared to the samples, which were heated to 400°C. This increase of length below 120°C can be attributed to a martensitic transformation, as the transformation of austenite into a body-centered phase, e.g. martensite is accompanied with a raise of volume. Thus, the reduction of austenite phase fraction in non-CT conditions occurs during cooling after heating.

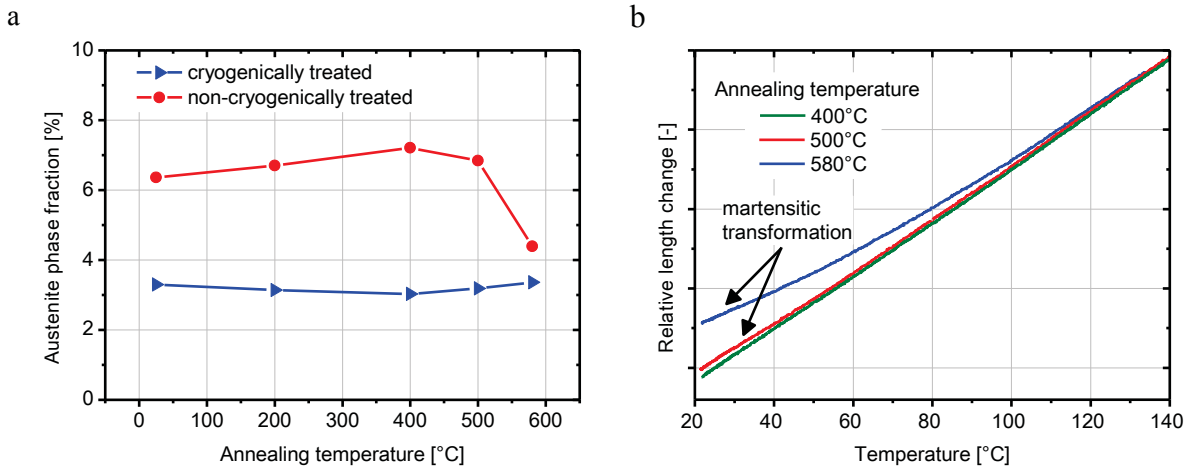

Figure 4.24: (a) Austenite phase fraction measurements before and after heating CT and non-CT samples to 200, 400, 500 or 580°C and immediately cooling down to room temperature. The heating rate was 20°C/ min and the cooling rate was 100°C/ min. (b) Relative length change during cooling after heating the non-CT samples to 400, 500 or 580°C. For a better comparability, the curves were shifted in y-direction. Therefore, the y-axis is not scaled [104].

Since neither dilatometer nor DSC heating curves indicate an austenite transition during heating, it is concluded that also for non-CT conditions no austenite decomposition into ferrite and carbides occurs during heating. Thus, the reduction of austenite phase fraction can be completely attributed to the austenite to martensite transformation during cooling.

For further characterization of the differences of microstructural evolution due to cryogenic treatment, the evolution of hardness was analyzed. The results of hardness measurements after heating CT and non-CT samples to various temperatures and cooling to room temperature are shown in Fig. 4.25. The CT samples show higher hardness values compared to the non-CT samples up to annealing temperatures of 500°C. Since non-CT samples exhibit a higher austenite phase fraction in this temperature region, the lower hardness values of non-CT conditions are predominately attributed to the higher austenite content. After heating to temperatures beyond 500°C, the hardness values of non-CT and CT samples are in the same range, since the austenite of non-CT samples has partially transformed into martensite upon cooling. In the region of cementite precipitation between 200°C and 400°C, a decrease of hardness, which is as strong for CT as for non-CT samples occurs. Furthermore, a massive increase of hardness proceeds for both conditions above temperatures of 480°C, which is a result of secondary hardening carbide formation. Secondary hardening carbide formation in this temperature region was also identified by dilatometer and DSC analyses. However, for non-CT specimens the raise of hardness due to secondary hardening carbide formation overlaps with the hardness increase due to austenite transformation upon cooling. Thus, no comparison between CT and non CT-conditions regarding the hardness increase as a result of secondary hardening carbide formation can be conducted.

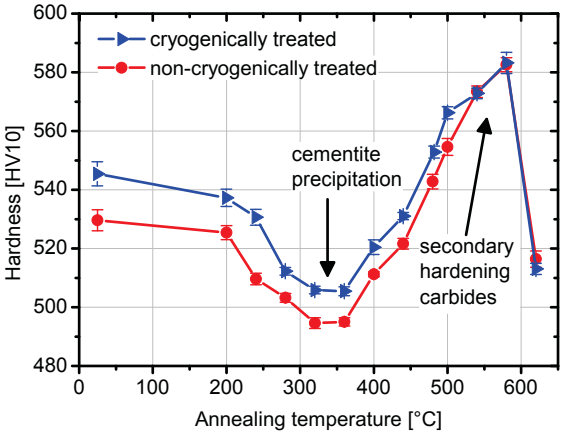

Figure 4.25: Hardness response due to heating of CT and non-CT samples to various temperatures (heating rate: 20°C/ min) and followed by immediate quenching to room temperature (100°C/ min) [104].

4.2.2 Transformation of austenite during cooling from tempering

Generally, the transformation behavior of retained and reverted austenite has a strong effect on the toughness properties of steels [9, 15, 16].
The austenite phase fraction measurements in Section 4.1.1 revealed that a reduction of austenite content occurs due to tempering of non-CT samples. A transformation of austenite by these phase fraction measurements is solely detectable when the austenite reduction is not overbalanced by a reverted austenite formation. Furthermore, it was determined in Section 4.2.1 that the austenite stays stable during heating of CT and non-CT samples beyond temperatures of 500°C but transforms during cooling to martensite. Thus, the section hereinafter concentrates on the austenite transformation and microstructure evolution processes during the holding and cooling segment of the tempering treatment. Parts of these dilatometry analyses are also subject of the Publications II and III [36, 117].

Tempering at 482°C

Dilatometry investigations were carried out for various tempering treatments at 482°C. The relative length change curves of CT and non-CT samples during tempering for 1 and 5 h and subsequent cooling to -100°C are presented in Fig. 4.26 (a). During holding at 482°C up to approximately 1 h a distinct increase of length can be observed for CT and non-CT samples. This increase is probably caused by secondary hardening carbide precipitation, which was also determined to occur during heating above 482°C by dilatometer heating curves (Fig. 4.22). Again this precipitation reaction is more pronounced for CT than for the non-CT conditions.
For holding times beyond 1 h, the length of the samples remains constant although the reverted austenite formation during tempering would cause a reduction of length. Hence, it is expected that the formation of reverted austenite at 482°C is too weak for a detectable impact on length or is counterbalanced by the formation of carbides.
After tempering at 482°C the samples were cooled to −100°C. The relative length change during this cooling treatment is illustrated as a function of temperature in Fig. 4.26 (b). It is identified that the non-CT samples exhibit a phase transformation upon cooling, which is accompanied with an increase of length. Therefore, it is attributed to a transformation of austenite into martensite. The M_s-temperature of the transformation in the non-CT samples is approx. 140°C. However, no significant martensitic transformation can be detected for the CT samples by dilatometer measurements. Nevertheless, there is a slight deviation from the linearity of the cooling curves in the region between 30°C to

140°C, indicating that there might also be a rather small martensitic transformation in CT samples. It is to note that the small kink at about 30°C is the result of gas floating for cryogenic treatment.

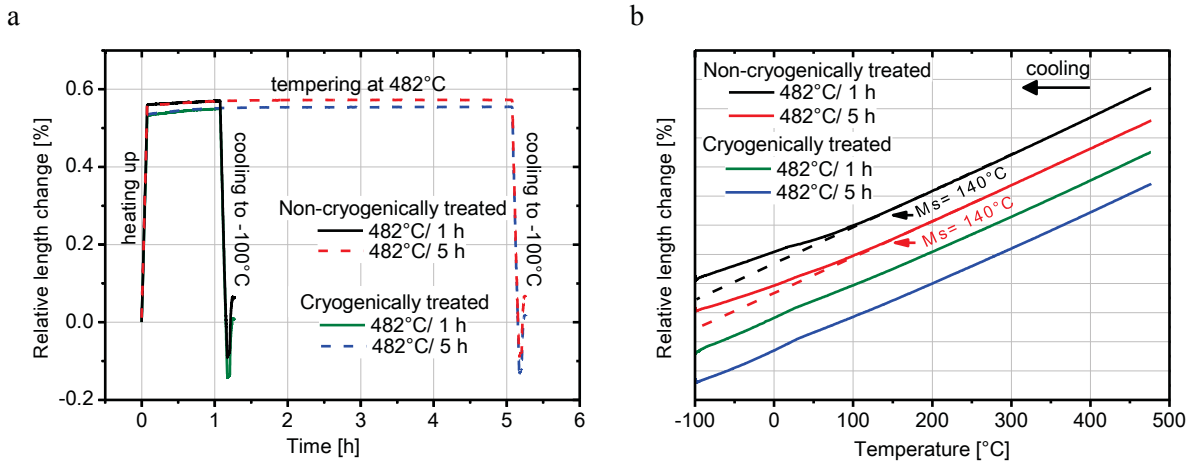

Figure 4.26: (a) Relative length change as a function of time of CT and non-CT samples during tempering at 482°C for 1 or 5 h. After tempering, the samples were cooled to −100°C and then reheated to room temperature. The heating and cooling rate was 100°C/ min. (b) Relative length change during cooling from tempering at 482°C for 1 or 5 h as a function of temperature. The non-CT samples exhibit a martensitic transformation during cooling starting at approximately 140°C. For a better visibility, the curves were shifted vertically to each other.

Also dilatometer investigations were carried out for the two-step tempering treatment at 482°C for 1+4 h. Fig. 4.27 (a) depicts the relative length change curves of CT and non-CT samples during tempering. During the first holding sequence at 482°C, again an increase of length occurs, which may be attributed to secondary hardening carbide formation.
Upon the first cooling segment a transformation of austenite proceeds for non-CT but not for CT samples, as shown in Fig. 4.27 (b). This leads to an increased length of the non-CT samples during the second tempering step compared to the CT samples. During holding at 482°C for 4 h the length of CT and non-CT samples remains constant, as already discussed earlier (Fig 4.26 (b)). However, during the second cooling segment no distinct phase transformation occurs for both, CT and non-CT conditions.

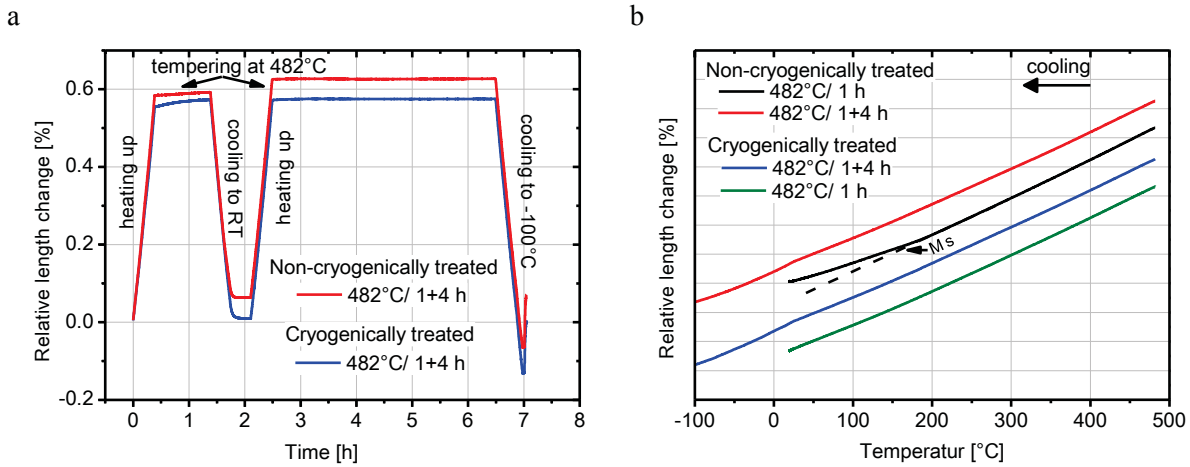

Figure 4.27: (a) Relative length change as a function of time of CT and non-CT samples during tempering at 482°C for 1 h, cooling to room temperature, heating again to 482°C and holding for 4 h. After tempering, the samples were cooled to −100°C and then reheated. The heating and cooling rate was 20°C/ min. (b) Relative length change during cooling from tempering at 482°C for 1 h and for 1+4 h as a function of temperature. During the first cooling sequence, the non-CT condition exhibits a martensitic transformation, whereas during the second cooling segment no significant transformation is observable for both conditions. For a better visibility, the curves were shifted vertically to each other.

Tempering at 540°C

Dilatometer investigations were also carried out for analyzing the tempering treatment at 540°C for 1 and 5 h. Fig. 4.28 (a) presents the relative length change curves of the CT and non-CT samples as a function of time. Within the first minutes of tempering at 540°C, again the length of the dilatometer samples increases probably due to carbide precipitation reactions. Holding times beyond 1 h cause a markedly decrease of length. This decrease is ascribed to the more enhanced formation of reverted austenite during tempering at 540°C (approx. 11 % after 5 h).

The cooling curves of CT and non-CT samples tempered at 540°C are plotted as a function of temperature in Fig. 4.28 (b). It was identified by the increase of volume upon cooling that in all conditions a martensitic transformation takes place. This transformation starts at lower temperatures for longer holding times. Accordingly, the transformation initiates at 210°C for the non-CT samples after tempering for 1 h and at 170°C after tempering for 5 h. Furthermore, the martensitic transformation proceeds at even lower temperatures for CT samples, since it starts at 166°C after tempering for 1 h and at 130°C after tempering for 5 h. Additionally, the martensitic transformations of these cooling curves are less intense for longer holding times and cryogenically treated samples.

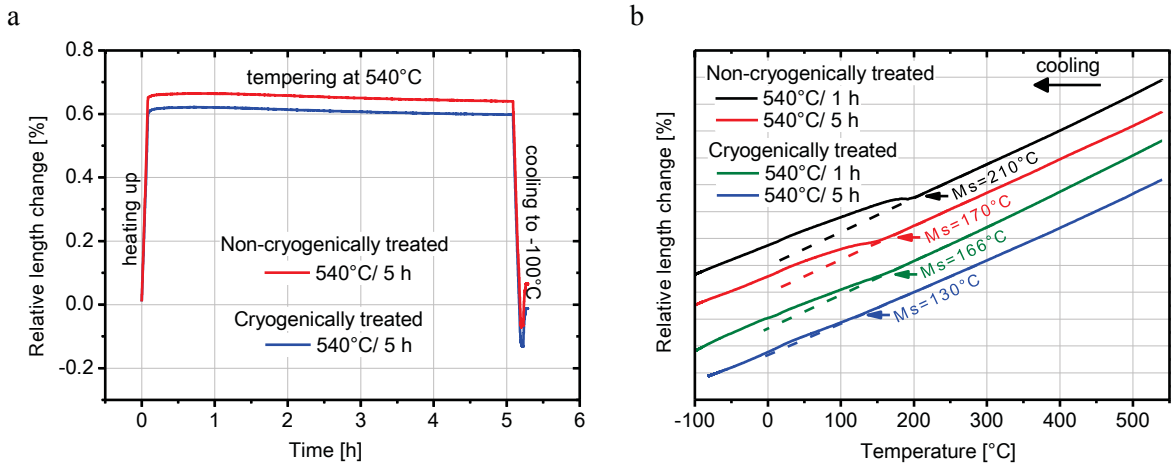

Figure 4.28: (a) Relative length change as a function of time of CT and non-CT samples during tempering at 540°C for 5 h. After tempering, the samples were cooled to -100°C and then reheated to room temperature. The heating and cooling rate was 100°C/ min. (b) Relative length change during cooling from tempering at 540°C for 1 and 5 h as a function of temperature. The samples exhibit martensitic transformations, which start at lower temperatures and are less pronounced for longer holding times and for cryogenically treated samples. For a better visibility, the curves were shifted vertically to each other [36, 117]

Tempering at 600°C

The results from dilatometer investigations of tempering CT and non-CT samples at 600°C for 1 h and for 5 h are depicted in Fig. 4.29. The strong reduction of length during holding at 600°C for 5 h is attributed to the formation of reverted austenite, as by this heat treatment approx. 22 % are formed.

The cooling curves of CT and non-CT samples tempered at 600°C are plotted as a function of temperature in Fig. 4.29 (b). These cooling curves also present martensitic transformations. It was again determined that the M_s-temperatures are lower with increasing tempering times. Hence, the transformation of non-CT samples starts at 150°C and 110°C due to holding for 1 h and for 5 h, respectively. Due to the application of a cryogenic treatment before tempering, the M_s-temperature of the sample tempered for 1 h decreases to 130°C. However, holding times for 5 h lead to a M_s-temperature of 115°C for the CT sample, which is similar to the one of the non-CT sample. Also for these heat treatment conditions, it was identified that the intensity of transformation is weaker for CT samples and for longer holding times.

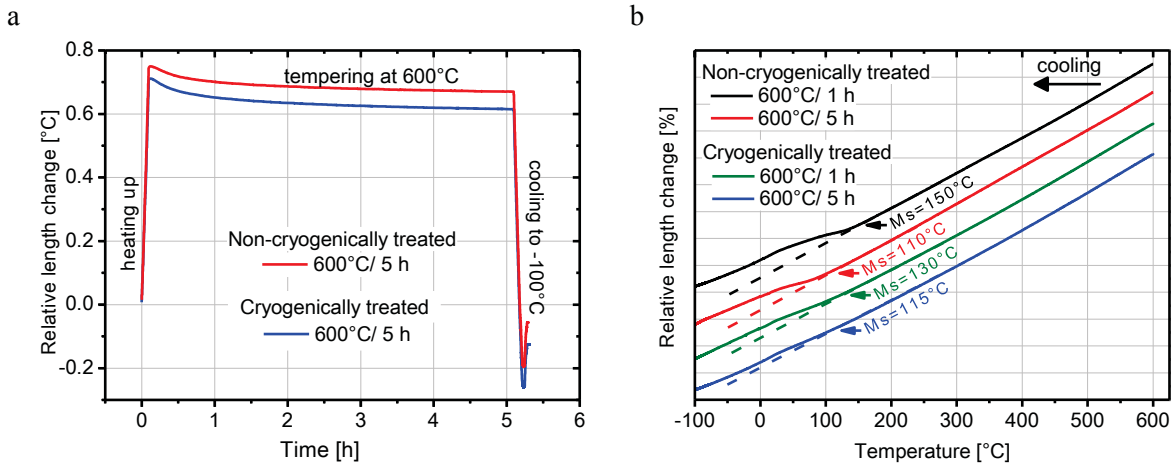

Figure 4.29: (a) Relative length change as a function of time of CT and non-CT samples during tempering at 600°C for 5 h. After tempering the samples were cooled to −100°C and then reheated to room temperature. The heating and cooling rate was 100°C/ min. (b) Relative length change during cooling from tempering at 600°C for 1 or 5 h as a function of temperature. The samples exhibit martensitic transformations, which start at lower temperatures and are less pronounced for longer holding times and for cryogenically treated samples. For a better visibility, the curves were shifted vertically to each other [36, 117].

Effect of tempering temperature

In Fig. 4.30 the derivatives of the length change curves during cooling of non-CT samples after tempering at 482°C, 540°C and 600°C for 5 h are illustrated. The martensitic transformations, which are indicated by the increase of the derivative of length change, are less intense and start at lower temperatures when tempering temperature increases from 540°C to 600°C. In contrast, when tempering is conducted at 482°C the intensity and the temperature of transformation is lower compared to tempering at 540°C, indicating that there might be different processes contributing to the temperature and intensity of austenite transformation during cooling.

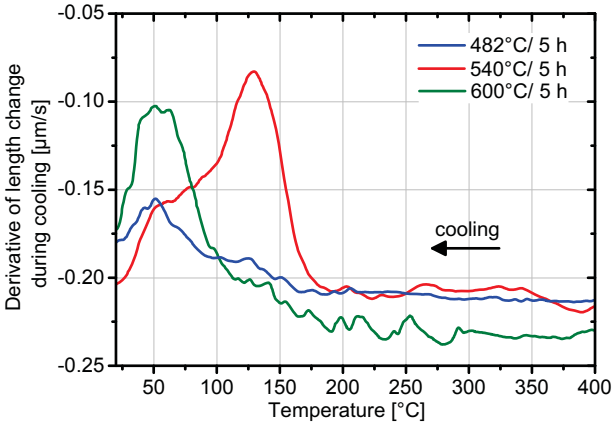

Figure 4.30: Derivatives of length changes as a function of temperature of non-CT samples during cooling after tempering at 482°C, 540°C and 600°C for 5 h. The heating and cooling rates were 100°C/ min.

4.2.3 Evolution of lattice parameters during tempering

The influence of cryogenic and tempering treatment was also characterized by XRD measurements of martensite and austenite lattice constants and lattice distortions. In general, lattice parameters are susceptible to chemical composition, temperature and hydrostatic (uniform) stress conditions [118]. As the measurements in this work were conducted at room temperature, the changes of lattice parameters upon tempering are mainly ascribed to chemical variations. Dislocations (lattice defects), non-uniform stresses and small crystallite sizes cause line broadening. Line broadening can be separated in broadening due to small crystallite sizes (size broadening) and in broadening due to lattice defects and stresses (strain broadening) [119].
Parts of this section are also treated in the Publication I [120].

Martensite lattice constant

In Fig. 4.31 the results from lattice constant measurements of martensite are depicted. As the carbon content of the material is relatively low, a separation of the lattice parameters a and c could not be conducted by XRD measurements [121].
The martensite lattice parameter decreases strongly within the first minutes of tempering at 540°C and 600°C and stays more or less constant when tempering is continued. Conversely, tempering at 482°C causes a decrease of lattice constant within the first 10 min and a subsequent increase up to approx. 1 h. Nonetheless, the lattice parameters decreases again for longer tempering times at 482°C.
For the conditions tempered at 540°C and 600° no distinct differences are detectable between CT and non-CT samples. In contrast, the reduction of the lattice parameter of CT samples tempered at 482°C occurs at shorter times and is more pronounced than the one for non-CT conditions.

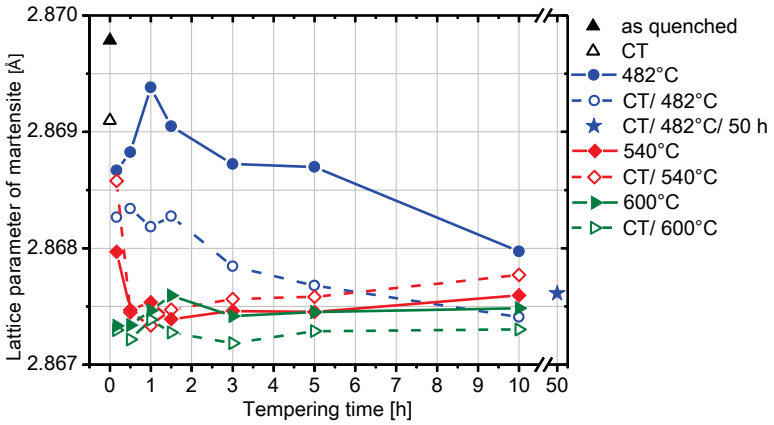

Figure 4.31: Measurement of the martensite lattice parameter changes due to tempering of CT and non-CT samples at 482°C, 540°C and 600°C for various times up to 50 h. The measurements were carried out at room temperature after tempering [120].

It is suggested that the decrease of lattice parameters can be ascribed to the depletion of alloying elements in martensite due to formation of carbides during tempering, since carbide forming elements, such as carbon, molybdenum, chromium would cause an increase of martensite lattice constant. Also a decrease of nickel content would lower the lattice parameter of martensite [39, 47–49, 51]. Conversely, it is assumed that the increase of lattice parameter because of tempering at 482°C for approx. 1 h is originated by secondary hardening carbide precipitation and the related effects, including the austenite transformation to martensite during cooling.

Austenite lattice constant

Also the influence of heat treatment on the evolution of austenite lattice constant (a) was analyzed as shown in Fig. 4.32. It is detected that the lattice parameter of austenite increases due to tempering for sufficient long tempering times and remains constant for even longer holding times. The increase proceeds within 10 min for tempering at 600°C and within 3 h for tempering at 540°C. However, due to tempering at 482°C the raise of lattice parameter takes up to 50 h. Additionally, it is identified that the lattice parameter increases due to tempering at 482°C within the first 10 min but decreases after approximately 1 h of tempering before it increases again. However, the reduction of lattice parameter after 1 h of tempering at 482°C occurs at somewhat shorter tempering times for the CT than for the non-CT samples.

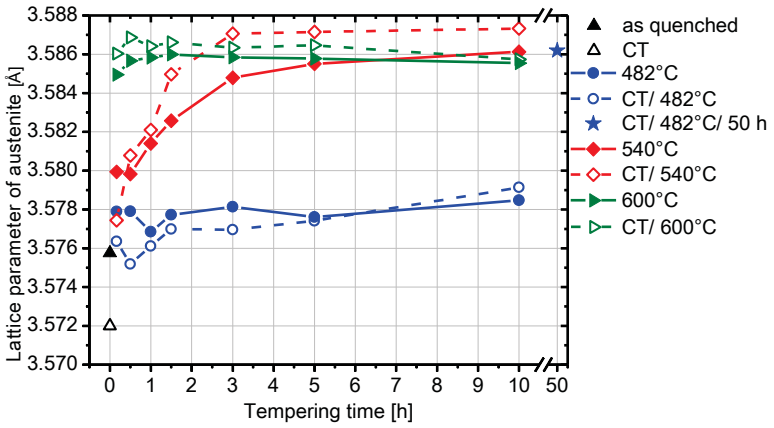

Figure 4.32: Measurement of austenite lattice parameter changes due to tempering of CT and non-CT samples at 482°C, 540°C and 600°C for various times up to 50 h. The measurements were carried out at room temperature after tempering [120].

Generally, reverted austenite in high Co-Ni is enriched in nickel and depleted in cobalt [25]. This is also demonstrated by APT measurements in Section 4.1.3. As the increase of Ni and the reduction of Co content in austenite would enhance the austenite lattice parameter [47, 50], the increase of the austenite lattice constant is assigned to the enrichment of Ni and the depletion of Co.

As carbon diffusion at these temperatures is much more enhanced than diffusion of substitutional elements, the decrease of austenite lattice constant due to tempering at 482°C for 1 h is probably caused by the reduction of carbon content [51, 52] due to secondary hardening carbide formation.

Martensite lattice distortion

The evolution of martensite lattice distortion during tempering is plotted in Fig. 4.33 The plot shows that tempering causes a reduction of this distortion, which is probably related to recovery processes, e.g. the decrease of the dislocation density. The reduction of martensite distortion is higher for longer tempering times and for higher tempering temperatures.

It was also determined that the CT samples exhibit a higher reduction of martensite lattice distortion than non-CT samples, suggesting that there are slight differences in microstructure evolution during tempering because of cryogenic treatment.

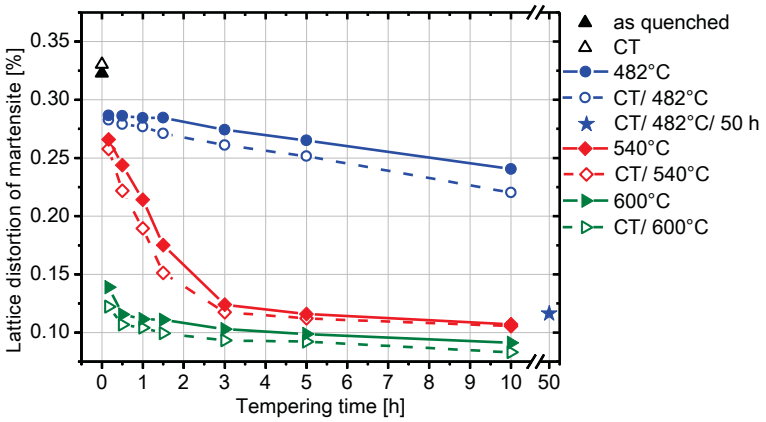

Figure 4.33: Measurement of martensite lattice distortion changes due to tempering of CT and non-CT samples at 482°C, 540°C and 600°C for various times up to 50 h. The measurements were carried out at room temperature after tempering.

4.2.4 Discussion and kinetic interpretation of the influence of heat and cryogenic treatment on the microstructural evolution

Influence of retained austenite on carbide precipitation processes

During heating of CT and non-CT samples the carbide precipitation processes were analyzed by means of dilatometer and DSC measurements. Significant differences during heating of CT and non-CT samples are observed in the regime of cementite and secondary hardening carbide precipitation (Fig. 4.22), as these processes are more enhanced and start at slightly lower temperatures for CT samples.
However, the decrease of hardness in the temperature regime of cementite precipitation is similar for CT and non-CT samples (Fig. 4.25). Basically, the hardness decrease in the region of cementite precipitation is a result of carbon rejection from martensite. In the as quenched condition of martensite, the carbon atoms are located in the octahedral interstitial sites and causing by that a tetragonal distortion of the lattice by lengthening the c axis and shortening the a axis of the unit cell [121]. Due to tempering the carbon atoms are rejected from martensite and form cementite. Consequently, the tetragonality of martensite is reduced, since the carbon atoms leave these octahedral sites. The reduction of tetragonality, causes a decrease of the lattice distortion, which in turn reduces the hardness. Cementite precipitations contribute to the hardness of the material. Since the hardness increase due to cementite precipitation is overbalanced by the much more pronounced hardness decrease because of the reduction of carbon dissolved in martensite, the hardness decreases in this temperature regime.
Thus, as the hardness decrease for both conditions in the temperature range of cementite precipitation is comparable, also the carbon reduction in martensite should be in the same range. It is estimated that carbon reduction in martensite is also caused by the diffusion of carbon atoms into retained austenite because of the higher carbon solubility of austenite than martensite. The non-CT samples contain about twice the retained austenite content compared to the CT samples, therefore, also the amount of carbon, which can solute in austenite is two times as much. Experimental results and calculations on other steel grades indicate that the austenite may enriched in carbon by 1.5 wt.% to 2.5 wt.% between temperatures of 240°C to 400°C [60, 61]. Hence, by assuming a maximum carbon enrichment in austenite of approx. 2 wt.% , in the non-CT samples 0.12 wt.% of carbon can dissolve in retained austenite while in the CT samples only 0.06 wt.% can dissolve. Based on that, in non-CT samples less carbon participate on cementite formation, causing a less pronounced cementite precipitation peak, as shown in Fig. 4.22.

Furthermore, the formation secondary hardening carbides in both conditions might also be influenced by cryogenic treatment and as a result of that by the preceding cementite precipitation reaction. Hence, the formation peak of secondary hardening carbides (observed by dilatometer analyses) is sharper, thus more intense and starts at somewhat lower temperatures for CT samples. The results from austenite lattice constant measurements (Fig. 4.32) also show an earlier decrease of lattice parameter in CT samples tempered at 482°C compared to the non-CT ones. This decrease is suggested to be caused by the reduction of carbon in the austenitic regions. Thus, these results also indicate that the formation of secondary hardening carbides might proceed at shorter tempering times in CT samples.

Transformation behavior of retained austenite in martensite upon cooling

The transformation behavior of retained austenite to martensite was analyzed for CT and non-CT samples, which were heated (20°C/ min) in the dilatometer to various temperatures up to 580°C and subsequently (without holding) cooled (100°C/ min) to room temperature (Fig. 4.24). Due to these heating experiments no distinct formation of reverted austenite occurs for both conditions. However, it was identified by dilatometry that the retained austenite transforms to martensite in non-CT samples during cooling after heating beyond 400°C. It is suggested that this transformation is influenced by the formation of secondary hardening carbides, which was also determined to occur in this temperature range by APT measurements (Fig. 4.11). Generally, the formation of secondary hardening carbides causes a depletion of elements in austenite, such as carbon and carbide forming elements, and thus, also a destabilization of austenite [34]. As a result, the austenite in non-CT samples transforms during cooling.
Since it was determined that the austenite in CT samples is stable during cooling, the transformation behavior has to be influenced by the preceding cryogenic treatment. Waitz et al. [58] described that smaller austenite particles exhibit a higher resistance against transformation, i.e. a higher stability. It was revealed that cryogenic treatment causes a reduction of austenite phase fraction, as determined by the austenite phase fraction measurements shown in Fig. 4.1. Since the thickness of retained austenite films varies as indicated by microstructural investigations in Fig. 4.4 and 4.5, it is assumed that preferentially the larger, less stable austenitic region transform to martensite during the cryogenic treatment. Thus, it is assumed that a decrease of the mean size of retained austenite films occurs, which results in a stabilization of retained austenite. However, a reduction of austenite particle size could not be evaluated by TEM investigations.

Accordingly, no transformation occurs in CT and non-CT samples, if they are heated up to 400°C followed by the cooling to room temperature, since no formation of secondary hardening carbides occurs. Conversely, due to heating of non-CT samples beyond 400°C a carbon reduction in austenite proceeds due to carbide precipitation and the less stable retained austenite films transform to martensite upon subsequent cooling. However, for the CT samples, the less stable austenitic regions have already transformed partially during the cryogenic treatment. Thus, no phase transformation takes place for these conditions during cooling after tempering.

Stabilizing of austenite against martensitic transformation due to tempering

The transformation behavior of austenite during cooling after tempering was also analyzed for CT and non-CT conditions, which were tempered at 482°C, 540°C and 600°C for 1 h, 5 h or 1+4 h (Section 4.2.2). The heating and cooling rates were 100°C/ min. Due to these tempering treatments reverted austenite is formed, which stands in contrast to the annealing treatments up to 580°C without holding (Section 4.2.1), where no reverted austenite formation occurs.
It was determined for the tempering treatments at 482°C, 540°C and 600°C for 1 h, 5 h and 1+4 h that the transformation of austenite is more pronounced and occurs at higher temperatures for non-CT compared to CT conditions. A higher transformation temperature as well as a higher amount of transformation can be ascribed to a lower resistance against transformation, i.e. a lower stability of austenite [46]. As a result, the differences between CT and non-CT samples were again ascribed to the stabilizing effect of cryogenic treatment on the retained austenite.
The two-step tempering process at 482°C for 1+4 h (Fig. 4.27) leads to an austenite transformation to martensite in non-CT samples during the first cooling but not during the second cooling sequence. Based on that, it is suggested that also a two-step tempering process induces similar austenite stabilization effects than cryogenic treatment. Additionally, by this two-step treatment no fresh, untempered martensite is present in CT and non-CT conditions and also the austenite content is in the same range for both conditions. Hence, it is assumed that by the two-step treatment the CT and non-CT conditions exhibit not only a comparable stability of austenite but also more or less comparable properties of martensite. However, the carbide precipitation behavior is suggested to be different in CT and non-CT samples tempered with two-steps.

The influence of tempering time and temperature on the austenite stability was also analyzed by characterizing the dilatometer cooling curves (Section 4.2.2). It was revealed

that the martensitic transformations start at lower temperatures and are less intense when tempering is conducted for longer times and at 600°C instead of 540°C (Fig. 4.28-4.30). However, the transformation temperature and the amount of transformation is lower after tempering at 482°C compared to the samples tempered at 540°C. Based on these findings, it is assumed that different phenomena contribute to the transformation behavior of austenite. A possible explanation for these phenomena is based on the results in Section 4.1 and is given in the following:
As nickel is the element, which might predominately affect the stability of austenite, it is necessary to enrich the present austenite with nickel. This is the fact for reverted austenite, as it was determined by APT experiments that the composition of reverted austenite after tempering at 482°C shows a clear nickel enrichment (Fig. 4.16). Furthermore, it was revealed that this reverted austenite exhibits nearly the same composition than the FCC phase in equilibrium (Table 4.5). As a result, it is estimated that also the reverted austenite formed at 540°C and 600°C exhibits its equilibrium composition. However, at the beginning of tempering the retained austenite may posses a composition, which is similar to an as-quenched martensite except for the C content. DICTRA investigations in Fig. 4.20 and 4.21 indicate that the composition of retained austenite would also move towards equilibrium composition, if the diffusion lengths of substitutional elements are sufficient, e.g. at higher tempering temperatures or longer times.
The equilibrium concentration of substitutional elements in austenite at 540°C and 600°C was calculated and is listed in Table 4.8.

	Ni	**Co**	**Cr**	**Mo**	**Fe**
	wt.%	**wt.%**	**wt.%**	**wt.%**	**wt.%**
540°C	34.0	5.2	1.5	0.6	Bal.
600°C	26.8	7.2	1.6	0.8	Bal.

Table 4.8: Equilibrium concentration of substitutional elements in austenite at 540°C and 600°C. For the calculations with Thermo-Calc (TCFE7) the the actual composition of the investigated material was used.

As the equilibrium Ni concentration in austenite is clearly higher at 540°C, the austenite should also exhibit a higher stability after tempering at 540°C than after tempering at 600°C. Since this does not correlate with the experimental results, it is suggested that the stabilizing process of retained austenite might be predominately controlled by transport of nickel atoms into austenite, i.e. by diffusional processes. The diffusion of Ni for retained austenite stabilization must proceed in the FCC phase. Hence, the mean diffusion path

x of nickel in austenite at 540°C and 600°C was calculated with Eq. 8 [122, 123]. The diffusion constant D is obtained from MatCalc calculations and the time for diffusion is termed as t.

$$x = \sqrt{4Dt} \tag{8}$$

The values of the mean diffusion path of nickel in austenite were correlated with the M_s-temperatures. The results are shown in Table 4.9.
As the diffusion of Ni in austenite gets more enhanced due to higher tempering temperatures or longer times, the M_s-temperature decreases. Thus, stability of austenite increases. The mean thickness of a half retained austenite film, which is about 10 nm, is in the range of the mean diffusion path of Ni in austenite. Due to that, it is reasonable to assume that the variation of M_s-temperatures occurs due to diffusion controlled stabilization with nickel. However, the Ni enrichment in austenite due to tempering at 540°C or 600°C might not be sufficient for stabilizing the reverted austenite completely. Hence, small amounts of austenite may transform upon cooling after tempering at elevated temperatures, as shown in Fig. 4.28 and 4.29.

		540°C/ 1 h	**540°C/ 5 h**	**600°C/ 1 h**	**600°C/ 5 h**
Diffusion path	nm	1.0	2.2	3.2	7.0
M_s of CT samples	°C	166	130	130	115
M_s of non-CT samples	°C	210	170	150	110

Table 4.9: The mean diffusion paths of nickel in austenite correlated with the M_s-temperatures obtained from the tempering treatments at 540°C and 600°C for 1 and 5 h. Higher diffusion lengths of Ni in austenite lead to lower M_s-temperatures, indicating a stabilizing effect due to nickel diffusion.

The variation of M_s-temperature of CT samples due to the applied heat treatments is weaker than the one of non-CT samples, as indicated in Table 4.9. It is suggested that this is caused by the smaller mean size of the austenite films in CT conditions, which results in a higher stability of austenite. Thus, stabilizing effects on austenite, such as the nickel enrichment, may have lower impacts in CT samples as the austenite in this condition is also stabilized by its size. Furthermore, it was found for the CT sample tempered at 600°C for 5 h that the M_s-temperature is higher compared to the non-CT sample of the same tempering conditions. This is expected to be a result of the measuring inaccuracy.

Conversely, the diffusion properties of austenite at 482°C are not sufficient for any stabilization of retained austenite up to 5 h, as the mean diffusion length of Ni is <1 nm during holding at tempering temperature. This was also determined by DICTRA calculations (Fig. 4.20). Therefore, it is assumed that the transformation behavior of austenite after tempering at 482°C does not fit into the tendency observed by tempering at 540°C or 600°C.

Measurements of the austenite lattice parameter (Fig. 4.32) also suggest that the enrichment of austenite with nickel occurs diffusion controlled, as the lattice parameter increases faster with increasing tempering temperature. It is to note that it is not possible by the results of austenite lattice parameter measurements to distinguish between retained and reverted austenite. Therefore, it is estimated that the increase of austenite lattice parameter is both; caused by nickel enrichment in retained austenite and a result of the formation of (Ni-enriched) reverted austenite.

To sum up, the application of a cryogenic treatment before tempering does not only influence the transformation behavior and the stability of austenite but also the precipitation processes of carbides. As it is indicated by the martensite lattice parameter and lattice distortion measurements (Section 4.2.3), there might also be slight differences in martensite in samples tempered at 482°C, 540°C and 600°C for 5 h due to cryogenic treatment .

4.3 Characterization of the mechanical properties at different heat treatment conditions

High Co-Ni steels exhibit excellent toughness properties combined with high hardness and strength values. It is reported in literature [15, 39, 40] that the toughness properties of these steels are heavily influenced by the stability of the austenite. In the Section 4.2.2 the transformation behavior of austenite to martensite after tempering was characterized by dilatometer measurements for the investigated high Co-Ni steel. It was demonstrated that the cryogenically treated (CT) samples, which were tempered at 482°C, 540°C or 600°C for 1 or 5 h, exhibit no or only a slight austenite transformation upon cooling after tempering, whereas for non-CT samples a much more pronounced austenite transformation to martensite takes place. In contrast to that, an austenite transformation does not occur during the second cooling step of both, CT and non-CT, samples tempered at 482°C for 1+4 h. Thus, no untempered martensite is present in the CT as well as in the non-CT samples tempered at 482°C for 1+4 h, which leads to more or less comparable properties of austenite and martensite for both of these conditions. Consequently, for analyzing the impact of these tempering and cryogenic treatments on mechanical properties, tensile tests and fracture toughness measurements were carried out.

4.3.1 Strength and ductility properties

The results from tensile tests of CT and non-CT samples tempered at 482°C, 540°C and 600°C for 5 h and at 482°C for 1+4 h are summarized in Table 4.10. Higher tempering temperatures lead to a reduction of the yield ($R_{p0.2}$) and the tensile strength (R_m) as well as to an increase of the fracture strain (A), the uniform elongation (A_g) and the reduction of area (Z). The Young's Modulus was determined for the steel to be appox. 188 GPa.
It was also identified that there is also an impact of cryogenic treatment on the strength and ductility properties. After equivalent tempering treatments, CT samples present higher yield strengths but lower tensile strengths (except the conditions tempered at 482°C) and uniform elongations compared to non-CT samples. Additionally, there are distinct differences between the conditions tempered at 482°C for 5 h or 1+4 h. CT and non-CT samples tempered for 1+4 h show lower tensile strengths and uniform elongations than the samples tempered for 5 h, respectively. Furthermore, the yield strength of the CT samples tempered for 1+4 h is higher, whereas the yield strength of the non-CT samples tempered for 1+4 h is lower compared to the samples tempered for 5 h.

Condition	$\mathbf{R_{p0.2}}$	$\mathbf{R_m}$	$\mathbf{A_g}$	**A**	**Z**
	MPa	**MPa**	%	%	%
CT/ 482°C/ 5 h	1700	2075	2.7	13.2	64
482°C/ 5 h	1640	2070	2.5	13.2	65
CT/ 540°C/ 5 h	1445	1525	4.5	16.1	72
540°C/ 5 h	1265	1555	4.8	16.2	72
CT/ 600°C/ 5 h	1275	1385	6.0	17.9	71
600°C/ 5 h	1100	1405	6.5	17.8	65
CT/ 482°C/ 1+4 h	1750	1960	1.9	12.7	66
482°C/ 1+4 h	1575	1965	2.4	12.8	64

Table 4.10: Results from tensile tests of CT and non-CT samples tempered at 482°C, 540°C and 600°C for 5 h and at 482°C for 1+4 h. The mean values were evaluated from two measurements, which were carried out for each condition.

In Fig. 4.34 the stress-strain curves of samples tempered at 482°C for 5 h and 1+4 h are plotted. These curves demonstrate that the plastic deformation during loading starts at lower strength levels for the non-CT compared to the CT conditions. As a consequence, the non-CT conditions present the lower yield strength values. It is to note that, the gap between CT and non-CT samples tempered for 5 h regarding the onset of yielding is smaller than the one for the samples tempered for 1+4 h.

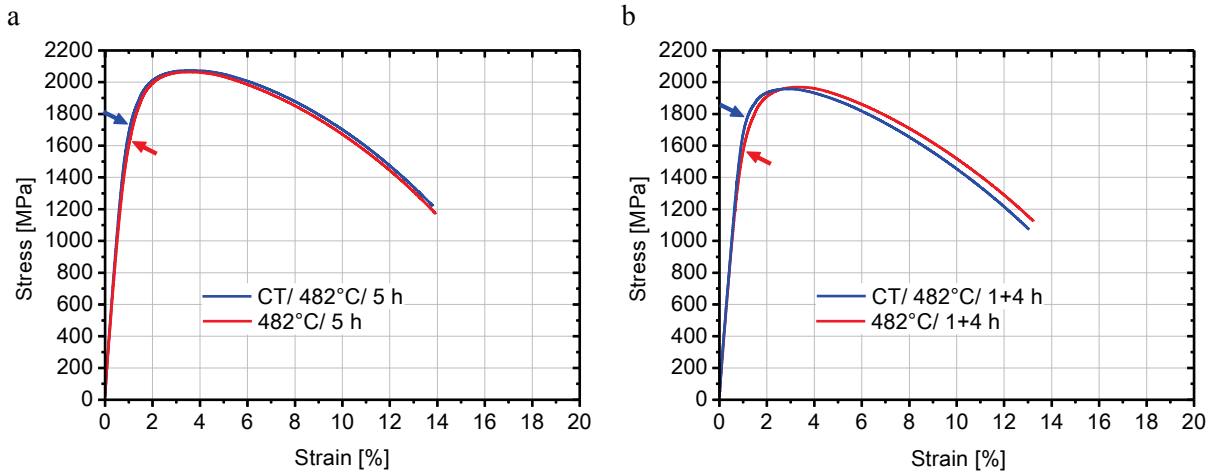

Figure 4.34: Stress-strain curves obtained from tensile tests. (a) Representative stress-strain curves of CT and non-CT samples tempered at 482°C for 5 h. (b) Representative stress-strain curves of CT and non-CT samples tempered at 482°C for 1+4 h. The onset of yielding in the CT and non-CT samples is marked by blue and red arrows, respectively.

The stress-strain curves of specimens tempered at 540°C or 600°C for 5 h are also strongly affected by cryogenic treatment, as shown in Fig. 4.35. The non-CT conditions exhibit a rather gradual increase of stress in the transition region from elastic to plastic. This behavior of the stress-strain curve leads to higher tensile stresses and to higher uniform strains for the non-CT samples. The profile of the stress-strain curve of CT samples shows a more or less sharp bend after reaching the yield strength. As a result, a region of almost constant stress values with increasing elongation occurs.

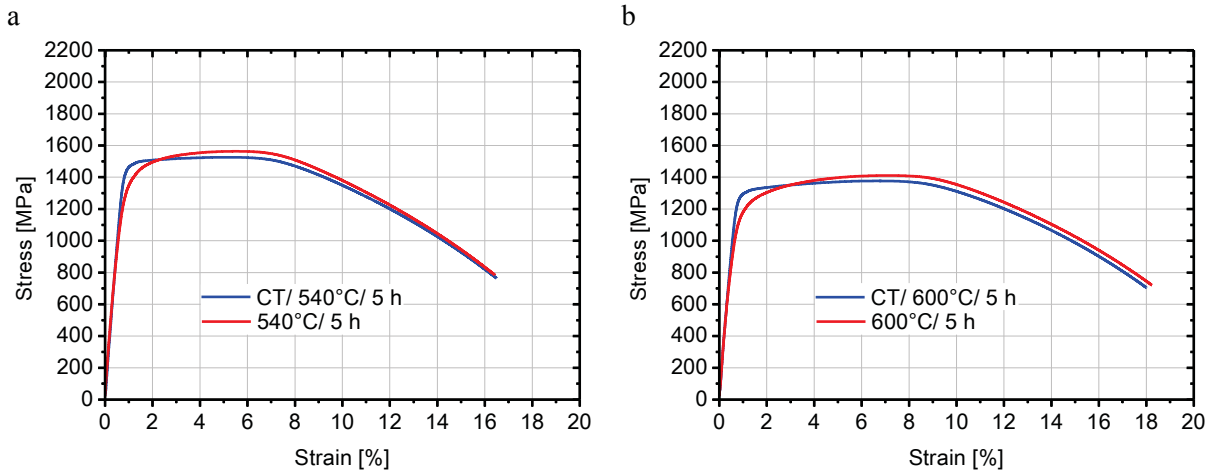

Figure 4.35: Stress-strain curves obtained from tensile tests. (a) Representative stress-strain curves of CT and non-CT samples after tempering at 540°C for 5 h. (b) Representative stress-strain curves of CT and non-CT samples after tempering at 600°C for 5 h.

4.3.2 Transformation behavior of austenite upon mechanical loading

The transformation behavior of austenite upon mechanical loading was analyzed for CT and non-CT samples, which were tempered at 600°C for 5 h by measuring the austenite phase fraction at defined stress levels during tensile testing. The results of the austenite phase fraction measurements and the stress-strain curves of these conditions are depicted in Fig. 4.36 (a) and (b).

For both conditions, the austenite phase fraction is between 24 % and 26 % at the initial stage of testing and stays more or less constant until the yield strength is reached and plastic deformation takes place. Beyond the yield strength, the austenite phase fraction is reduced, indicating that for both, CT and non-CT, conditions a significant transformation of austenite proceeds during testing. For the CT sample, the transformation of austenite starts at higher stress levels as the yield strength is also higher and the decrease of austenite fraction is more abrupt compared to the non-CT sample. It is assumed that during straining of the non-CT sample also some austenite transformation might occur below the yield strength. As the measuring inaccuracy is about 2 %, the transformation of austenite in this range can only be supposed. However, it is reasonable to expect that in the non-CT specimen the austenite transforms to martensite also before plastic deformation occurs, i.e. stress-assisted, as the austenite in this condition exhibits a lower stability. The lower stability of austenite in non-CT conditions was also determined by dilatometry measurements in Fig. 4.29.

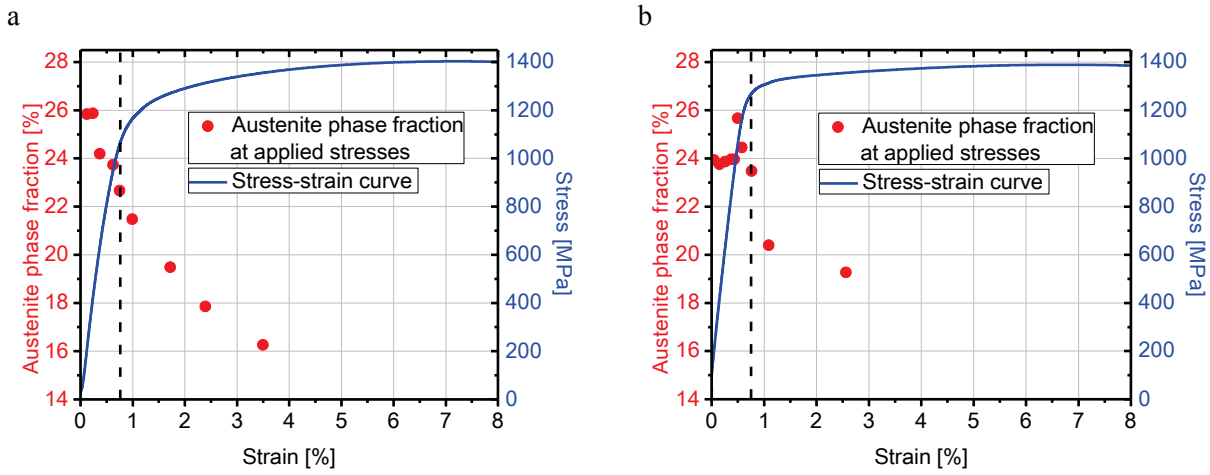

Figure 4.36: Results from austenite phase fraction measurements at distinct stress levels during tensile tests. For comparison also the stress-strain curves are plotted. (a) Non-CT specimen tempered at 600°C for 5 h. (b) CT specimens tempered at 600°C for 5 h. The measuring inaccuracy of austenite phase fraction determination was about 2 %. The vertical dashed lines indicate the positions of the yield strength.

Austenite phase fraction measurements were also carried out on fractured specimens after tensile testing. The analyses were conducted near the fracture on the cutting plane as shown in Fig. 4.37. The cutting plane was about 2-3 mm away from the fracture surface. The results of the measurements on CT and non-CT specimens tempered at 482°C, 540°C and 600°C for 5 h and on specimens tempered at 482°C for 1+4 h are presented in Table 4.11. For comparison, also the austenite phase fractions of samples before (austenitized and cryogenically treated) and after tempering are listed. These measurements reveal that the austenite phase fraction decreases for all conditions during testing compared to the austenite phase fraction after tempering, indicating that austenite is not stable upon mechanical loading and transforms. Moreover, it was found that for the conditions tempered at 482°C, the austenite phase fraction is even below detection limit near the fracture of the tensile test specimens.

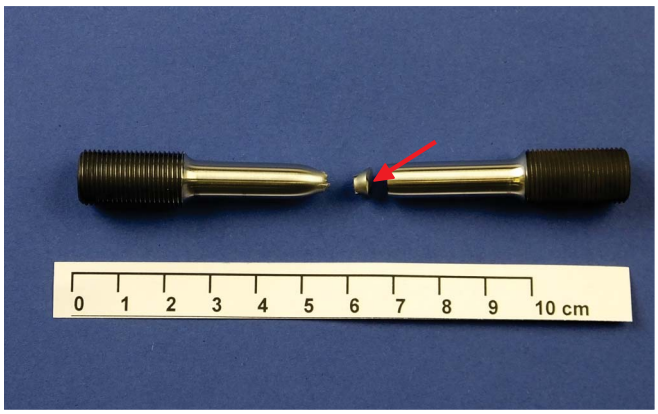

Figure 4.37: Fractured tensile test sample. The arrow indicates the position of XRD analyses.

Condition	Austenite phase fraction [%]		
	Retained austenite before tempering	**After tempering**	**Broken tensile test samples**
	Section 4.1.1	Section 4.1.1	near the fracture, Fig. 4.37
CT/ 482°C/ 5 h	3.5	4.0	-
482°C/ 5 h	6.5	3.5	-
CT/ 540°C/ 5 h	3.5	13.0	5.5
540°C/ 5 h	6.5	15.0	5.0
CT/ 600°C/ 5 h	3.5	24.5	6.0
600°C/ 5 h	6.5	25.5	6.5
CT/ 482°C/ 1+4 h	3.5	4.0	-
482°C/ 1+4 h	6.5	4.0	-

Table 4.11: Austenite phase fraction measurements on fractured tensile test samples. For comparison, also the retained austenite phase fractions of the samples before tempering (austenitized and cryogenically treated) and the austenite phase fractions after tempering are listed (these measurements are also shown in Fig. 4.1 and Table 4.1). For the samples tempered at 482°C the austenite phase fraction after tensile testing was below detection limit, which was about 1 %.

4.3.3 Fracture toughness properties

The results of fracture toughness measurements of CT and non-CT samples tempered at 482°C, 540°C and 600°C for 5 h and at 482°C for 1+4 h are presented in Table 4.12. As a result of the too small sample sizes and of the large plastic deformations at crack tip in the samples tempered at 540°C and 600°C, valid K_{IC} values according to the standard ASTM E399-09 [90] are only obtained for non-CT samples tempered at 482°C for 5 h. The fracture toughness of this condition was determined to be 92 MPa$\sqrt{m}$. However, for comparison of the heat treatment conditions the K_Q values were used. Furthermore, also the K_{max} values were evaluated, which present the values at the force maximum.

Condition	$\mathbf{K_Q}$	$\mathbf{K_{max}}$
	MPa$\sqrt{m}$	**MPa**$\sqrt{m}$
CT/ 482°C/ 5 h	110 ± 5	112 ± 4
482°C/ 5 h	92* ± 5	92 ± 5
CT/ 540°C/ 5 h	111 ± 3	146 ±3
540°C/ 5 h	95 ± 2	141 ± 4
CT/ 600°C/ 5 h	100 ± 1	157 ± 2
600°C/ 5 h	79 ± 7	150 ± 2
CT/ 482°C/ 1+4 h	124 ± 1	140 ± 6
482°C/ 1+4 h	112 ± 1	129 ± 7

Table 4.12: Results from fracture toughness measurements of CT and non-CT samples tempered at 482°C, 540°C and 600°C for 5 h and at 482°C for 1+4 h. The K_Q values were evaluated according to the Standard ASTM E399-09 [90] and the K_{max} values were taken at the force maximum. For each condition three measurements were carried out and the mean values and the standard deviations were calculated. * Valid K_{IC} value.

The K_Q value of the CT condition tempered at 482°C for 5 h was determined with 110 MPa$\sqrt{m}$. This values is about 18 MPa$\sqrt{m}$ higher than the K_{IC} value of the non-CT condition (92 MPa$\sqrt{m}$). Higher toughness values for CT compared to non-CT samples are also observed for the conditions tempered at 482°C for 1+4 h. However, the difference of K_Q values between these conditions is only 12 MPa$\sqrt{m}$. Furthermore, there are also variations of the toughness properties between the samples tempered for 5 h and 1+4 h. Tempering of CT samples for 1+4 h instead of 5 h causes about 14 MPa$\sqrt{m}$ higher K_Q values. Thus, the largest K_Q value of the conditions tempered at 482°C was obtained for the CT sample tempered for 1+4 h and was determined with 124 MPa$\sqrt{m}$.

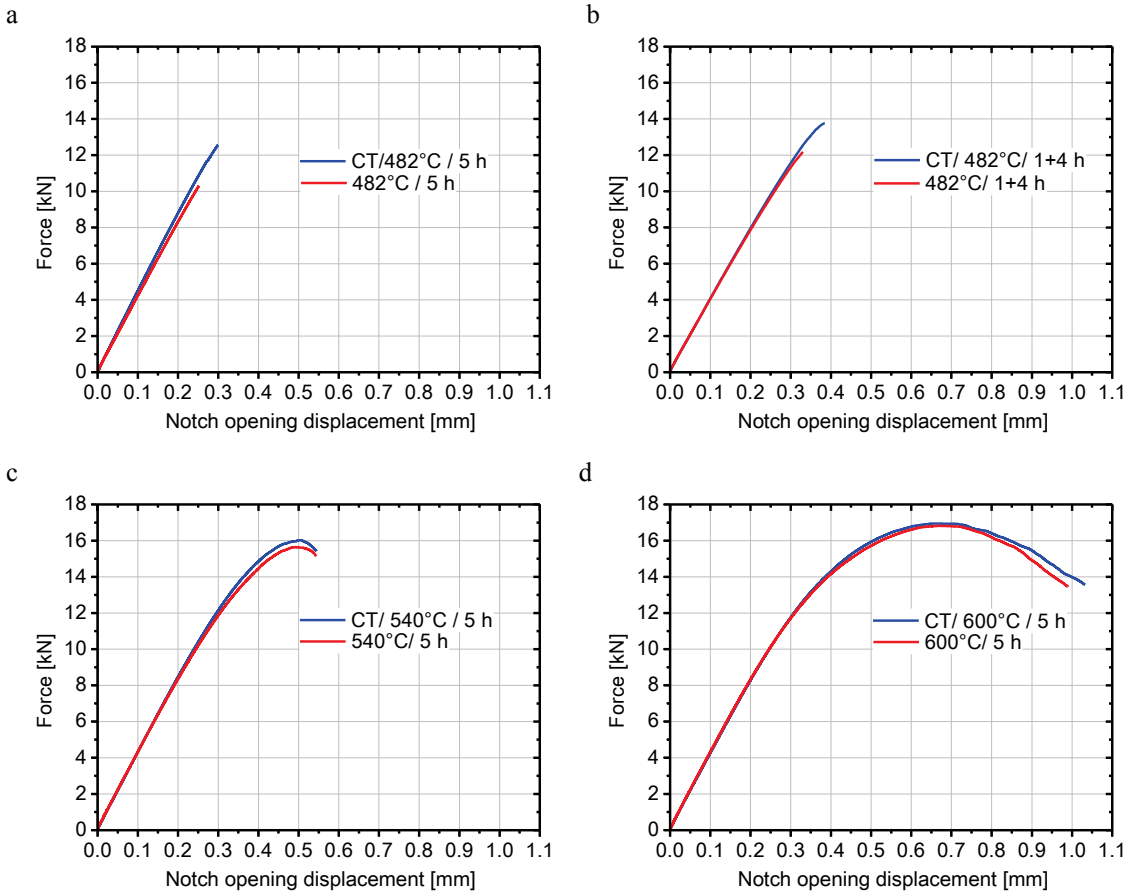

Figure 4.38: Representative load-notch opening displacement curves of CT and non-CT samples tempered at 482°C, 540°C and 600°C for 5 h and at 482°C for 1+4 h.

The load-notch opening displacement curves of samples tempered at 482°C for 5 h and for 1+4 h are depicted in Fig. 4.38 (a) and (b). These curves show a merely linear behavior. Conversely, the load-notch opening displacement curves of the samples tempered at 540°C or 600°C indicate large plastic deformations. The curves are presented in Fig. 4.38 (c) and (d). Also these tempering conditions are influenced by cryogenic treatment, as the CT samples exhibit clearly higher K_Q values than the non-CT conditions. The K_Q values of CT and non-CT samples tempered at 540°C are 111 MPa$\sqrt{m}$ and 95 MPa$\sqrt{m}$. However, the K_Q values decrease slightly due to tempering at 600°C to about 100 MPa$\sqrt{m}$ for CT and to 79 MPa$\sqrt{m}$ for non-CT samples. The K_{max} values of the conditions tempered at 540°C and 600°C increase strongly compared to the values of the samples tempered at 482°C. Nevertheless, concerning the K_{max} values only small differences are observable between CT and non-CT conditions tempered at higher temperatures.

4.3.4 Fractography

The fracture surfaces of broken SENB specimens were analyzed. Fig. 4.39 presents the fracture surfaces of the CT and non-CT samples tempered at 482°C for 5 h. A predominately ductile fracture is present for both conditions. Apparently the CT sample presents a slightly rougher surface.

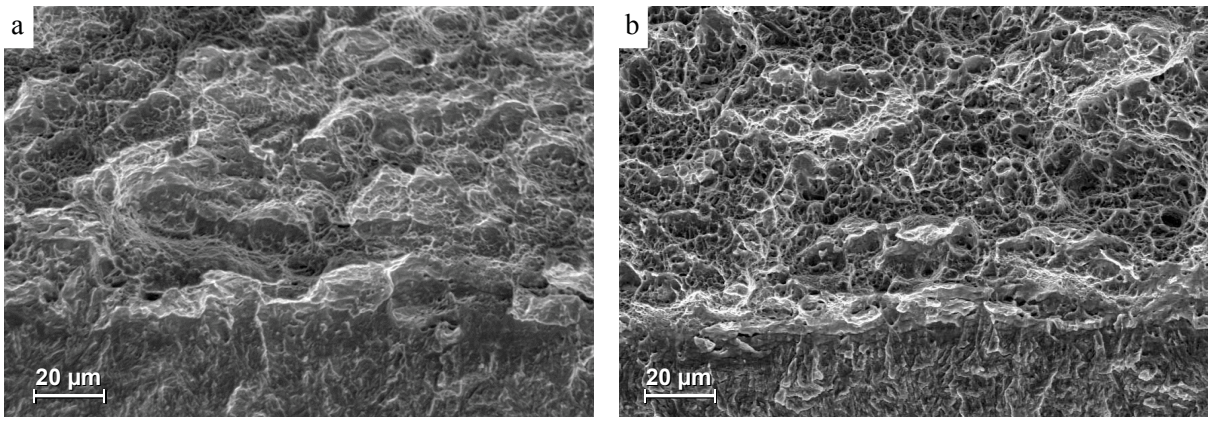

Figure 4.39: SEM analysis of fractured SENB samples tempered at 482°C for 5 h. (a) Ductile fracture of the CT sample. (b) Ductile fracture of the non-CT sample.

Also, the samples tempered at 482°C for 1+4 h present a mostly ductile fracture as shown by the dimple structure in Fig. 4.40 (a) and (b). However, for this tempering condition no differences are observable for CT and non-CT samples.

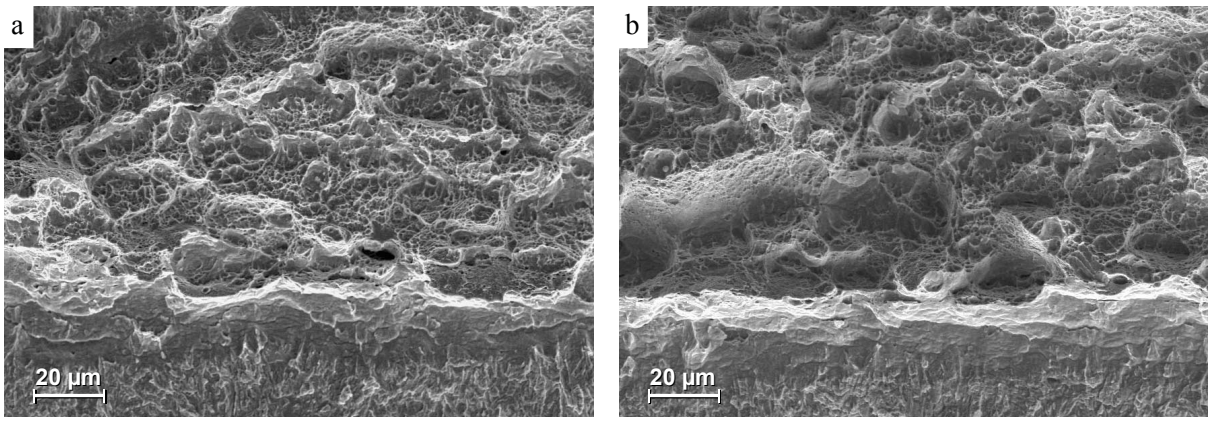

Figure 4.40: SEM analysis of fractured SENB samples tempered at 482°C for 1+4 h. (a) Ductile fracture of the CT sample. (b) Ductile fracture of the non-CT sample.

The fracture surface of the CT sample tempered at 540°C is depicted in Fig. 4.41. It presents a merely ductile fracture in the first 300 μm. Due to further extension of the crack, the fracture mode passes over to an intergranular fracture with ductile regions. As shown in Fig. 4.42, tempering at 600°C leads again to a mainly ductile fracture. This heat treatment condition leads to significantly larger dimples than tempering at 482°C.

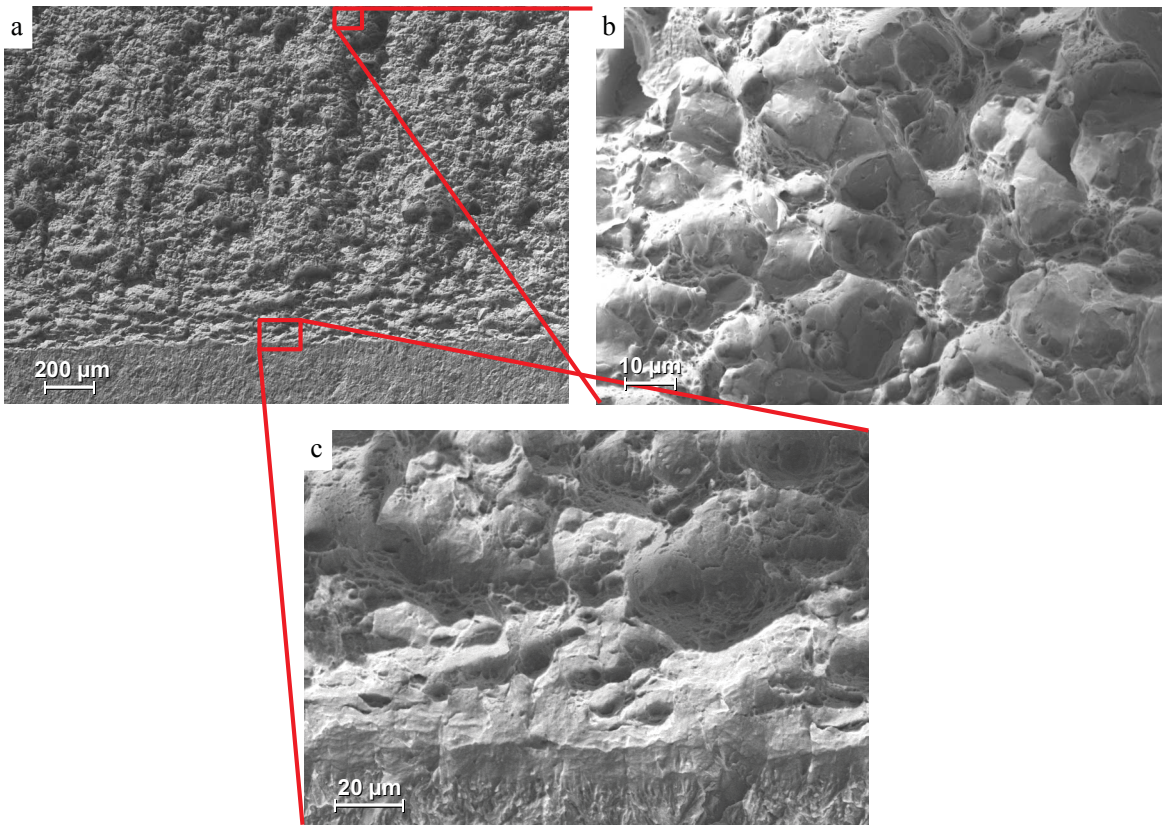

Figure 4.41: SEM analysis of a fractured SENB sample, which was cryogenically treated and tempered at 540°C for 5 h. (a) Overview image from the fracture surface. (b) Fracture surface about 1.3 mm away from the precrack. (c) Fracture surface near the fatigue precrack.

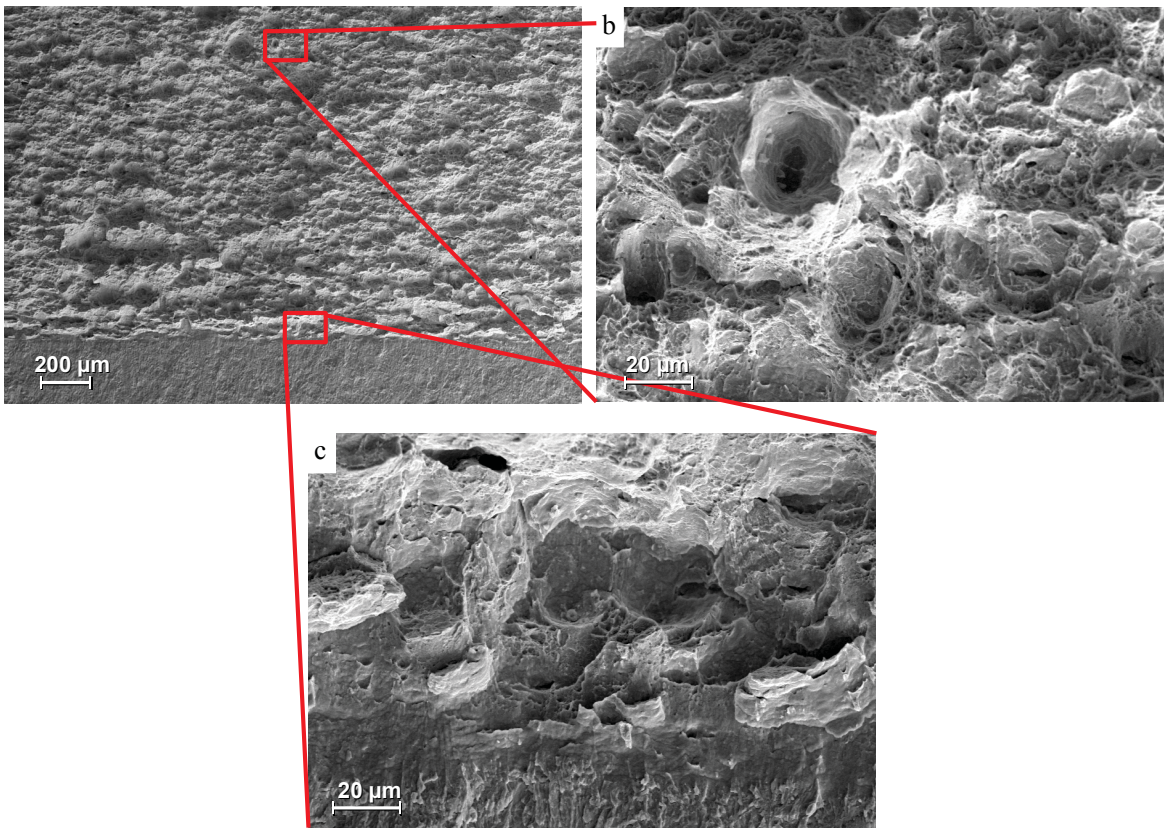

Figure 4.42: SEM analysis of a fractured SENB sample, which was cryogenically treated tempered at 600°C for 5 h. (a) Overview image from the fracture surface. (b) Fracture surface about 1.2 mm away from the precrack. (c) Fracture surface near the fatigue precrack.

4.3.5 Analyses of crack tip opening displacement

As a result of the too small sample sizes for measuring valid K_{IC} values, the crack tip opening displacement at crack initiation (COD_i) and during crack growth was also analyzed as a criterion for toughness properties. The COD values were determined with stereophotogrammetric analyses according to Kolednik and Stampfl [91, 92] by evaluating the height profiles of both sides of the fracture surface of SENB samples by using SEM. The measurements were carried out on CT and non-CT samples tempered at 482°C for 5 h and 1+4 h. For each condition, representative SEM images of the same position on both sides of the fracture surface accompanied with one representative height profile pair are shown in Fig. 4.43-4.46.

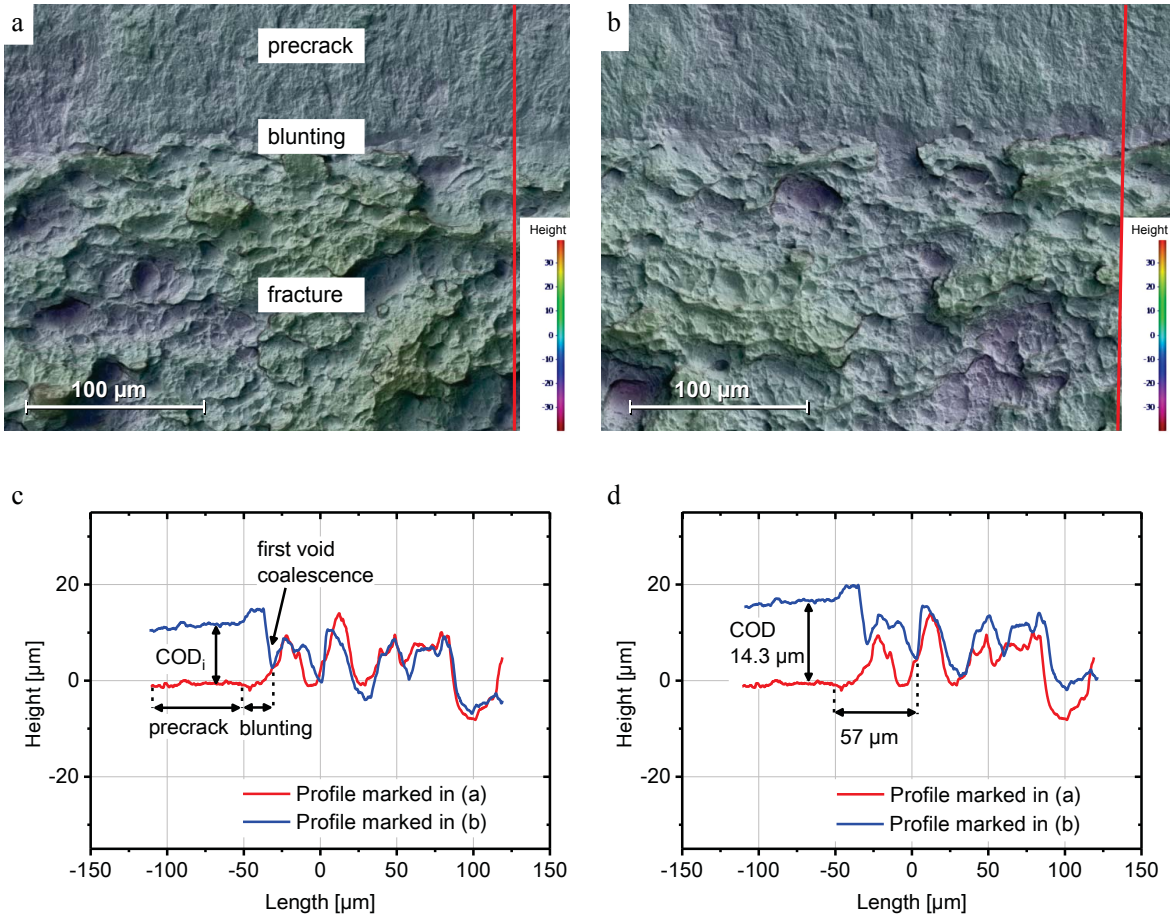

Figure 4.43: Stereophotogrammetric measurements on the same positions from both sides of the fracture surface of a SENB specimen, which was cryogenically treated and tempered at 482°C for 5 h. In (a) and (b) the SEM images of both sides of the fracture surface are depicted. The surface in (b) is mirrored in the horizontal direction. In (c) and (d) the height profiles are plotted. The the positions of the profiles are indicated in (a) and (b) by red lines. In the diagrams, the profile marked in (b) was turned upside down. In (c) the profiles were adjusted in the way that they touch starting from the precrack in the point of the first void coalescence. In (d) the profiles were shifted vertically so that they touch at the next point, which is 57 μm away from end of the precrack.

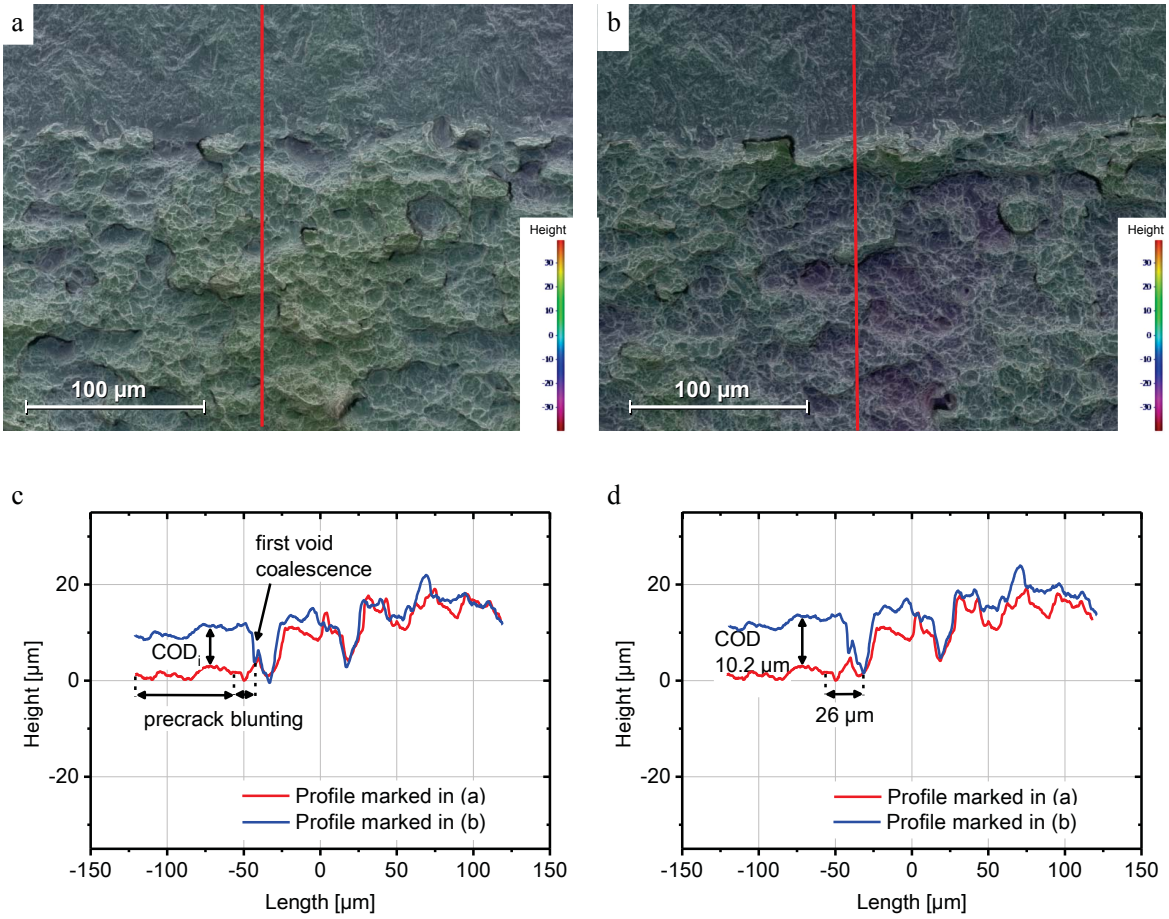

Figure 4.44: Stereophotogrammetric measurements on the same positions from both sides of the fracture surface of a SENB specimen, which was tempered at 482°C for 5 h. In (a) and (b) the SEM images of both sides of the fracture surface are depicted. The surface in (b) is mirrored in the horizontal direction. In (c) and (d) the height profiles are plotted. The the positions of the profiles are indicated in (a) and (b) by red lines. In the diagrams, the profile marked in (b) was turned upside down. In (c) the profiles were adjusted in the way that they touch starting from the precrack in the point of the first void coalescence. In (d) the profiles were shifted vertically so that they touch at the next point, which is 26 μm away from end of the precrack.

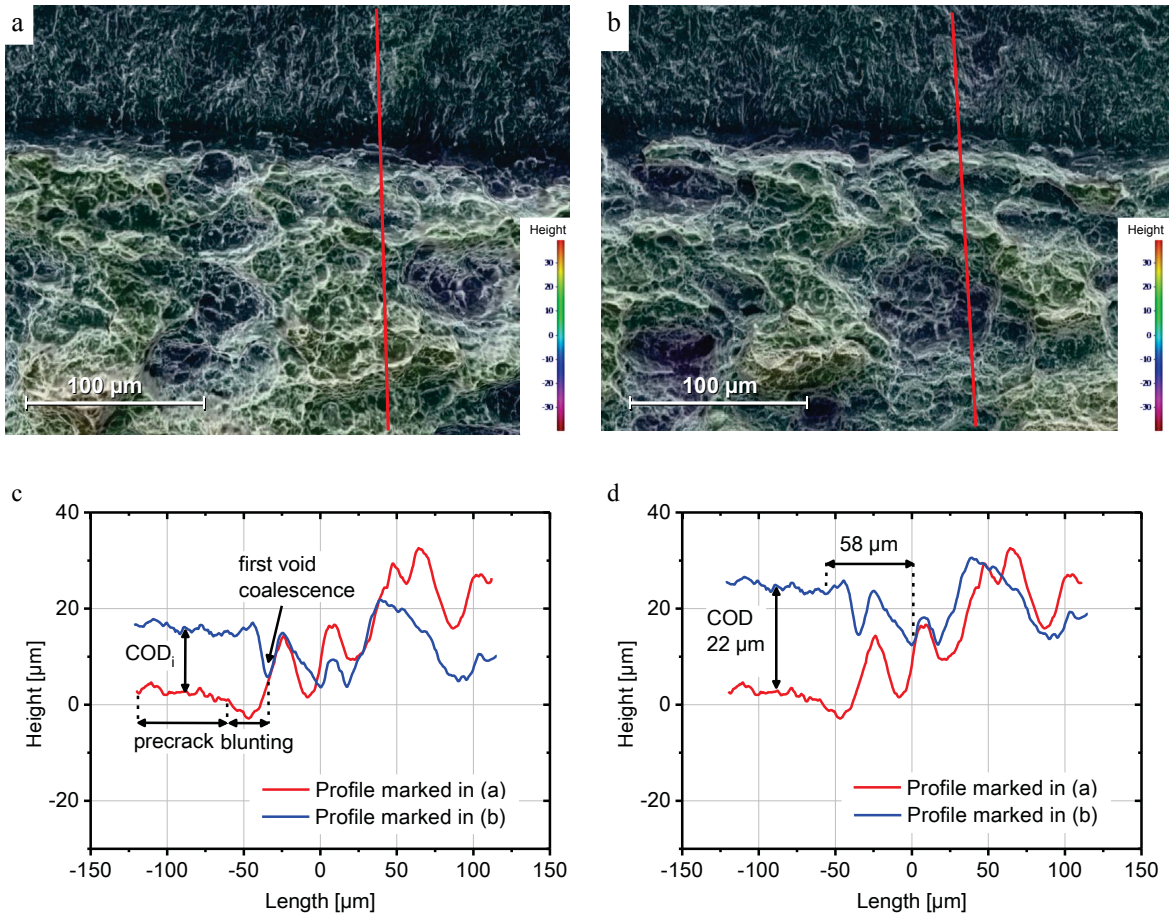

Figure 4.45: Stereophotogrammetric measurements on the same positions from both sides of the fracture surface of a SENB specimen, which was cryogenically treated and tempered at 482°C for 1+4 h. In (a) and (b) the SEM images of both sides of the fracture surface are depicted. The surface in (b) is mirrored in the horizontal direction. In (c) and (d) the height profiles are plotted. The the positions of the profiles are indicated in (a) and (b) by red lines. In the diagrams, the profile marked in (b) was turned upside down. In (c) the profiles were adjusted in the way that they touch starting from the precrack in the point of the first void coalescence. In (d) the profiles were shifted vertically so that they touch at the next point, which is 58 μm away from end of the precrack.

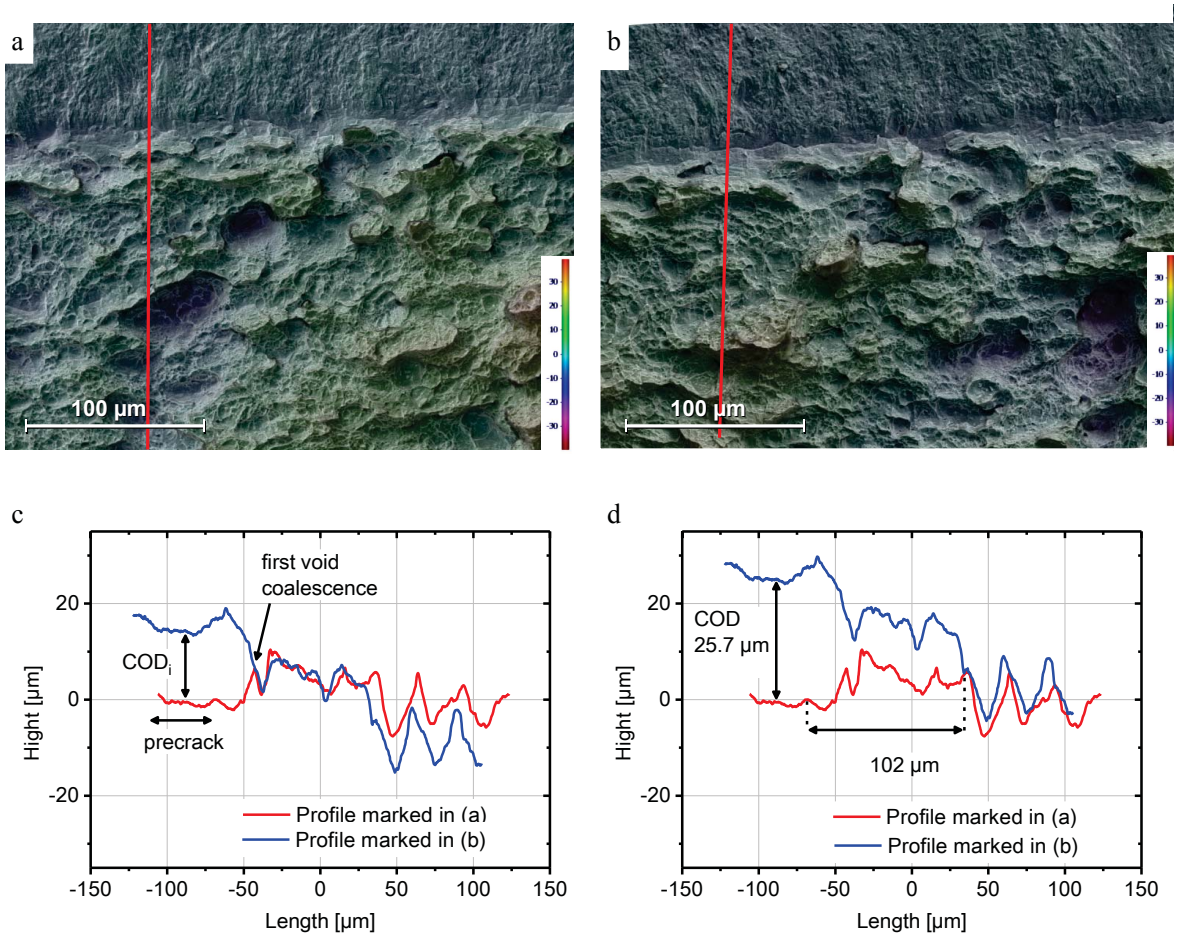

Figure 4.46: Stereophotogrammetric measurements on the same positions from both sides of the fracture surface of a SENB specimen, which was tempered at 482°C for 1+4 h. In (a) and (b) the SEM images of both sides of the fracture surface are depicted. The surface in (b) is mirrored in the horizontal direction. In (c) and (d) the height profiles are plotted. The the positions of the profiles are indicated in (a) and (b) by red lines. In the diagrams, the profile marked in (b) was turned upside down. In (c) the profiles were adjusted in the way that they touch starting from the precrack in the point of the first void coalescence. In (d) the profiles were shifted vertically so that they touch at the next point, which is 102 μm away from end of the precrack.

The COD values as a function of crack extension for the investigated conditions are presented in Fig. 4.47. The starting point of crack growth was set to the onset of blunting, as shown by the Fig. 4.43-4.46. The COD_i values obtained at the point of the first void coalescence and the $COD_{\Delta a=160\ \mu m}$ values at a crack extension Δa of 160 μm are listed in Table 4.13.

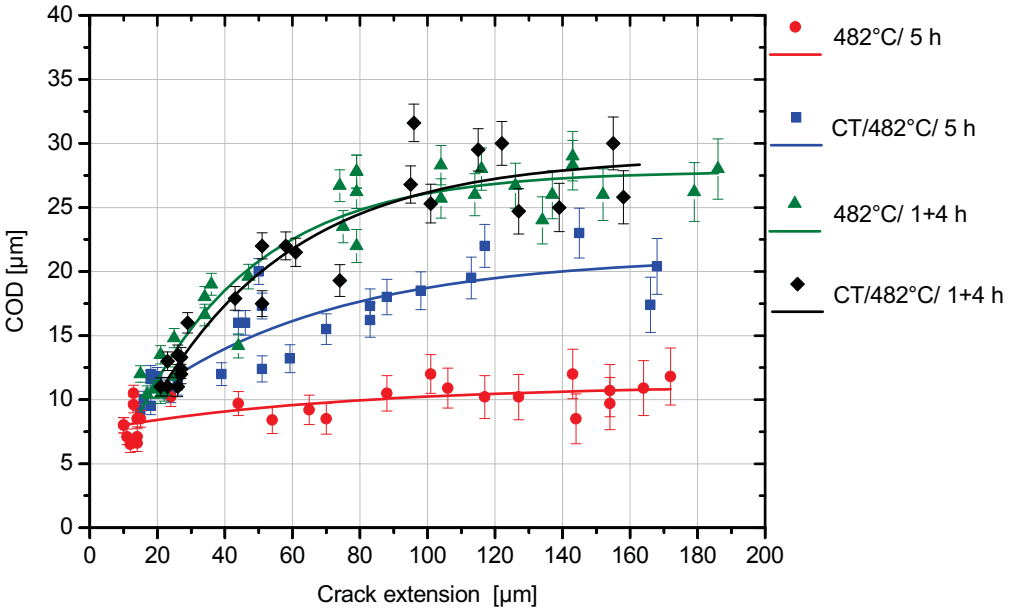

Figure 4.47: COD values of CT and non-CT samples tempered at 482°C for 5 h and 1+4 h plotted as a function of crack extension. The starting point of crack growth was set to the onset of blunting. The measuring inaccuracy of the crack extension was about ± 5 μm. The measuring inaccuracy of the COD was estimated to be ± 0.5 μm plus/minus 1 % of the respective crack extension to take angle errors into account.

Generally, the COD raises with increasing crack extension. The non-CT sample, which was tempered at 482°C for 5 h, exhibits only a slight enhancement of COD values from about 8 μm at crack initiation to 11 μm at a crack extension of 160 μm. For this condition also the height profile of the fracture surface is rather smooth compared to the other conditions. The CT sample with the same tempering treatment shows a somewhat higher COD_i of about 11 μm and a significant raise to approx. 20 μm at 160 μm crack extension. Distinct differences can not be observed regarding the behavior of COD between CT and non-CT conditions tempered for 1+4 h. Both conditions show relatively high COD_i values of approx. 12 μm and a huge raise of COD to approx. 28 μm for a crack extension of about 160 μm.

The results of the calculations of K_{COD} from COD values are presented in Table 4.14. The non-CT sample tempered at 482°C for 5 h has the lowest K_{COD_i} and $K_{COD_{\Delta a=160\ \mu m}}$ values as they are 91 MPa$\sqrt{m}$ and 106 MPa$\sqrt{m}$, respectively. Higher toughness values are obtained from the CT condition with the same tempering treatment. A K_{COD_i} of 105 MPa$\sqrt{m}$ and a $K_{COD_{\Delta a=160\ \mu m}}$ of 144 MPa$\sqrt{m}$ was evaluated for this heat treatment

condition. Furthermore, there are only slight differences between the calculated K values of the CT and the non-CT conditions tempered at 482°C for 1+4 h . However, they present a K_{COD_i} value of approx. 108 MPa$\sqrt{m}$ and a $K_{COD_{\Delta a=160\ \mu m}}$ value of approx. 163 MPa$\sqrt{m}$, which are much higher than the values of the other conditions tempered at 482°C.

Condition	$\mathbf{COD_i}$ μ**m**	$\mathbf{COD_{\Delta a=160\ \mu m}}$ μ**m**
CT/ 482°C/ 5 h	10.7 ± 1.0	20.3 ± 2.2
482°C/ 5 h	8.1 ± 0.9	10.7± 2.2
CT/ 482°C/ 1+4 h	12.5 ± 1.7	28.3 ± 2.2
482°C/ 1+4 h	11.5 ± 1.2	27.5 ± 2.2

Table 4.13: Determined COD values at crack initiation (COD_i) and at a crack extension of 160 μm ($COD_{\Delta a=160\ \mu m}$) of the CT and non-CT samples tempered at 482°C for 5 h and 1+4 h. For each condition nine measurements in form of height profiles were carried out.

It is to note that the results from stereophotogrammetric analyses by and large support the results from fracture toughness tests in Section 4.3.3, as also by these measurements slight differences between the CT and non-CT conditions tempered for 1+4 h but large differences between the conditions tempered for 5 h are present. Furthermore, the K_{COD_i} values correlate quite well with the K_Q values.

Condition	$\mathbf{K_{COD_i}}$ **MPa**$\sqrt{m}$	$\mathbf{K_{COD_{\Delta a=160\ \mu m}}}$ **MPa**$\sqrt{m}$	$\mathbf{K_Q}$ **MPa**$\sqrt{m}$	$\mathbf{K_{max}}$ **MPa**$\sqrt{m}$
CT/ 482°C/ 5 h	105 ± 6	144 ± 8	110 ± 5	112 ± 4
482°C/ 5 h	91 ± 7	106 ± 11	92 ± 5	92 ± 5
CT/ 482°C/ 1+4 h	108 ± 6	162 ± 6	124 ± 1	140 ± 6
482°C/ 1+4 h	107 ± 6	164 ± 7	112 ± 1	129 ± 7

Table 4.14: Calculated K_{COD_i} and $K_{COD_{\Delta a=160\ \mu m}}$ values of the CT and non-CT samples tempered at 482°C for 5 h and 1+4 h. The values were calculated from the COD_i by using Eq. 6 and 7. The K_Q evaluated in Section 4.3.3 by fracture toughness tests is listed for comparison.

4.3.6 Discussion of the influence heat treatment and microstructure on mechanical properties

The analyses of the mechanical properties revealed that there are distinct differences in toughness and strength between CT and non-CT conditions, regardless of the tempering temperature and time.
In Section 4.1.1 it was determined that the austenite contents of CT and non-CT samples, which were tempered for 5 h or 1+4 h at the same temperatures, are comparable. Thus, it is suggested that the phase fraction of austenite is not the critical factor regarding the differences of mechanical properties.
The results of austenite phase fraction measurements on fractured tensile test specimens (Table 4.11) revealed that austenite transforms in martensite at least partially during testing in all conditions. This implies that some austenite in non-CT as well as in CT samples is unstable during the tests. It is suggested that upon mechanical loading first of all the retained austenite transforms because of its low stability (Section 4.2.2). The maximum retained austenite phase fraction is about 3.5 % in CT and 6.5 % in non-CT samples. Nevertheless, it was determined by dilatometry in Section 4.2.2 that in most cases some retained austenite transforms due to tempering. So the actual retained austenite content in the tempered CT and non-CT samples is probably lower than 3.5 % and 6.5 %, respectively. As for the CT and non-CT conditions tempered at 540°C and 600°C for 5 h the reduction of austenite content during tensile testing is definitely more than 3.5 % for CT and 6.5 % for non-CT samples, also the reverted austenite present in theses specimens has to transform partially during loading. For the conditions tempered at 482°C, the reverted austenite phase fraction is approx. 1 %, as shown in Fig. 4.1. As the detection limit by XRD measurements of the austenite phase fraction is about 1 %, no statement can be made, if also the reverted austenite transforms in these samples during tensile testing. However, as the reverted austenite formed at 482°C exhibits a higher Ni content than the austenite formed at 600°C (Fig. 4.20 and 4.21), it is probable that the reverted austenite in the samples tempered at 482°C is more stable and does not transform during tensile testing. It is to mention that the reduction of austenite phase fraction due to tensile testing is almost equal for CT and non-CT samples tempered with the same parameters (Table 4.11).
Furthermore, the analyses of the transformation behavior of austenite during the tensile tests (Fig. 4.36) showed that a pronounced austenite transition starts for CT and non-CT samples tempered at 600°C, when the loading stress exceeds the yield strength of the

material. However, as the yield strength values of the CT sample are higher compared to the non-CT sample, also the stress levels, at which the pronounced austenite transformation begins, are higher. It is suggested that when the loading stress exceeds the yield strength, plastic deformation occurs and thus, new potential nucleation sites are created in austenite for its transformation as described by Haidemenopoulos [15]. As a result, the strain-induced transition of austenite into martensite is triggered. However, some of the austenite might also transform in the non-CT sample tempered at 600°C before the loading stress exceeds the yield strength (stress-assisted). Since the transformation of austenite into martensite is connected with a volume increase, it is possible that this transformation contributes to the lower yield strength of non-CT samples, as explained in the following:
A transformation of the retained austenite in martensite would lead to a volume increase of up to 3 % [53, 54, 59]. If 2 % austenite transform into martensite in the non-CT sample tempered at 600°C before the loading stress reached the yield strength (estimated from Fig. 4.36 (a)), a volume increase would proceed, which might cause about 0.06 % additional plastic elongation. Since the transformation of austenite into martensite during testing is directed, the resulting additional plastic elongation due to transformation is probably higher. Nevertheless, the additional plastic elongation may contribute and lead to the lower yield strength values of non-CT samples. As a result, it is not clear if austenite transformation at higher stress levels in the CT samples is a result of the higher stability of austenite or of the higher strength of the material. Thus, the influence of cryogenic treatment on the stability of austenite could not be quantified.
Furthermore, it is assumed that the region of constant stress values of the stress-strain curves of the samples tempered at 540°C and 600°C (Fig 4.35) is caused by the transformation of austenite. A significant austenite transformation in martensite in this region was determined for the samples tempered at 600°C as shown by Fig. 4.36. However, a pronounced amount of austenite is still present after 5 % plastic strain. It is suggested that the transformation of austenite into martensite causes an increase of strength, which counterbalances the softening due to necking. For the conditions tempered at 482°C the effect of the transforming austenite on the stress-strain curves is not identifiable. This is probably a consequence of the low austenite phase fractions.

Distinct differences between CT and non-CT conditions were also found regarding fracture toughness properties. It was determined that regardless of the tempering condition, the K_Q values of CT samples are higher compared to them of the non-CT samples, as

shown in Table 4.12. It was also determined that the K_Q values are more enhanced for the specimens tempered at 482°C for 1+4 h (two step tempering treatment) compared to the samples tempered for 5 h (one step tempering). However, this may be ascribed to the lower strength of these conditions. Furthermore, it was evaluated that the difference between the K_Q values of CT and non-CT conditions is lower for the samples tempered for 1+4 h than for the samples tempered for 5 h at 482°C.

The evaluation of the COD_i and K_{COD_i} values at crack initiation (Table 4.13 and 4.14), revealed that the toughness of the CT condition tempered for 5 h is slightly lower but also comparable to the toughness of the CT and non-CT conditions tempered for 1+4 h. Only the non-CT sample tempered for 5 h has significantly lower toughness values at crack initiation. Additionally, it was found that the largest differences between the non-CT condition tempered at 482°C for 5 h and the other conditions tempered at 482°C are concerning the crack resistance curves (Fig. 4.47). Whereas the other conditions show a strong raise of the COD with an increasing crack extension Δa, the crack resistance curve of the non-CT sample tempered for 5 h is very flat.

From these results, it can be concluded that the omission of the cryogenic treatment deteriorates the toughness values of the sample tempered at 482°C for 5 h but has less influence on fracture toughness of the samples tempered for 1+4 h. A possible explanation for this behavior is discussed hereinafter:

The dilatometer investigations of samples tempered at 482°C for 1+4 h (Fig. 4.27) demonstrated that the austenite remains stable in CT as well as in non-CT conditions during the second cooling segment. Thus, as a result of this two-step tempering treatment no untempered martensite is present in both conditions. Furthermore, as no phase transformation was identified upon cooling to −100°C, also the stability of austenite of both conditions is expected to be similar. Conversely, for the non-CT samples tempered at 482°C for 5 h (Fig. 4.26) the austenite transforms during cooling, whereas again for CT conditions no phase transition occurs. As a consequence, microstructural differences are present, which may comprise untempered martensite and a lower stability of austenite in the non-CT samples tempered for 5 h. Since untempered martensite and a low stability of austenite would rather decrease fracture toughness, it is assumed that this leads to the lower toughness values of non-CT samples. Therefore, it is expected that the missing austenite transformation after tempering in non-CT sample tempered for 1+4 h causes the higher fracture toughness compared to the non-CT sample tempered for 5 h (Table 4.14). Furthermore, as the most significant difference between the CT and the non-CT samples was found in the crack resistance behavior, it is suggested that a untempered marten-

site or a low stability austenite has also a pronounced impact on crack growth behavior (Fig. 4.47).

It is to mention that both, the yield strength and the K_Q values, are higher for the CT than for the non-CT specimens, even for the samples tempered at 482°C for 1+4 h. Thus, it is suggested that also other microstructural differences than the stability of austenite contribute to these properties. Microstructural differences were also found by dilatometer and DSC heating experiments in Section 4.2.1. By these experiments it was determined that carbide precipitation is much more pronounced in CT than in non-CT conditions. As a result, it is assumed that the higher yield strength of the CT conditions is predominately originated by the more pronounced carbide formation. These alteration in carbide precipitation behavior might also determine the differences between the K_Q values of CT and non-CT conditions. Thus, during tensile tests the non-CT samples tempered for 5 h and 1+4 h do not present distinct differences, although austenite stability is varying.

5 Summary and outlook

In prior investigations [15, 18, 25, 35, 39, 40], the influence of heat treatment on fracture toughness properties was thoroughly analyzed for high Co-Ni steels. In these works it is described that the precipitation of reverted austenite during tempering predominately affects the toughness properties. However, the influence of heat and cryogenic treatment on evolution of microstructural elements is still to clarify. Thus, the scope of this work comprises a detailed analyses of the microstructure, of the evolution of the various phases during tempering and of their influence on the mechanical properties.

It was found in Section 4.1 that retained austenite is present after austenitizing and subsequent cooling to room temperature as well as after cryogenic treatment. During tempering at 482°C reverted austenite is formed by nucleating at retained austenite. The reverted austenite is enriched in nickel and chromium and depleted in cobalt. Thus, a remarkable diffusion of elements has to proceed during tempering, which takes mainly place in the adjacent martensite, because of the higher diffusion coefficient of alloying elements in martensite or ferrite compared to austenite. Accordingly, zones of nickel and chromium depletion and a zone of cobalt enrichment were found in martensite by APT measurements (Fig. 4.18) and DICTRA calculations (Fig. 4.20).
Additionally, it was found by APT measurements and kinetic calculations in Section 4.1 that the reverted austenite exhibits a concentration near the equilibrium concentration at tempering temperature. Hence, it is suggested that reverted austenite is formed when it is stable at tempering temperature and this is when the reverted austenite exhibits its equilibrium concentration. As a result, it is concluded that the formation of reverted austenite is not only influenced by Ni diffusion but also the diffusion of Co, Cr and Mo atoms.
Furthermore, the APT investigations (Fig. 4.18) indicate that in the retained austenite adjacent to the reverted austenite almost no elemental redistribution occurs, as the diffusion of substitutional elements in FCC is neglectable at 482°C for up to 50 h. Thus, the retained austenite exhibits a composition, except for the carbon content, similar to the as-quenched martensite or the overall composition of the alloy.
Moreover, it was found by APT investigations that carbon is mainly precipitated in form of carbides due to tempering at 482°C and thus neither enriched in reverted nor in retained austenite. As a result of the findings from microstructure characterization, it is concluded that the reverted austenite has a higher stability against stress or strain induced phase

transformation to martensite than retained austenite since it is remarkably enriched in nickel, which stabilizes the austenite.

From dilatometry analyses in Section 4.2.2 it was determined that in the non-cryogenically treated (non-CT) condition tempered at 482°C for 5 h predominately the retained austenite transforms into martensite during cooling after tempering, probably due to its low stability. Conversely, in the cryogenically treated (CT) sample tempered at 482°C for 5 h the retained austenite does not transform. As a result, it is concluded that this transformation of retained austenite is significantly influenced by the application of a preceding cryogenic treatment, which causes a transformation of the less stable austenite to martensite. Thus, for cryogenically treated samples no transition of austenite to martensite occurs during cooling to room temperature after tempering at 482°C for 5 h.
Additionally, a two-step tempering treatment was performed at 482°C, which comprises first a tempering step of 1 h and a second tempering step of 4 h. It was found by dilatometry investigations of this tempering treatment that during cooling after the second tempering, no further phase transformation of austenite to martensite occurs for CT as well as for non-CT specimens and thus no untempered martensite is present in both of these conditions. As the austenite remains stable also in the non-CT condition after two-step tempering, it is assumed that this two-step tempering treatment causes a similar austenite stability than a cryogenic treatment followed by tempering.

The effect of cryogenic treatment on mechanical properties was analyzed in Section 4.3 by tensile and fracture toughness tests. By these experiments it could be revealed that for specimens tempered at 482°C for 5 h the mechanical properties are strongly influenced by cryogenic treatment, as CT samples exhibit higher yield strength and fracture toughness (K_Q) values but lower tensile strength values. It is expected that this is either an effect of austenite stability or an effect of the influence of alternations in the carbide evolution. Conversely, for the CT and non-CT samples tempered at 482°C for 1+4 h distinct differences regarding the strength but only slight differences regarding the K_Q values were observed. As for these conditions the austenite stability should be more or less the same and no untempered martensite should be present, it was concluded that mainly the carbide precipitation processes (Section 4.2.1) cause these differences between these conditions. Furthermore, as the differences of carbide precipitation processes are probably caused by the different amounts of retained austenite, it is concluded that the phase fraction of

retained austenite has also in this regard a powerful impact on microstructural evolution in these steel grades.

Additionally, it was determined in Section 4.3.5 that the COD_i and the K_{COD_i} values are almost the same for the CT and non-CT conditions tempered at 482°C for 1+4 h, as the COD_i values were 12.5 μm and 11.5 μm and the K_{COD_i} were 108 MPa$\sqrt{m}$ and 107 MPa$\sqrt{m}$, respectively. For these conditions it was found that also the austenite stability is comparable. Conversely, the non-CT sample tempered at 482°C for 5 h exhibits a significantly lower COD_i value (8.1 μm) and a lower K_{COD_i} value (91 MPa$\sqrt{m}$) than the CT one, which presents a COD_i value of 10.7 μm and a K_{COD_i} value of 105 MPa$\sqrt{m}$. Since in the non-CT condition tempered at 482°C for 5 h a part of the austenite even transforms during cooling after tempering, it is suggested that the lower stability of retained austenite deteriorates the fracture toughness (COD_i and the K_{COD_i} values) of the investigated high Co-Ni steel.
Moreover, it was found that the crack resistance curve of the non-CT sample tempered at 482°C for 5 h is very flat and the COD does not raise with increasing crack extension (Fig. 4.47). In contrast, for all the other conditions tempered at 482°C the crack resistance curves show an increase with increasing crack extension. But it has to be recognized that the onset of instability occurs after a small crack extension of about 100 to 200 μm. As a consequence, it is concluded that the low stability of the austenite in the non-CT samples tempered at 482°C for 5 h has not only a significant influence on the fracture toughness but also on the crack resistance curve.

The results of this work give a new perspective on the microstructural evolution in high Co-Ni steels. By the evaluation of the influence of retained austenite on the phase evolution and on the mechanical properties the basis for possible new developments in the field high Co-Ni steels is laid. Moreover, by these findings the influence of cryogenic treatment on mechanical properties could be considered from a new point of view.

6 List of abbreviations

Δa	Crack extension
A	Fracture strain
A_g	Uniform strain
APT	Atom probe tomography
at.%	Atomic percent
BCC	Body-centered-cubic
BF	Bright-field
COD	Crack opening displacement
COD_i	Crack opening displacement at first void coalescence
COD_{160}	Crack opening displacement at 160 μm crack extension
CT	Cryogenically treated
DF	Dark-field
DSC	Differential scanning calorimetry
E	Young's Modulus
EDS	Energy dispersive X-ray spectroscopy
FCC	Face-centered-cubic
HCP	Hexagonal-close packed
K_{COD}	Calculated fracture toughness from COD
K_Q	Fracture toughness value without (check of) validation
n	Work hardening exponent
R_m	Tensile strength
$R_{p0.2}$	Yield strength
SEM	Scanning electron microscopy
SENB	Single edge-notched bend
TEM	Transmission electron microscopy
TRIP	Transformation induced plasticity

wt.%	Weight percent
XRD	X-ray diffraction
XRF	X-ray fluorescence
Z	Reduction of area
α	Ferrite
γ	Austenite

7 Bibliography

[1] W. Bergmann, *Werkstofftechnik 1.* Carl Hanser Verlag München, (2008).

[2] H. K. D. H Bhadeshia and R. W. K. Honeycombe, *Steels, Microstructure and Properties.* Elsevier, Butterworth-Heinemann, 3rd ed., (2006).

[3] G. A. Roberts, G. Krauss, and R. L. Kennedy, *Tool steels.* ASM International, 5th ed., (1998).

[4] H. Okamoto, "Co-Fe (Cobalt-Iron)," *Journal of Phase Equilibria and Diffusion*, vol. 29, pp. 383–384, (2008).

[5] H. Berns and W. Theisen, *Eisenwerkstoffe - Stahl und Gusseisen.* Springer Berlin Heidelberg, (2008).

[6] Y. Ustinovshikov, B. Pushkarev, I. Shabanova, and A. Ulianov, "Phase Transformations in the Fe-Co System," *Interface Science*, vol. 10, pp. 311–321, (2002).

[7] K. Ishida, "Calculation of the effect of alloying elements on the Ms temperature in steels," *Journal of Alloys and Compounds*, vol. 220, pp. 126–131, (1995).

[8] C. Liu, Z. Zhao, D. O. Northwood, and Y. Liu, "A new empirical formula for the calculation of Ms temperatures in pure iron and super-low carbon alloy steels," *Journal of Materials Processing Technology*, vol. 113, pp. 556–562, (2001).

[9] H. K. D. H. Bhadeshia and D. V. Edmonds, "Bainite in silicon steels: new composition–property approach Part 1," *Metal Science*, vol. 17, pp. 411–419, (1983).

[10] A. S. Podder and H. K. D. H. Bhadeshia, "Thermal stability of austenite retained in bainitic steels," *Materials Science and Engineering: A*, vol. 527, pp. 2121–2128, (2010).

[11] J. G. Speer, F. C. R. Assuncao, D. K. Matlock, and D. V. Edmonds, "The "Quenching and Partitioning" Process: Background and Recent Progress," *Materials Research*, vol. 8, (2005).

[12] D. V. Edmonds, K. He, F.C. Rizzo, B.C. De Cooman, D.K. Matlock, and J.G. Speer, "Quenching and partitioning martensite—a novel steel heat treatment," *Materials Science and Engineering: A*, vol. 438–440, pp. 25–34, (2006).

[13] I. B. Timokhina, P. D. Hodgson, and E. V. Pereloma, "Effect of microstructure on the stability of retained austenite in transformation-induced-plasticity steels," *Metallurgical and Materials Transactions A*, vol. 35, pp. 2331–2341, (2004).

[14] A. Kokosza and J. Pacyna, "Retained austenite in the cracking process of 70MnCrMoV9-2-4-2 tempered steel," *Journal of achievements in materials and manufacturing engineering*, vol. 29, pp. 39–46, (2008).

[15] G. N. Haidemenopoulos, *Dispersed-phase transformation toughening in ultrahigh-strength steels*. PhD thesis, Massachusetts Institute of Technology, (1988).

[16] R. H. Leal, *Transformation toughening of metastable austenitic steels*. PhD thesis, Massachusetts Institute of Technology, (1984).

[17] R. Ayer and P. M. Machmeier, "Microstructural basis for the effect of chromium on the strength and toughness of AF1410-based high performance steels," *Metallurgical and Materials Transactions A*, vol. 27, pp. 2510–2517, (1996).

[18] G. N. Haidemenopoulos, M. Grujicic, G.B. Olson, and M. Cohen, "Thermodynamics-based alloy design criteria for austenite stabilization and transformation toughening in the Fe-Ni-Co system," *Journal of Alloys and Compounds*, vol. 220, pp. 142–147, (1995).

[19] M. J. Van Genderen, M. Isac, A. Böttger, and E. J. Mittemeijer, "Aging and tempering behavior of iron-nickel-carbon and iron-carbon martensite," *Metallurgical and Materials Transactions A*, vol. 28, pp. 545–561, (1997).

[20] R. Schnitzer, R. Radis, M. Nöhrer, M. Schober, R. Hochfellner, S. Zinner, E. Povoden-Karadeniz, E. Kozeschnik, and H. Leitner, "Reverted austenite in PH 13-8 Mo maraging steels," *Materials Chemistry and Physics*, vol. 122, pp. 138–145, (2010).

[21] L. T. Shiang and C. M. Wayman, "Maraging behavior of an Fe-19.5Ni-5Mn alloy II: Evolution of reverse-transformed austenite during overaging," *Metallography*, vol. 21, pp. 425–451, (1988).

[22] B. Fultz, J. I. Kim, Y. H. Kim, H. J. Kim, G. O. Fior, and J. W. Morris, "The stability of precipitated austenite and the toughness of 9Ni steel," *Metallurgical Transactions A*, vol. 16, pp. 2237–2249, (1985).

[23] B. Fultz, J. I. Kim, Y. H. Kim, and J. W. Morris, "The chemical composition of precipitated austenite in 9Ni steel," *Metallurgical Transactions A*, vol. 17, pp. 967–972, (1986).

[24] J. I. Kim, C. K. Syn, and J. W. Morris, "Microstructural sources of toughness in QLT-Treated 5.5Ni cryogenic steel," *Metallurgical Transactions A*, vol. 14, pp. 93–103, (1983).

[25] R. Ayer and P. M. Machmeier, "Transmission electron microscopy examination of hardening and toughening phenomena in Aermet 100," *Metallurgical Transactions A*, vol. 24, pp. 1943–1955, (1993).

[26] H. Nakagawa, T. Miyazaki, and H. Yokota, "Effects of aging temperature on the microstructure and mechanical properties of 1.8Cu-7.3Ni-15.9Cr-1.2Mo-low C, N martensitic precipitation hardening stainless steel," *Journal of Materials Science*, vol. 35, pp. 2245–2253, (2000).

[27] C. Wang, J. Shi, C. Y. Wang, W. J. Hui, M. Q. Wang, H. Dong, and W. Q. Cao, "Development of Ultrafine Lamellar Ferrite and Austenite Duplex Structure in 0.2C 5Mn Steel during ART-annealing," *ISIJ International*, vol. 51, pp. 651–656, (2011).

[28] P. P. Sinha, D. Sivakumar, N. S. Babu, K. T. Tharian, and A. Natarajan, "Austenite reversion in 18 Ni Co-free maraging steel," *Steel Research*, vol. 66, pp. 490–494, (1995).

[29] O. Dmitrieva, D. Ponge, G. Inden, J. Millán, P. Choi, J. Sietsma, and D. Raabe, "Chemical gradients across phase boundaries between martensite and austenite in steel studied by atom probe tomography and simulation," *Acta Materialia*, vol. 59, pp. 364–374, (2011).

[30] D. Raabe, S. Sandlöbes, J. Millán, D. Ponge, H. Assadi, M. Herbig, and P.-P. Choi, "Segregation engineering enables nanoscale martensite to austenite phase transformation at grain boundaries: A pathway to ductile martensite," *Acta Materialia*, vol. 61, pp. 6132–6152, (2013).

[31] M. Farooque, H. Ayub, A. Ul Haq, and A. Q. Khan, "The formation of reverted austenite in 18Science, vol. 33, pp. 2927–2930, (1998).

[32] Xiaodong Li and Zhongda Yin, "Reverted austenite during aging in 18Ni(350) maraging steel," *Materials Letters*, vol. 24, pp. 239–242, (1995).

[33] J. Wang and S. Van Der Zwaag, "Stabilization mechanisms of retained austenite in transformation-induced plasticity steel," *Metallurgical and Materials Transactions A*, vol. 32, pp. 1527–1539, (2001).

[34] C. Lerchbacher, S. Zinner, and H. Leitner, "Retained Austenite Decomposition and Carbide Formation During Tempering a Hot-Work Tool Steel X38CrMoV5-1 Studied by Dilatometry and Atom Probe Tomography," *Metall. Mater. Trans. A*, vol. 43A, pp. 4989–4998, (2012).

[35] K. Sato, *Improving the toughness of ultrahigh strength steel*. PhD thesis, University of California, Berkeley, (2002).

[36] M. Gruber, S. Ploberger, G. Ressel, M. Wiessner, M. Hausbauer, S. Marsoner, and R. Ebner, "Effects of the combined heat and cryogenic treatment on the stability of austenite in a high Co-Ni steel," *Archives of Metallurgy and Materials, Vol 60, Issue 3*, pp. 2131–2137, (2015).

[37] R. H. J. Hannink, P. M. Kelly, and B. C. Muddle, "Transformation Toughening in Zirconia-Containing Ceramics," *Journal of the American Ceramic Society*, vol. 83, pp. 461–487, (2000).

[38] P. M. Kelly and L. R. Francis Rose, "The martensitic transformation in ceramics — its role in transformation toughening," *Progress in Materials Science*, vol. 47, pp. 463–557, (2002).

[39] C. J. Kuehmann, *Thermal processing optimization of nickel-cobalt ultrahigh-strength steels*. Phd thesis, Northwestern University, Evanston Illinois, (1994).

[40] H. E. Lippard, *Microanalytical Investigations of Transformation Toughened Co-Ni Steels*. Phd thesis, Northwestern University, Evanston, Illinois, (1999).

[41] W. W. Geberich, P. L. Hemmings, V. F. Zackay, and E. R. Parker, "Interactions between crack growth and strain-induced transformation," *International Conference on Fracture*, (1969).

[42] S. D. Antolovich and B. Singh, "On the toughness increment associated with the austenite to martensite phase transformation in TRIP steels," *Metallurgical and Materials Transactions B*, vol. 2, pp. 2135–2141, (1971).

[43] I. Tamura, "Deformation-induced martensitic transformation and transformation-induced plasticity in steels," *Metal Science*, vol. 16, pp. 245–253, (1982).

[44] S. Chatterjee and H. K. D. H. Bhadeshia, "Transformation induced plasticity assisted steels: stress or strain affected martensitic transformation?," *Materials Science and Technology*, vol. 23, pp. 1101–1104, (2007).

[45] V. F. Zackay, E. R. Parker, D. Fahr, and R. Busch, "The Enhancement of Ductiliy in High-Strength Steels," *Transactions of the ASM*, pp. 252–259, (1967).

[46] A. Perlade, O. Bouaziz, and Q. Furnémont, "A physically based model for TRIP-aided carbon steels behaviour," *Materials Science and Engineering: A*, vol. 356, pp. 145–152, (2003).

[47] R. P. Reed and R. E. Schramm, "Lattice Parameters of Martensite and Austenite in Fe-Ni Alloys," *Journal of Applied Physics*, vol. 40, pp. 3453–3458, (1969).

[48] E. P. Abrahamson II and S. L. Lopata, "The lattice parameters and solubility limits of alpha iron as affected by some binary transition-element additions," *Transactions of the Metallurgical Society of AIME*, vol. 236, pp. 76–87, (1966).

[49] L. Zwell, D. E. Carnahan, and G. R. Speich, "Lattice parameter of ferritic and martensitic Fe−Ni alloys," *Metallurgical Transactions*, vol. 1, pp. 1007–1009, (1970).

[50] R. J. Weiss, "The Origin of the "INVAR" effect," *Materials Research Laboratory, U.S. Army Materials Research Agency, Watertown Massachussetts*, vol. (1963).

[51] L. Cheng, A. Böttger, Th. H. de Keijser, and E. J. Mittemeijer, "Lattice parameters of iron-carbon and iron-nitrogen martensites and austenites," *Scripta Metallurgica et Materialia*, vol. 24, pp. 509–514, (1990).

[52] N. Ridley and H. Stuart, "Partial Molar Volumes from High-Temperature Lattice Parameters of Iron–Carbon Austenites," *Metal Science*, vol. 4, pp. 219–222, (1970).

[53] J. M. Moyer and G. S. Ansell, "The volume expansion accompanying the martensite transformation in iron-carbon alloys," *Metallurgical Transactions A*, vol. 6, pp. 1785–1791, (1975).

[54] A. Shibata, H. Yonezawa, K. Yabuuchi, S. Morito, T. Furuhara, and T. Maki, "Relation between martensite morphology and volume change accompanying fcc to bcc

martensitic transformation in Fe–Ni–Co alloys," *Materials Science and Engineering: A*, vol. 438–440, pp. 241–245, (2006).

[55] K.J. Kim and L.H. Schwartz, "On the effects of intercritical tempering on the impact energy of fe-9ni-0.1c," *Materials Science and Engineering*, vol. 33, pp. 5–20, (1978).

[56] C. K. Syn, B. Fultz, and J. W. Morris, "Mechanical stability of retained austenite in tempered 9Ni steel," *Metallurgical Transactions A*, vol. 9, pp. 1635–1640, (1978).

[57] A. Kokosza and J. Pacyna, "Mechanical Stability of Retained Austenite in Unalloyed Structural Steels of Various Carbon Content," *Archives of Metallurgy and Materials*, vol. 55, (2010).

[58] T. Waitz, T. Antretter, F. D. Fischer, and H. P. Karnthaler, "Size effects on martensitic phase transformations in nanocrystalline NiTi shape memory alloys," *Materials Science and Technology*, vol. 24, pp. 934–940, (2008).

[59] M. Grujicic, "Design of precipitated austenite for dispersed-phase transformation toughening in high strength Co-Ni steels," *Materials Science and Engineering: A*, vol. 128, pp. 201–207, (1990).

[60] J. Speer, D. K. Matlock, B. C. De Cooman, and J. G. Schroth, "Carbon partitioning into austenite after martensite transformation," *Acta Materialia*, vol. 51, pp. 2611–2622, (2003).

[61] C. Garcia-Mateo, F. G. Caballero, M. K. Miller, and J. A. Jimenez, "On measurement of carbon content in retained austenite in a nanostructured bainitic steel," *Journal of Materials Science*, vol. 47, pp. 1004–1010, (2012).

[62] G. B. Olson and M. Cohen, "Stress-Assisted Isothermal Martensitic Transformation: Application to TRIP Steels," *Metallurgical Transactions A*, vol. 13A, pp. 1907–1914, (1982).

[63] P. M. Novotny and G. E. Maurer, "Ultra-high-strength steels VS titanuim alloys," (2007).

[64] K. S. Cho, J. H. Choi, H. S. Kang, S. H. Kim, K. B. Lee, H. R. Yang, and H. Kwon, "Influence of rolling temperature on the microstructure and mechanical properties of secondary hardening high Co–Ni steel bearing 0.28 wt% C," *Materials Science and Engineering: A*, vol. 527, pp. 7286–7293, (2010).

[65] J. H. Graves, "Effect of Heat Treatment on the Microstructure and Properties of AerMet 100 Steel," (1994). Diploma thesis, Worchester Polytechnic Institute.

[66] Aermet 100 Data sheet. http://cartech.ides.com/datasheet.aspx?i=101&e=161&c, Juni 2015.

[67] Aermet 310 Data sheet. http://cartech.ides.com/datasheet.aspx?i=103&e=158&c=techart, Juni 2015.

[68] Aermet 340 Data sheet. http://cartech.ides.com/datasheet.aspx?i=101&e=338&c, Juni 2015.

[69] AF1410 Data sheet. http://customer.cartech.com/assets/documents/datasheets/AF1410.pdf, Juni 2015.

[70] HY 180 Data sheet. http://customer.cartech.com/assets/documents/datasheets/HY-180.pdf, Juni 2015.

[71] M. Gruber, *Microstructure and mechanical properties of the AerMet® 100 alloy.* (2012). Diploma Thesis, Montanuniversity of Leoben.

[72] H. M. Lee, H. Sohn, and C. H. Yoo, "Isothermal M2C carbide growth in ultrahigh strength high Co-Ni steels," *Scripta Materialia*, vol. 37, pp. 1931–1937, (1997).

[73] H. Zhengfei and W. Xingfang, "High resolution electron microscopy of precipitates in high Co–Ni alloy steel," *Micron*, vol. 34, pp. 19–23, (2003).

[74] K. J. Handerhan, W. M. Garrison, and N. R. Moody, "A comparison of the fracture behavior of two heats of the secondary hardening steel AF1410," *Metallurgical Transactions A*, vol. 20, pp. 105–123, (1989).

[75] W. M. Garrison and N. R. Moody, "The influence of inclusion spacing and microstructure on the," vol. 18, pp. 1257–1263, 1987.

[76] W. M. Garrison and K. J. Handerhan, "Fracture Toughness: Particle-Dispersion Correlation," *Innovations in Ultrahigh-Strength Steel Technology, Proceedings of the 34th Sagamore Conference held August 30 - September 3, 1987 Lake George, New York*, pp. 443–466.

[77] W. Sha, *Maraging steels, Modelling of microstructure, properties and applications*. Woodhead Publishing Limited, (2009).

[78] U. K. Viswanathan, G. K. Dey, and M. K. Asundi, "Precipitation hardening in 350 grade maraging steel," *Metallurgical Transactions A*, vol. 24, pp. 2429–2442, (1993).

[79] U. K. Viswanathan, G. K. Dey, and V. Sethumadhavan, "Effects of austenite reversion during overageing on the mechanical properties of 18 Ni (350) maraging steel," *Materials Science and Engineering: A*, vol. 398, pp. 367–372, (2005).

[80] R. Schnitzer, G. A. Zickler, E. Lach, H. Clemens, S. Zinner, T. Lippmann, and H. Leitner, "Influence of reverted austenite on static and dynamic mechanical properties of a PH 13-8 Mo maraging steel," *Materials Science and Engineering: A*, vol. 527, pp. 2065–2070, (2010).

[81] A. Markfeld and A. Rosen, "The effect of reverted austenite on the plastic deformation of maraging steel," *Materials Science and Engineering*, vol. 46, pp. 151–157, (1980).

[82] M. K. Miller, *Atom probe field ion microscopy*, vol. 52. Clarendon Press and Oxford University Press, (1996).

[83] EN ISO 6507 - 1, Standard for Metallic-materials - Vickers hardness test, (1997).

[84] A. Young, *The Rietveld Method*. Oxford Universitiy Press, (2002).

[85] A. Le Bail, H. Duroy, and J. L. Fourquet, "Ab-initio structure determination of LiSbWO6 by X-ray powder diffraction," *Materials Research Bulletin*, vol. 23, pp. 447–452, (1988).

[86] G. S. Pawley, "Unit-cell refinement from powder diffraction scans," *Journal of Applied Crystallography*, vol. 14, pp. 357–361, (1981).

[87] *DIFFRACplus, TOPAS 4.2 User Manual*. BRUKER AXS GmbH, Karlsruhe, Germany, (2009).

[88] H. Leitner, *Kinetics of secondary hardening precipitations in high-speed steels*. PhD thesis, (2002).

[89] EN ISO 6892 - 1, Standard for Metallic-materials - Tensile testing, (2009).

[90] ASTM E 399 - 09, Standard Test Method for Linear-Elastic Plane-Strain Fracture Toughness KIC of Metallic Materials, (2009).

[91] O. Kolednik and H. P. Stüwe, "The stereophotogrammetric determination of the critical crack tip opening displacement," *Engineering Fracture Mechanics*, vol. 21, pp. 145–155, (1985).

[92] J. Stampfl, S. Scherer, M. Berchthaler, M. Gruber, and O. Kolednik, "Determination of the fracture toughness by automatic image processing," *International Journal of Fracture*, vol. 78, pp. 35–44, (1996).

[93] O. Kolednik and H. P. Stüwe, "An extensive analysis of a JIC-test," *Engineering Fracture Mechanics*, vol. 24, pp. 277–290, (1986).

[94] ESIS P2-92, "ESIS Procedure for determining the fracture behaviour of materials," 1992.

[95] TCFE7-TCS steels/Fe-alloys database, Thermo-Calc version 3.0.1, Foundation of Computational Thermodynamics Stockholm.

[96] MOB2 - TCS Alloy Mobility Database, DICTRA version 24, Foundation for Computational Thermodynamics Stockholm.

[97] TCFE3-TCS steels/Fe-alloys database, Thermo-Calc version R, Foundation of Computational Thermodynamics Stockholm.

[98] E. Kozeschnik, "MatCalc Version 5.61, Vienna University of Technology."

[99] MatCalc, Thermodynamic Database mc_fe_v2.040.tdb, Vienna University of Technology.

[100] MatCalc, Mobility Database mc_fe_v2.006.ddb, Vienna University of Technology.

[101] M. Gruber, G. Ressel, F. Mendez Martin, S. Ploberger, S. Marsoner, and R. Ebner, "Formation and growth kinetics of reverted austenite during tempering of a high Co-Ni steel," *to be submitted to Metallurgical and Materials Transactions A*, (2016).

[102] O. C. Hellman, J. A. Vandenbroucke, J. Rüsing, D. Isheim, and D. N. Seidman, "Analysis of Three-dimensional Atom-probe Data by the Proximity Histogram," *Microscopy and Microanalysis Vol. 6*, pp. 437–444, (2000).

[103] P. V. Morra, A. J. Böttger, and E. J. Mittemeijer, "Decomposition of iron-based martensite; A kinetic analysis by means of differential scanning calorimetry and dilatometry," *Journal of Thermal Analysis and Calorimetry*, vol. 64, pp. 905–914, (2001).

[104] M. Gruber, G. Ressel, S. Ploberger, S. Marsoner, and R. Ebner, "Characterization of the effect of cryogenic treatment on the tempering behavior of a secondary hardening high Co-Ni steel high Co-Ni steel," *IOP Conference Series: Materials Science and Engineering*, vol. 119, (2016).

[105] G. R. Speich and W. C. Leslie, "Tempering of steel," *Metallurgical Transactions*, vol. 3, pp. 1043–1054, (1972).

[106] T. Waterschoot, K. Verbeken, and B. C. De Cooman,, "Tempering Kinetics of the Martensitic Phase in DP Steel," *ISIJ International*, vol. 46, pp. 138–146, (2006).

[107] L. Cheng, C. M. Brakman, B. M. Korevaar, and E. J. Mittemeijer, "The tempering of iron- carbon martensite; dilatometric and calorimetric analysis," *Metallurgical Transactions A*, vol. 19, pp. 2415–2426, (1988).

[108] J. Pacyna, "Dilatometric investigations of phase transformations at heating and cooling of hardened, unalloyed, high carbon steels," *Journal of Achievements in Materials and Manufacturing Engineering*, vol. 46, pp. 7–17, (2011).

[109] P. Bala, J. Pacyna, and J. Krawczyk, "The kinetics of phase transformations during tempering in the new hot working steel," *Journal of Achievements in Materials and Manufacturing Engineering*, vol. 22, pp. 15–18, (2007).

[110] P. Bala, J. Pacyna, and J. Krawczyk, "Continuous heating from as-quenched state in a new hot-work steel," vol. 28, pp. 517–524, 2007.

[111] K.-E. Thelning, *Steel and its heat treatment.* Butterworth & Co Publishers Ltd, (1978).

[112] Z. Guo, *The Limit of Strength and Toughness of Steel.* PhD thesis, University of California, Berkeley, (2001).

[113] R. Kapoor, L. Kumar, and I. Batra, "A dilatometric study of the continuous heating transformations in 18wt.% Ni maraging steel of grade 350," *Materials Science and Engineering: A*, vol. 352, pp. 318–324, (2003).

[114] F. Moszner, E. Povoden-Karadeniz, S. Pogatscher, P. J. Uggowitzer, Y. Estrin, S. S. A. Gerstl, E. Kozeschnik, and J. F. Löffler, "Reverse α'- γ transformation mechanisms of martensitic fe–mn and age-hardenable fe–mn–pd alloys upon fast and slow continuous heating," vol. 72, pp. 99–109, 2014.

[115] B. Jeyaganesh, S. Raju, S. Murugesan, E. Mohandas, and M. Vijayalakshmi, "A Study on the Effect of Thermal Ageing on the Specific-Heat Characteristics of 9Cr–1Mo–0.1C (mass%) Steel," *International Journal of Thermophysics*, vol. 30, pp. 619–634, (2009).

[116] S. Raju, B. Jeya Ganesh, A. K. Rai, R. Mythili, S. Saroja, E. Mohandas, M. Vijayalakshmi, K. Rao, and B. Raj, "Measurement of transformation temperatures and specific heat capacity of tungsten added reduced activation ferritic–martensitic steel," *Journal of Nuclear Materials*, vol. 389, pp. 385–393, (2009).

[117] M. Gruber, S. Ploberger, M. Wiessner, S. Marsoner, and R. Ebner, "Influence of heat treatment on the stability of austenite in a high Co-Ni secondary hardening steel," *Proceedings of the International Conference on Solid-Solid Phase Transformations in Inorganic Materials 2015, Whistler*, pp. 115–122.

[118] L. Spieß, G. Teichert, R. Schwarzer, B. H., and G. C., *Moderne Röntgenbeugung, Röntgendiffraktometrie für Materialwissenschaftler, Physiker und Chemiker*. Vieweg+Teubner GWV Fachverlage GmbH, Wiesbaden, (2009).

[119] *DIFFRACplus, TOPAS/TOPAS R/TOPAS P Version 3.0 User's Manual*. BRUKER AXS GmbH, Karlsruhe, West Germany, (2005).

[120] M. Gruber, S. Ploberger, M. Wiessner, S. Marsoner, and R. Ebner, "Influence of Heat Treatment on the Microstructure of a High Co-Ni Secondary Hardening Steel," *Materials Today: Proceedings*, vol. 2, pp. 949–952, (2015).

[121] L. Xiao, Z. Fan, Z. Jinxiu, Z. Mingxing, K. Mokuang, and G. Zhenqi, "Lattice-parameter variation with carbon content of martensite. I. X-ray-diffraction experimental study," *Physical Review B*, vol. 52, pp. 9970–9978, (1995).

[122] A. Einstein, "Über die von der molekularkinetischen Theorie der Wärme geforderte Bewegung von in ruhenden Flüssigkeiten suspendierten Teilchen," *Annalen der Physik*, vol. (1905), pp. 549–560.

[123] H. K. D. H. Bhadeshia, "Materials Science & Metallurgy, Course MP6, Ki-

netics and Microstructure Modelling, Lecture 3: Introduction to Diffusion." http://www.msm.cam.ac.uk/phase-trans/mphil/MP6-3.pdf, (2015).

8 Publications

Publication I M. Gruber, S. Ploberger, M. Wiessner, S. Marsoner, and R. Ebner, "Influence of Heat Treatment on the Microstructure of a High Co-Ni Secondary Hardening Steel", Materials Today: Proceedings, vol. 2, pp. 949-952, (2015).

Publication II M. Gruber, S. Ploberger, M. Wiessner, S. Marsoner, and R. Ebner, "Influence of heat treatment on the stability of austenite in a high Co-Ni secondary hardening steel", Proceedings of the International Conference on Solid-Solid Phase Transformations in Inorganic Materials 2015, Whistler, pp. 115-122.

Publication III M. Gruber, S. Ploberger, G. Ressel, M. Wiessner, M. Hausbauer, S. Marsoner, and R. Ebner, "Effects of the combined heat and cryogenic treatment on the stability of austenite in a high Co-Ni steel", Archives of Metallurgy and Materials, Vol 60, Issue 3, pp. 2131-2137, (2015).

Publication IV M. Gruber , G. Ressel, S. Ploberger, S. Marsoner, and R. Ebner, "Characterization of the effect of cryogenic treatment on the tempering behavior of a secondary hardening high Co-Ni steel high Co-Ni steel", IOP Conference Series: Materials Science and Engineering, vol. 119, (2016).

Publication V M. Gruber, G. Ressel, F. Mendez Martin, S. Ploberger, S. Marsoner, and R. Ebner, "Formation and growth kinetics of reverted austenite during tempering of a high Co-Ni steel", to be submitted to Metallurgical and Materials Transactions A, (2016).

Publication I

Available online at www.sciencedirect.com

ScienceDirect

materialstoday: PROCEEDINGS

Materials Today: Proceedings 2S (2015) S949 – S952

International Conference on Martensitic Transformations, ICOMAT-2014

Influence of heat treatment on the microstructure of a high Co-Ni secondary hardening steel

M. Gruber[a,*], S. Ploberger[b], M. Wiessner[a], S. Marsoner[a], R. Ebner[a]

[a]*Materials Center Leoben Forschung GmbH, Roseggerstrasse 12, A-8700 Leoben, Austria*
[b]*Böhler Edelstahl GmbH & Co KG, Mariazeller Strasse 25, A-8605 Kapfenberg, Austria*

Abstract

The aim of this study was to analyze the influence of combined heat and cryogenic treatment on the evolution of martensite and reverted austenite in a high Co-Ni steel. To this end the evolution of phase fractions and lattice constants after thermal treatments were characterized by using X-ray diffraction (XRD) investigations and dilatometer analyses. The arrangement of phases and the element distribution in martensite, austenite and carbides were analyzed by using energy filtered transmission electron microscopy (EFTEM).

Selection and Peer-review under responsibility of the chairs of the International Conference on Martensitic Transformations 2014.

Keywords: Reverted austenite; cryogenic treatment; lattice parameter measurements; EFTEM investigations;

1. Introduction

High Co-Ni secondary hardening steels are known for their excellent properties concerning high fracture toughness combined with high hardness [1, 2]. The unique mechanical properties of this martensitic steel grade are ascribed to the formation of reverted austenite after aging and its stability during plastic deformation. Reverted austenite can be varied in composition, size and phase fraction due to heat treatment parameters. Haidemenopoulos [3] described that the stability is so much higher the smaller the austenite particles are and the

* Corresponding author. Tel.: +43-3842-45922502
E-mail address: Marina.Gruber@mcl.at

Selection and Peer-review under responsibility of the chairs of the International Conference on Martensitic Transformations 2014.
doi:10.1016/j.matpr.2015.07.439

more the austenite is enriched in austenite stabilizers like carbon, nickel and manganese. Ayer and Machmeier [1] and Lippard [4] found that reverted austenite in high Co-Ni steels is enriched in nickel which is known as an austenite stabilizing element.

The aim of this investigation was to gain a deeper understanding of the influence of the applied combined heat and cryogenic treatment on the evolution of microstructure including martensite and austenite.

2. Experimental

The investigated material was a martensitic steel with a chemical composition according to Table 1.

Table 1. Chemical composition of the investigated alloy in weight percent.

	C	Ni	Co	Cr	Mo
wt.-%	0.22	11	13.5	2.9	1.2

Heat treatment of test samples comprised in a first step of austenitization at 885 °C for 1 h in a vacuum furnace followed by a cryogenic treatment in a freezing unit. In a second step the specimens were tempered in a batch furnace for various times and at specific temperature levels. Dilatometer measurements were carried out by heating samples to 885 °C/1 h and cooling down to -100 °C with a cooling rate of about 1.67 K/s.

The dilatometer investigations were applied on a DIL 805A dilatometer from TA Instruments (formerly BAEHR) to characterize the phase evolution during martensitic transformation while cooling down to cryogenic temperatures.

Phase fraction analysis after cryogenic treatment at different temperatures was carried out by X-ray diffraction (XRD) on a Xstress 3000 G2 diffractometer from Stresstech.

The influence of cryogenic and subsequent aging treatment on the evolution of phase fraction and lattice parameters of austenite and martensite was analyzed ex-situ by means of XRD using a D8 Discover diffractometer from Bruker AXS.

The morphology and chemical composition of austenite and martensite in the quenched and tempered microstructure were characterized by energy filtered transmission electron microscopy (EFTEM) using a FEI Tecnai F20 microscope as well as by dark field microscopy using a Philips CM20 TEM at the Austrian Centre for Electron Microscopy and Nanoanalysis.

3. Results and discussion

3.1. Martensitic transformation behavior during quenching

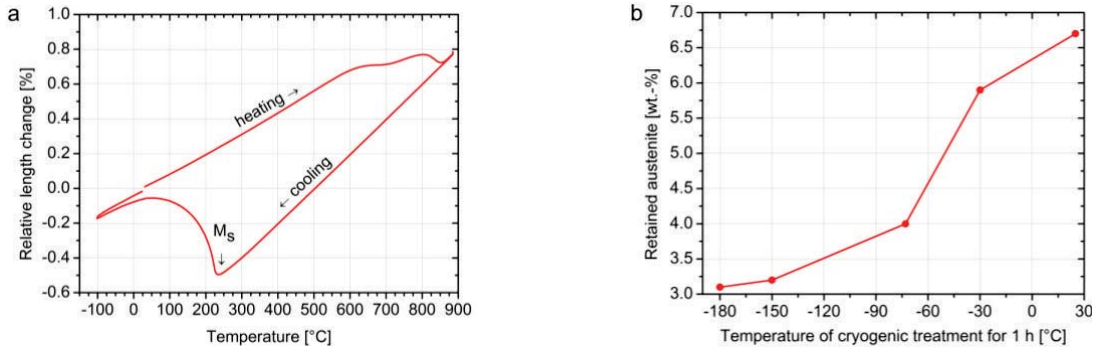

Fig. 1. (a) Dilatometer measurement during heating to 885 °C/1 h and cooling down to -100 °C; (b) XRD measurements after austenitizing at 885 °C/1 h and cooling down to temperatures between 25 °C and -180 °C.

The dilatometer and XRD measurements are summarized in Fig. 1. From the dilatometer investigations it can be concluded that most of the martensitic transformation is completed after cooling to about -50 to -80 °C as the slope

of the curve is not changing any more on further cooling. XRD measurements indicate about 7 wt.-% retained austenite after cooling to room temperature. During further cooling the retained austenite decreases, but about 3 wt.-% of retained austenite are still present even after cryogenic treatment at -180 °C.

3.2. Morphology and chemical composition of phases

A bright-field image of the martensitic microstructure is displayed in Fig. 2a and the corresponding dark field image which was taken using austenite reflections for imaging is shown in Fig. 2b. The bright areas in the dark-field image are indicating austenite films which are located at martensite lath boundaries. These austenite films have a thickness ranging from 20 to 100 nm.

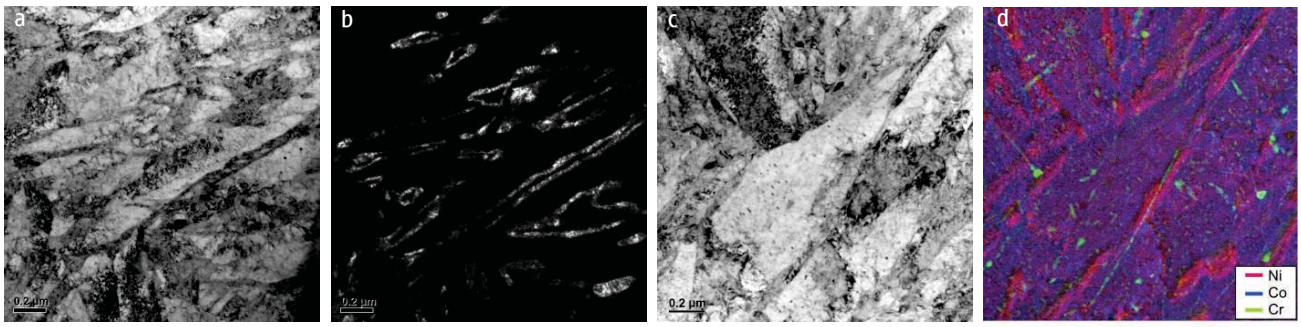

Fig. 2. (a) Bright-field image; (b) dark-field image from same position as (a) using austenite reflections for imaging; (c) bright field image; (d) corresponding nickel, cobalt and chromium map after austenitizing at 885 °C/1 h, cryogenic treatment at -73 °C/1 h and aging at 600 °C/5 h.

As reported in former studies [3, 4] reverted austenite tends to be enriched in nickel. Hence it was tried to evaluate the austenite distribution via EFTEM. A bright-filed image and the corresponding element distribution map of nickel, cobalt and chromium are depicted in Fig. 2c and d. The nickel enriched zones shown in the EFTEM investigations have similar form and morphology as the austenite films shown in the dark-field image. This leads to the conclusion that the nickel enriched and cobalt depleted regions are austenite films. Chromium is mainly precipitated in carbides.

3.3. Development of phase fraction and lattice parameters during tempering

The phase fraction analysis of austenite after isothermal tempering at 482 °C, 540 °C and 600 °C for different tempering times is presented in Fig. 3a. Tempering generally causes an increase of austenite phase fraction. Austenite that is formed during tempering is referred to reverted austenite. It is to emphasize that austenite phase fraction of non-cryogenically treated samples decreases from about 6 wt.-% after austenitizing to 2 wt.-% during tempering at 482 °C up to tempering times of about 1 h while the austenite phase fraction then again slightly increases for longer tempering times.

Fig. 3b shows the results of lattice parameter measurements of martensite. Aging at 540 °C and 600 °C causes a fast reduction of martensite lattice parameter within less than 10 min of aging. For aging at 482 °C this decrease of the lattice parameter takes 5 h to 10 h. It is assumed that the reason for this reduction is the depletion of carbon and carbide forming alloying elements from martensite as this causes a decrease of martensite lattice parameter [5, 6].

Austenite lattice parameters are illustrated in Fig. 3c. During tempering at 600 °C the lattice constant is raised to a more or less constant value within less than 10 min. For tempering at 540 °C it takes about 3 h and for tempering at 482 °C it takes up to 50 h to achieve a steady value of the lattice parameter. The increase of lattice parameter of austenite can be correlated with nickel enrichment and cobalt depletion which is in agreement with findings of lattice parameters described in literature [4, 7] and with EFTEM investigations highlighted in Fig. 2d.

Tempering at 482 °C causes a fast increase of austenite lattice parameter and a corresponding decrease of the martensite lattice parameter within a few minutes but the lattice parameters do not reach the same values as for

tempering at the higher temperatures. As carbon increases the lattice parameters in both austenite and martensite [6] the observed effects can be assigned to carbon enrichment in austenite and carbon depletion in martensite due to formation of carbides in martensite. The development of the lattice parameter for tempering at 482°C around 1 hour tempering time is attributed to the formation of secondary hardening carbides as peak hardness is reached at this time [8]. It is assumed that austenite lattice parameter is reduced after 482 °C/0.5 - 1 h as a result of carbon depletion due to carbide precipitation.

It is argued from the reduction of the austenite content during tempering of the non-cryogenically treated specimens at 482 °C that this is mainly caused by carbon depletion especially for short tempering times, at longer tempering times the nickel enrichment of the austenite starts to re-stabilize the austenite. The austenite content prior to tempering is higher without cryogenic treatment than with cryogenic treatment which causes differences in the mass balances between austenite and martensite. It is expected that lower initial austenite content results in thinner austenite films which can be more easily enriched with carbon and nickel and depleted from cobalt than thicker films. Therefore, no reduction of austenite is observed after tempering of cryogenically-treated samples at 482 °C because of the higher austenite stability.

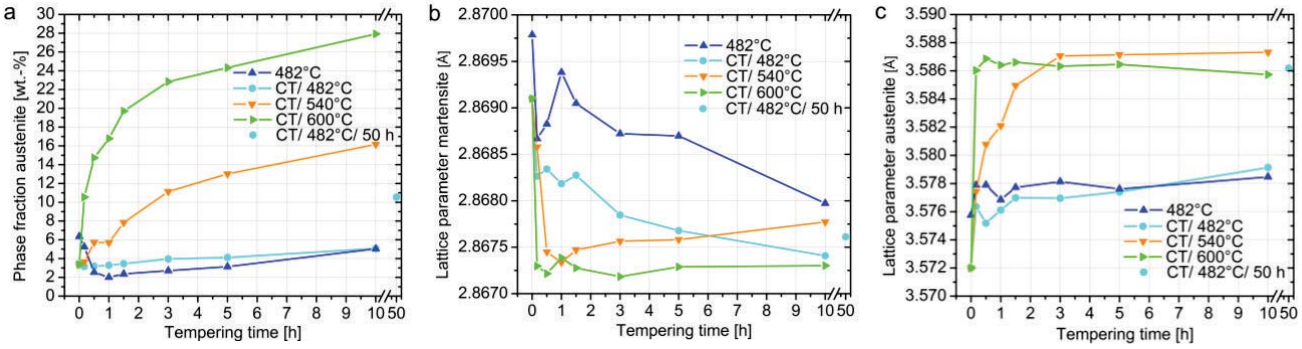

Fig. 3. (a) Evolution of phase fraction of austenite; (b) evolution of martensite lattice parameter; (c) evolution of austenite lattice parameter after austenitizing at 885 °C with and without cryogenic treatment (CT) at -73 °C/1 h and aging at 482 °C, 540 °C and 600 °C.

4. Conclusion

From dilatometer and XRD investigations it is concluded that most of the martensitic transformation has not been fully completed and about 3 wt.-% of retained austenite are still present after cryogenic treatment at -180 °C.

EFTEM investigations reveal that austenite has been nickel enriched and cobalt depleted during tempering at 600 °C/5 h. For shorter tempering times and lower tempering temperatures the alloying element separation is less pronounced.

It is expected that reduction of austenite content at 482 °C without refrigeration is a consequence of destabilization of austenite due to depletion of carbon which is not counterbalanced by sufficient nickel enrichment. Austenite is stabilized again as tempering continues due to continuous nickel enrichment of austenite.

References

[1] R. Ayer, P.M. Machmeier, Metall. Trans. A 24 (1993) 1943-1955.
[2] K. Sato, Dissertation, Universitiy of California, Berkeley (2002).
[3] G.N. Haidemenopoulos, Dissertation, Massachusetts Institute of Technology (1988).
[4] E. H. Lippard, Dissertation, Northwestern Universitiy, Evanston Illinois (1999).
[5] E.P. Abrahamson, S.L. Lopata, Trans. AIME 236 (1966) 76-87.
[6] L. Cheng, A. Böttger, Th.H. Keijser, E. Mittemeijer, Scripta Metall. Mater. 24 (1990) 509-514.
[7] R.P. Reed, R.E Schramm, J. Appl. Phys. 40 (1969) 3453-3458.
[8] C.H. Yoo, H.M. Lee, J.W. Chan, J.W. Morris, Metall. Trans. A 27 (1996) 3466-3472.

Publication II

Proceedings of the International Conference on Solid-Solid Phase Transformations in Inorganic Materials 2015
Edited by: Matthias Militzer, Gianluigi Botton, Long-Qing Chen, James Howe, Chadwick Sinclair, and Hatem Zurob

INFLUENCE OF HEAT TREATMENT ON THE STABILITY OF AUSTENITE IN A HIGH Co-Ni SECONDARY HARDENING STEEL

Marina Gruber[1], Sarah Ploberger[2], Manfred Wiessner[1], Stefan Marsoner[1], Reinhold Ebner[1]

[1] Materials Center Leoben Forschung GmbH, Roseggerstrasse 12, Leoben, A-8700 Austria
[2] Böhler Edelstahl GmbH & Co KG, Mariazeller Strasse 25, Kapfenberg, A-8605 Austria

Keywords: high Co-Ni steel, heat treatment, phase evolution, reverted austenite, retained austenite, X-ray diffraction, dilatometer investigations

Abstract

Mechanical properties of high Co-Ni high strength steels like Aermet 100 and AF1410 are strongly influenced by the stability of austenite. As austenite plays a major role regarding the mechanical properties in this class of steel, the aim of this work was to get a deeper understanding on the influence of heat treatment on transformation behavior of retained and reverted austenite.
The investigations focus on the evolution of the phase fraction of austenite after tempering at different temperatures and times and on the stability of the austenite formed during tempering. The austenite phase fraction after tempering was determined quantitatively by means of X-ray diffraction analyses and the stability of the austenite was characterized by means of dilatometry investigations by studying the transformation behavior of the austenite during cooling from tempering temperature down to -100°C.

Introduction

Steels like maraging steels or high Co-Ni steels obtain parts of their excellent toughness properties from reverted austenite [1, 2, 3]. The stability of austenite, i.e. its resistance against martensitic phase transformation during straining, has major influence on toughness of these types of steels. Haidemenopoulos [4] concluded that the stability of austenite is influenced by its chemical composition, the size of austenite precipitates, the stress state and the strength of the matrix. The strength of the matrix indirectly influences the stability of austenite by providing mechanical driving force additionally to the total driving force for martensitic transformation. The hydrostatic stress state is influencing austenite to martensite transformation due to the volume change during transformation. Several investigations also describe that austenite shows increasing resistance to transformation with decreasing grain size [4, 5, 6]. This is explained by Haidemenopoulos [7] by the fact that smaller austenite grains have lower number of preexistent nucleation sites for phase transformation. Others claim that in shape memory alloys transformation of small austenite grains is harder due to increasing energy barrier for transformation with decreasing grain size [8]. In steels with reverted austenite, at least one austenite stabilizing element, which enables austenite formation during tempering, is present. Typical elements for such austenite stabilizers are nickel and manganese. The more austenite is enriched with these elements the more it gets stabilized [7, 9, 10].
However, in Aermet 100 there are two types of austenite present after tempering. Retained austenite occurs just after quenching from austenitization temperature and even after cryogenic

treatment [11]. Retained austenite tends to be unstable, even though its small size because chemical stabilization cannot be easily obtained by tempering parameters. Compared to retained austenite, reverted austenite starts to grow in Aermet 100 above tempering temperatures of approximately 450°C [12]. Lippard [10] described that reverted austenite is enriched in nickel in Aermet 100.
For high Ni-Co steels there are many calculations and thermodynamic simulations which predict the stability for different kinds of austenite [3, 7, 9, 10]. However, there is lack of experimental results on stability of austenite in this class of steels. It is the intention of this work to present experimental results on the stability of austenite in a 0.22 % C, 11 % Ni, 13.5 % Co, 2.9 % Cr, 1.2 % Mo steel.
To this end quantitative X-ray diffraction analyses were carried out before and after tempering treatment to determine the austenite content. Dilatometry measurements were employed to characterize transformation behavior of austenite when cooling specimens after tempering to room or even lower temperature. The investigations allow to draw conclusions on the effect of different tempering treatments on the stability of austenite.

Experimental

The composition of the material investigated in this paper is displayed in Table I.

Table I. Chemical composition of the investigated steel in wt.-%.

	C	Ni	Co	Cr	Mo
wt.-%	0.22	11	13.5	2.9	1.2

In order to study the effect of heat treatment on austenite phase fraction and austenite stability all specimens were austenitized in a vacuum furnace at 885°C/ 1 h followed by controlled cooling with a cooling rate of 10°C/ min. Subsequently, tempering of the samples for X-ray analyses was carried out in a batch furnace at temperatures of 540°C and 600°C at various times between 10 min to 5 h.
The heat treated specimens were then characterized regarding phase composition by means of quantitative high precision X-ray diffraction (XRD). The XRD measurements were carried out on a D8 Discover diffractometer from Bruker AXS in the as quenched condition and after tempering. Cr-K_α radiation was used with a wavelength of 2.29 Å. For the quantitative determination of phase fractions the Rietveld method was applied [13].
Dilatometer measurements were carried out on a DIL 805A dilatometer from TA Instruments (formerly BAEHR). The samples for the dilatometer measurements were tubular and had a length of 10 mm, an outer diameter of 4 mm and a wall thickness of 1 mm. Tempering treatment of the austenitized samples was done in dilatometer at 540°C and 600°C for 1 h and 5 h. Heating up to tempering temperature and cooling after tempering was performed at 100°C/ min. Quenching was done down to -100°C with a freezing unit from TA instruments. Freezing was carried out with the aid of helium, which was cooled before with liquid nitrogen and guided through the hollow dilatometer samples. Discontinuous length changes of the specimen during the thermal cycle were taken as indication for austenite to martensite phase transformation, which is connected with a volume change.

Results

Phase Fraction Analysis after Tempering

In Figure 1 the result of phase fraction analyses after quenching and after different tempering treatments is shown. Just after quenching the alloy exhibits retained austenite with a phase fraction of about 6 wt.%, as indicated by the values for tempering time 0 h. The austenite content varies due to tempering at 540°C and 600°C. While the austenite content steadily increases in the investigated time regime (> 10 min) after tempering at 600°C, it decreases after tempering at 540°C within less than 10 min before it increases again for increasing tempering times.
The increase of austenite content is connected with the formation of reverted austenite. After 5 h of tempering the fraction of austenite reaches about 25 wt.% for the at 600°C and 15 wt.% for the at 540°C tempered sample. The increase of austenite fraction at 600°C is thus much more pronounced than for tempering at 540°C.
The reduction of austenite after tempering at 540°C for tempering times less than 60 min is argued to be related to martensite transformation during cooling. It is supposed that reverted austenite formation during tempering (austenite gain) and austenite to martensite phase transformation (austenite loss) during cooling are competitive processes. In order to study the austenite to martensite phase transformation during cooling dilatometry investigations were conducted.
Please note that the austenite content during tempering is higher than indicated in Figure 1 because parts of the austenite transform to martensite during cooling as pointed out in the following chapter. High temperature XRD experiments, which are not shown in this work, revealed that the austenite phase fraction is between 1 to 5 wt.% higher than indicated by the curves displayed in Figure 1.

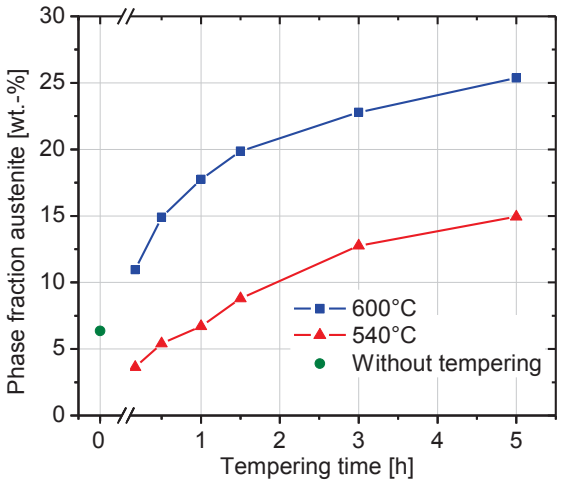

Figure 1. Measurements of phase fraction of austenite just after quenching from austenitization temperature (tempering time: 0 h) and after tempering for various tempering times at 540°C and 600°C; measurements were carried out at room temperature; measuring inaccuracy ±1 %.

Investigation of Transformation Behavior

In Figure 2 relative length change of cooling curves determined in the dilatometer after tempering at 540°C for 1 h and 5 h and subsequent cooling to -100°C are displayed. Due to different tempering times, different start values of the length change curves are present. There is clear evidence from the volume increase that a phase transformation from austenite to martensite is starting at about 210°C in the sample tempered for 1 h while martensitic phase transformation is starting at about 170°C in the sample tempered for 5 h.

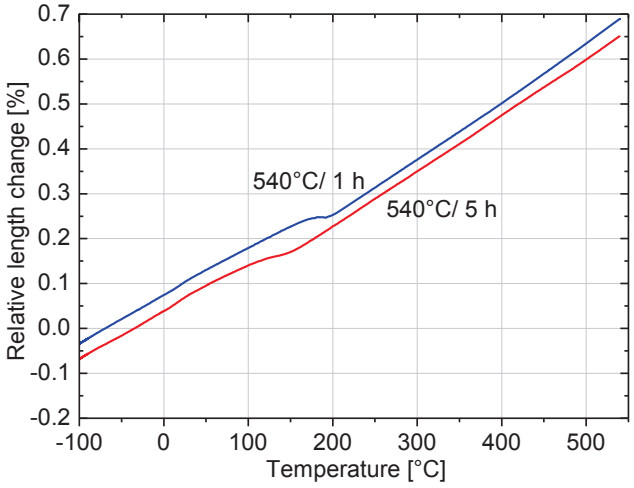

Figure 2. Relative length change during cooling after tempering for 1 h and 5 h at 540°C; rate for heating up to tempering temperature and cooling from tempering temperature was 100°C/ min.

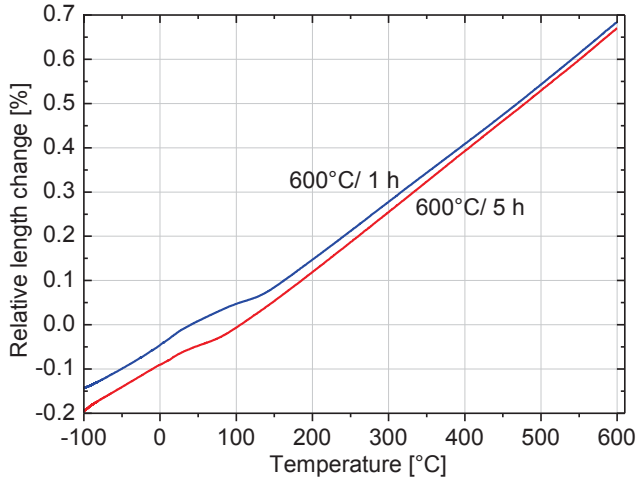

Figure 3. Relative length change during cooling after tempering for 1 h and 5 h at 600°C; rate for heating up to tempering temperature and cooling from tempering temperature was 100°C/ min.

Similar investigations were also conducted for tempering at 600°C and subsequent cooling. Figure 3 displays the cooling curves from dilatometer investigations after tempering at 600°C for 1 h and 5 h. Again, due to different tempering times different martensite start temperatures can be found. Compared to tempering at 540°C the austenite fraction is higher at 600°C. The initial length of the specimens tempered at 600°C is close to that of the specimens tempered at 540°C because the larger thermal dilatation due to the higher tempering temperature is almost counterbalanced by the higher austenite fraction which causes a length reduction due to the lower specific volume compared to the martensite structure. From the cooling curves in Figure 3 it can be concluded that martensitic phase transformation is starting at 150°C after tempering at 600°C for 1 h, while martensite start temperature is at 110°C after tempering at 600°C for 5 h.

In Figure 4 the differential length change during cooling from tempering temperature is illustrated. By comparison of the results of the dilatometer investigations at both tempering temperatures, it can be concluded that austenite to martensite phase transformation occurs at significantly lower temperatures after tempering for 5 h than after tempering for 1 h. And, martensite start temperature for both tempering times is lower after tempering at 600°C than after tempering at 540°C. It should be further noted that the differential length change becomes smaller for the higher tempering temperatures and the longer tempering times.

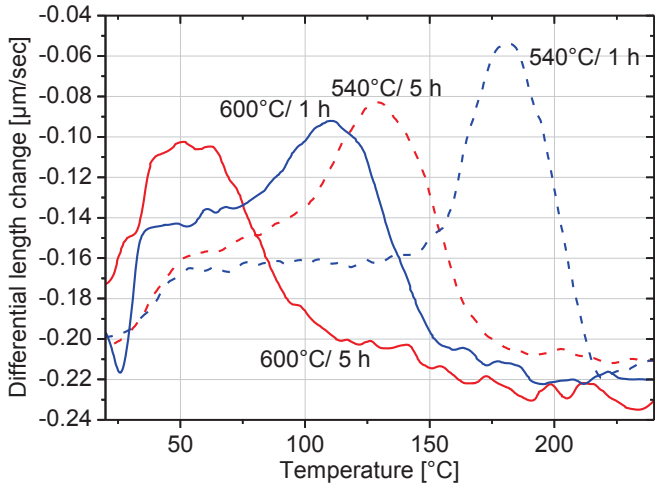

Figure 4. Differential length change during cooling from tempering at 540°C and 600°C for 1 h and 5 h.

Discussion

The increase of austenite phase fraction in the XRD measurements of the samples tempered at 540°C and 600°C clearly indicates that reverted austenite forms during tempering at 540°C and 600°C.
From the dilatometry investigations it can be concluded that austenite partially transforms into martensite during cooling after tempering. During tempering the austenite content was thus higher than displayed in Figure 1. From length change due to phase transformation obtained from dilatometer measurements and from investigation of volume change because of austenite to

martensite transition in [14, 15] it is estimated that 1-5 % of austenite present at tempering temperature transforms into martensite during cooling. This leads to the conclusion that some parts of the austenite are not stable enough to prevent martensite formation. It is suspected that this destabilization is mainly related to the retained austenite. This assumption is supported by the experimentally determined reduction of carbon content of austenite because of the formation of carbides as reported in [15]. This carbon reduction in austenite is suspected to cause a destabilization of austenite. Destabilization due to carbon reduction takes place very fast within the first minutes of tempering.

It is concluded from cooling curves of dilatometer measurements that austenite to martensite transformation starts at lower temperatures and is less intense with higher tempering temperatures and with longer tempering times. Lower martensite start temperatures can be interpreted as an indication for higher stability of the retained austenite against phase transformation. It was described in [15] that austenite becomes stabilized again at longer tempering times because of nickel diffusion into austenite.
Thermodynamic predictions lead to the conclusion that in equilibrium austenite gets enriched in nickel. A summary of the thermodynamic equilibrium calculations is shown in Table II. In [7] it was described that nickel is an important element for stabilizing austenite. By comparison of equilibrium phase compositions of austenite and martensite it is indicated that they do not alter that much between tempering at 540 and 600°C. From this it can be concluded that the austenite formation during tempering is rather controlled by diffusion than by thermodynamics. From mobility data from MatCalc [16, 17, 18] the diffusion coefficients of substitutional elements such as nickel increase by a factor of about 10 in martensite and austenite while increasing the temperature from about 540°C to 600°C.
Taking into account that the reverted austenite is highly enriched in nickel from the beginning of its formation [19] and that the reverted austenite is mainly nucleated at retained austenite it can be expected that also the retained austenite gets enriched by nickel diffusion from the reverted austenite to the retained austenite. This nickel enrichment of the retained austenite can be expected especially for the higher tempering temperatures and times, which is in accordance with the experimental results of lowering the martensite start temperature.

Table II. Equilibrium calculations of phase fractions and phase composition of austenite and martensite of the investigated steel at 540°C and 600°C with MatCalc [16, 18]; carbides are considered in the calculation but not displayed in the table for the sake of clarity.

Equilibrium at		540°C		600°C	
		Martensite	Austenite	Martensite	Austenite
Phase fraction	[mol %]	72.7	24.2	65.4	31.6
C	[wt.-%]	3.2×10^{-5}	1.9×10^{-3}	2.3×10^{-4}	1.1×10^{-2}
Ni	[wt.-%]	4.5	31.6	4.5	25.3
Co	[wt.-%]	16.8	5.1	17.2	7.0
Cr	[wt.-%]	1.3	2.4	1.2	2.3
Mo	[wt.-%]	0.1	0.5	0.1	0.5
Fe	[wt.-%]	77.3	60.4	77.0	64.9

Conclusion

From the combined XRD and dilatometry investigations the following conclusions can be drawn regarding the phenomena taking place during tempering of high Ni-Co steels:

- After quenching from austentization temperature the high Ni-Co steel exhibits a retained austenite content of about 6 wt.-%.
- Tempering of this quenched steel at 540°C and 600 °C for more than 30 min causes in any case an increase of the austenite phase fraction in the investigated high Ni-Co steel compared to the as quenched condition. Tempering of times below 60 min at 540°C causes a reduction of the austenite due to austenite destabilization as a consequence of carbon reduction.
- Reduction of austenite content due to martensite formation during cooling is in the range of 1-5 % for the investigated tempering temperatures (540 and 600°C) and time regime (10 min up to 5 h).
- From dilatometer measurements it is concluded that transformation of austenite to martensite during cooling from tempering temperature occurs at lower temperatures and is less intense when tempering was performed at higher temperatures and for longer times. Restabilization of retained austenite is suspected due to nickel diffusion into retained austenite. Stabilization of retained austenite is thus more pronounced at higher tempering temperatures and longer tempering times because nickel diffusion and the accompanying stabilization of austenite is more enhanced for these conditions.

References

1. R. Ayer and P.M. Machmeier, „Transmission Electron Microscopy Examination of Hardening and Toughening Phenomena in Aermet 100," Metallurgical Transactions A, Vol. 24A (1993), 1943-1955.

2. U. Viswanathan, G. Dey and V. Sethumadhavan, „Effects of austenite reversion during overageing on the mechanical properties of 18 Ni (350) maraging steel," Materials Science and Engineering A 398 (2005), 367-372.

3. K. Sato, „Improving the Toughness of Ultrahigh Strength Steel," Dissertation, University of California, (2002).

4. G. Haidemenopoulos et al., „Thermodynamics-based alloy design criteria for austenite stabilisation and transformation toughening in Fe-Ni-Co system," Journal of Alloys and Compounds 220 (1995), 142-147.

5. H. K. D. H. Bhadeshia and D. V. Edmonds, „Bainite in silicon steels: new composition-property approach Part 1," Metal Science Vol. 17 (1983), 411-419.

6. J. Wang and S. v. d. Zwaag, „Stabilization Mechanisms of Retained Austenite in Transformation-Induced Plasticity Steel," Metallurgical and Materials Transactions A, Volume 32A (2001), 1527-1539.

7. G. Haidemenopoulos, Dissertation, Massachusetts Institute of Technology, (1988).

8. T. Waitz et al., „Size effects on martensitic phase transformations in nanocrystallinge NiTi sahpe memory alloys," Materials Schience and Technology, vol. 24, No. 8 (2008), 934-940.

9. C. J. Kuehmann, "Thermal processing optimation of nickel-cobalt ultrahigh-strength steels", Evanston, Illinois: Northwestern University, (1994).

10. H. E. Lippard, "Microanalytical Investigations of Transformation Toughened Co-Ni Steels", Evanston Illinois: Northwestern Universitiy, (1999).

11. M. Gruber, „Mikrostruktur und mechanische Eigenschaften der Aermet 100 Legierung", Diploma thesis, Montanuniversity of Leoben, (2012).

12. R. Ayer and P. M. Machmeier, „Microstructural Basis for the Effect of Chromium on the Strength and Toughness of AF1410- Based High Performance Steels," Metallurgical and Materials Transactions A, Vol. 27 A (1996) 2510-2517.

13. A. Young, The Rietveld Method, Oxford Universitiy Press, (2002).

14. A. Shibata et al., "Relation between martensite morphology and volume change accompanying fcc to bcc martensitic transformation in Fe–Ni–Co alloys," Materials Science and Engineering A 438–440, pp. 241-245, (2006).

15. M. Gruber et al., „Influence of heat treatment on the microstructure of a high Co-Ni secondary hardening steel", Work presented at the International Conference on Martensitic Transformations 2014, Bilbao Spain.

16. E. Kozeschnik, MatCalc Version 5.60, Institute of Materials Science and Technology, Vienna University of Technology.

17. Mobility Database "mc_fe_V2.006", Institute of Materials Science and Technology, Vienna University of Technology.

18. Thermodynamic Database "mc_fe_V2.024", Institute of Materials Science and Technology, Vienna University of Technology.

19. R. Schnitzer et al., „Reverted austenite in PH 13-8 Mo maraging steels," Materials Chemistry and Physics 122 (2010), 138-145.

Publication III

A R C H I V E S O F M E T A L L U R G Y A N D M A T E R I A L S
Volume 60 2015 Issue 3
DOI: 10.1515/amm-2015-0358

M. GRUBER*#, S. PLOBERGER**, G. RESSEL*, M. WIESSNER*, M. HAUSBAUER**, S. MARSONER*, R. EBNER*

EFFECTS OF THE COMBINED HEAT AND CRYOGENIC TREATMENT ON THE STABILITY OF AUSTENITE IN A HIGH CO-NI STEEL

WPŁYW ZŁOŻONEJ OBRÓBKI CIEPLNEJ – GRZANIA I KRIOGENICZNEGO CHŁODZENIA NA STABILNOŚĆ AUSTENITU W WYSOKOSTOPOWEJ STALI CO-NI

The stability of austenite is one of the most dominant factors affecting the toughness properties of high Co-Ni steels such as Aermet 100 and AF1410. Thus, the aim of this work was to get a deeper understanding on the impact of combined heat and cryogenic treatment on the stability of retained and reverted austenite. In order to characterize the evolution of the phase fraction of austenite during tempering at different temperatures and times, X-ray diffraction analyses were carried out. The stability of austenite, which was formed during tempering, was analyzed with dilatometric investigations by studying the transformation behavior of the austenite during cooling from tempering temperature down to -100°C. Additionally, transmission electron microscopy investigations were performed to characterize the chemical composition and phase distribution of austenite and martensite before and after tempering.

Keywords: high Co-Ni steel, reverted austenite, retained austenite, high temperature X-ray diffraction, dilatometer investigations

Stabilność austenitu jest jednym z najbardziej dominujących czynników mających wpływ na ciągliwość stali Co-Ni, takiej jak Aermet 100 i AF1410. Celem pracy było głębsze zrozumienia wpływu skojarzonego nagrzewania i obróbki kriogenicznej na stabilność austenitu szczątkowego i przemienionego. Ewolucję udziału fazy austenitycznej podczas odpuszczania w różnych temperaturach i czasach przeprowadzono stosując rentgenowskie badania dyfrakcyjne. Stabilność austenitu, który powstał podczas odpuszczania, badano metodą dylatometryczną, analizując zachowanie się austenitu podczas odpuszczania w temperaturach poniżej –100°C. Zrealizowano badania metodą mikroskopii elektronowej w celu określenia składu chemicznego i rozkładu austenitu i martenzytu przed i po odpuszczaniu.

Słowa kluczowe: stal Co-Ni, austenite przemieniony, austenite szczątkowy, rentgenowska dyfraktometria wysokotemperaturowa, dylatometria

1. Introduction

High Co-Ni hardening steels are well-known for their excellent toughness properties in combination with good hardness and strength values [1-3]. Their favorable mechanical properties are mainly related to the toughening effect of austenite. In particular, in this type of steel it must be distinguished between retained and reverted austenite. Retained austenite is defined as the untransformed austenite after quenching from austenitization temperature to room temperature or even after cryogenic treatment. Conversely, reverted austenite is formed after quenching during a subsequent tempering treatment [2,4]. Generally, the toughening effect of austenite can be characterized by its stability – the resistance against transformation [5]. It is assumed that the higher the stability of austenite is, the higher is also the toughening effect of austenite. The stability of austenite is affected by its chemical composition and the size of austenite grains [6]. It is reported that austenite grains exhibit increasing resistance against transformation with decreasing size [7]. Haidemenopoulos [5] claimed that this is a result of the lower number of potential nucleation sites for phase transformation due to smaller grain sizes. In contrast to this, it is described in [8] that transformation of small austenite grains in shape memory alloys is harder because of the increasing energy barrier for transformation with decreas-

* MATERIALS CENTER LEOBEN FORSCHUNG GMBH, ROSEGGERSTRASSE 12, LEOBEN, A-8700 AUSTRIA
** BÖHLER EDELSTAHL GMBH & CO KG, MARIAZELLER STRASSE 25, KAPFENBERG, A-8605 AUSTRIA
# corresponding Author: Marina.Gruber@mcl.at

ing grain size. Additionally, chemical stabilization of austenite can occur owing to an enrichment of austenite stabilizers, such as carbon, nickel or manganese [5,6,9,10]. In Aermet 100, which is one of the most prominent steel types of high Co-Ni hardening steels, both retained and reverted austenite are present [2]. Compared to reverted austenite the size and composition of retained austenite cannot easily be varied for toughening effects due to tempering treatment [5]. Consequently, cryogenic treatment is commonly applied to reduce the content of retained austenite and subsequent tempering treatment is employed in order to get an intended formation of reverted austenite [5]. In Aermet 100 reverted austenite is created above tempering temperatures of approximately 450°C [2,11]. Lippard [12] and Ayer, Machmeier [2] described that in Aermet 100 reverted austenite is formed predominantly at martensite lath boundaries and is enriched in nickel and depleted in cobalt.

Literature dealing with stabilization of retained austenite of steels, which are tempered above 400°C, i.e. in the temperature range where carbide precipitation occurs, is limited. In contrast to this, there are several calculations and qualitative evaluations of the stability of reverted austenite in high Ni-Co steels [5,12,13]. However, there are only a few experimental results on the stability of austenite in high Co-Ni steels at all. Consequently, the aim of this work is to present experimental results on the stability of retained and reverted austenite due to tempering and cryogenic treatment in a 0.22% C, 11% Ni, 13.5% Co, 2.9% Cr, 1.2% Mo steel.

To this end quantitative X-ray diffraction (XRD) analyses were carried out before and during tempering treatment to determine the austenite content. Transmission electron microscopy (TEM) investigations were conducted before and after tempering to analyze austenite distribution and composition. Dilatometric measurements were employed on cryogenically and on non-cryogenically treated samples to characterize the transformation behavior of austenite during cooling of specimens to room or even lower temperature after the tempering treatment. The investigations allow to draw conclusions on the effect of cryogenic treatment (CT) and different tempering treatments on the stability of austenite.

1. Experimental

The experiments were employed on a steel with a chemical composition listed in Table 1. The contents of substitutional elements were determined by X-ray fluorescence analysis and the carbon content was characterized by thermal combustion analysis.

TABLE 1

Chemical composition of the investigated steel in wt.%

	C	Ni	Co	Cr	Mo
wt.%	0.22	11.0	13.5	2.9	1.2

In order to study the effect of heat treatment on austenite phase fraction and austenite stability, all specimens were austenitized in a vacuum furnace at 885°C for 1 h followed by controlled cooling with a cooling rate of 10°C/ min. Half of the samples were treated cryogenically in a freezing unit at –73°C for 1 h. For TEM investigations the samples were tempered at 600°C for 5 h in a batch furnace.

In-situ XRD measurements were conducted to determine the austenite phase fraction in the as quenched and refrigerated condition as well as during tempering at 540°C and 600°C for 5 h. All XRD investigations were carried out using a Bruker™ AXS Advance diffractometer with an Anton Paar™ (HTK2000) high temperature chamber. Cr-K_α radiation was used with a wavelength of 2.29 Å. For the quantitative determination of phase fractions the Rietveld method [14] was applied. Measuring time for each diffractogram was set to 37 min. Because of the relatively short measuring time, measuring inaccuracy of austenite phase fraction was about ±1-3 wt.%.

TEM measurements were performed with a Philips™ CM12 microscope. Samples of 3 mm in diameter were ground to 80 μm and subsequently electrolytically etched using a Struers™ A2 electrolyte. Chemical composition was studied via an energy dispersive X-ray spectroscopy (EDS) detector attached to the microscope.

Dilatometric measurements were carried out using a TA Instruments™ (formerly BAEHR™) DIL 805A dilatometer. Tempering treatment was performed at 540°C and 600°C for 1 h and 5 h. The samples for the dilatometer analysis were tubular with a length of 10 mm, an outer diameter of 4 mm and a wall thickness of 1 mm. The heating and cooling rate was set to 100°C/ min. Quenching to –100°C was done by a freezing unit from TA instruments™ with the aid of helium, which was cooled before with liquid nitrogen and passed through the hollow dilatometer samples. Discontinuous length changes of the specimen during the thermal cycle were taken as indication for austenite to martensite phase transformation, as this phase transformation is linked with a volumetric change. Measuring inaccuracy of martensite start (Ms) temperature was ~10°C.

2. Results

2.1. *In-situ* measurements of austenite phase fraction during tempering

(Fig. 1) presents the results of phase fraction analyses of austenite during tempering at different temperatures. After quenching from austenitizing temperature retained austenite is present as indicated by the values for tempering time 0 h. The content of retained austenite in this condition is ~6 wt.%. By performing a cryogenic treatment the austenite phase fraction is reduced to approximately 2 wt.%.

Subsequent tempering treatment after austenitization or after cryogenic treatment causes an increase of austenite phase fraction. This increase is related to the formation of reverted

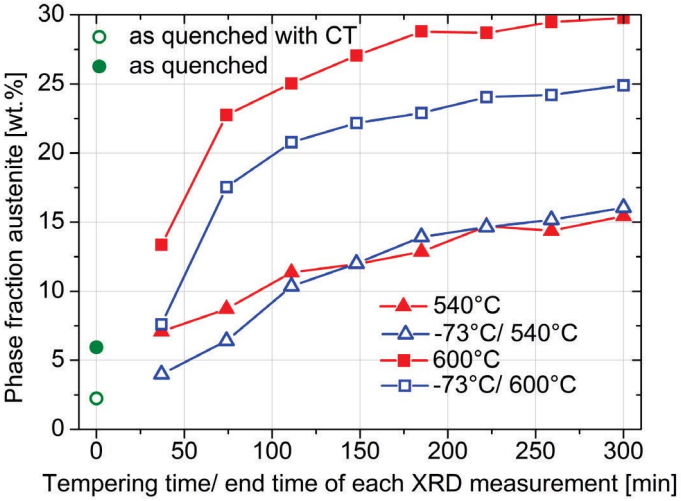

Fig. 1. Analysis of the phase fraction of austenite directly after quenching from austenitization temperature or cryogenic treatment (CT) (circles) and during tempering at 540°C (triangles) and 600°C (squares) for 5 h for CT and non-CT samples. Each measuring point indicates a XRD measurement during tempering or before tempering. The time increment of these graphs correspond to the measurement time for each XRD measurement, i.e. 37 min

austenite. After 5 h of tempering at 600°C the fraction of austenite raises up to ~30 wt.% for the non-CT samples and to ~25 wt.% for the CT samples. Differences in austenite phase fractions at 600°C due to CT may be a result of the measuring inaccuracy. Additionally, it is suggested that CT, which causes a lower phase fraction of retained austenite, may influence the formation process of reverted austenite. After 5 h of tempering at 540°C about 15 wt.% austenite are present for CT as well as for non-CT samples. Consequently, tempering at 600°C causes a much more pronounced formation of reverted austenite than tempering at 540°C.

2.2. Characterization of the microstructure after heat treatment

In (Fig. 2a) the martensitic microstructure after austenitizing is illustrated. Retained austenite films are determined at martensite lath boundaries via selected area diffraction and corresponding dark-field images (Fig. 2b). The average thickness of retained austenite films is approximately 20 nm.

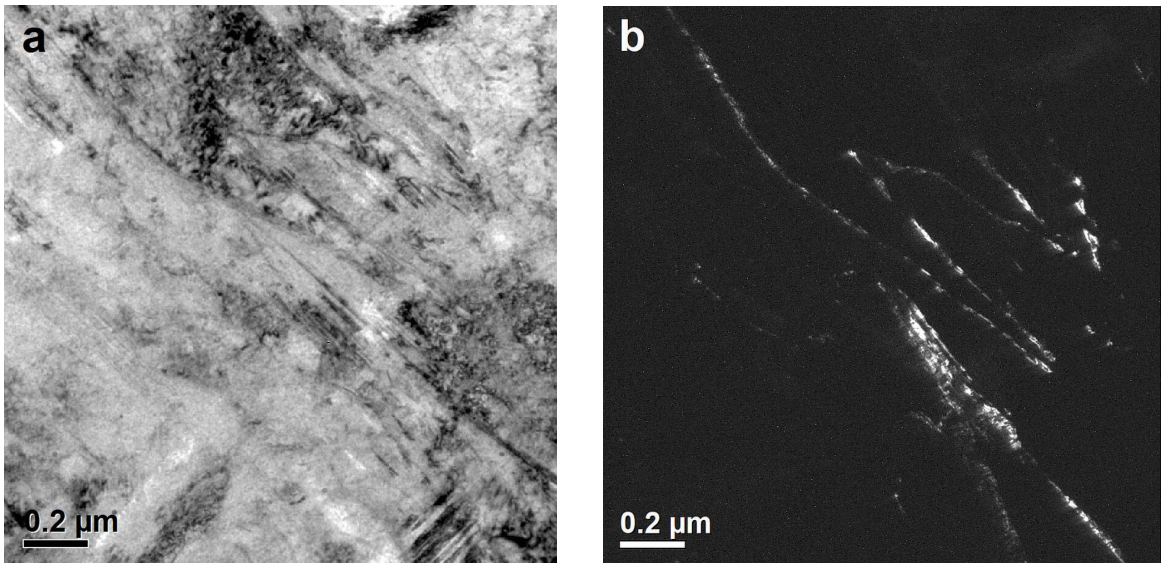

Fig. 2. TEM analysis of martensitic matrix and retained austenite of a sample, which was austenitized at 885°C for 1 h and quenched to room temperature. The bright-field image (a) and the corresponding dark-field image (b) show retained austenite films at martensite lath boundaries

In (Fig. 3) the microstructure of a sample tempered at 600°C for 5 h without CT is depicted. In this case austenite is still present at martensite lath boundaries and austenite films have grown to size of approximately 200 nm in thickness. It should also be noticed that carbide precipitation occurs, as described in [15].

In order to study chemical compositions of austenite and martensite after tempering at 600°C EDS, measurements were employed. The results are summarized in (Table 2). Apparently, the nickel content of the reverted austenite is enhanced in contrast to the nickel content of martensite. In contrast to that, cobalt content in reverted austenite is reduced.

As TEM investigations on CT samples do not show any distinct differences to non-CT samples, analyses are not presented in this paper.

TABLE 2

Measurement of the chemical composition via EDS analyses of austenite and martensite after 885°C/ 1 h/ 600°C/ 5 h

	Ni [wt.%]	Co [wt.%]	Cr [wt.%]	Mo [wt.%]	Fe [wt.%]
Reverted austenite	18.2	11.0	5.6	1.5	63.7
Martensite	9.2	13.3	5.4	1.2	70.8

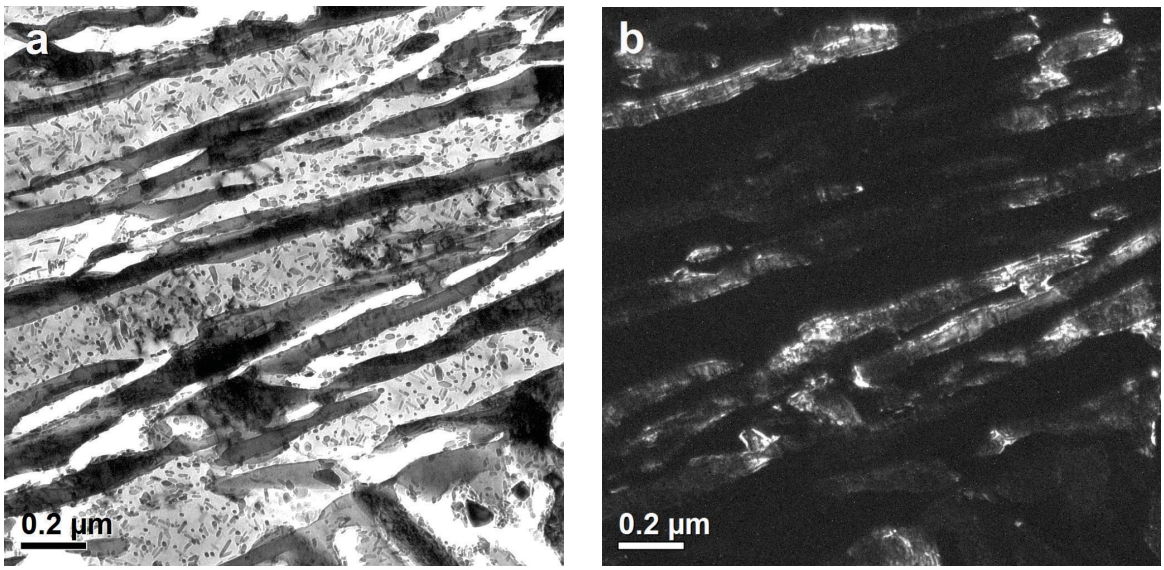

Fig. 3. TEM images showing tempered martensite, reverted austenite and carbides. Samples were austenitized at 885°C for 1 h, quenched to room temperature and tempered at 600°C for 5 h. The bright field image (a) and the corresponding dark field image (b) show reverted austenite films at martensite lath boundaries

2.3. Characterization of the transformation behavior of austenite

For characterizing the stability of austenite, its transformation behavior during cooling was studied by dilatometric investigations. In (Fig. 4) the relative length change during cooling to –100°C after tempering at 540°C for 1 h and for 5 h with and without CT is illustrated. For the purpose of good comparability of the results, the cooling curves were shifted in the direction of the relative length change axis. Therefore, no scaling is shown for this axis. From these measurements it can be deduced that a volume increase occurs during cooling after tempering at 540°C for 1 h and for 5 h with and without CT. The increase of volume during cooling is related to a phase transformation of austenite to martensite, as the phase transition from austenite to martensite is accompanied by a volume increase. (Fig. 4) shows that transformation of austenite is less intense with increasing holding time and with previous cryogenic treatment.

Additionally, dilatometric investigations were carried out for tempering at 600°C for 1 h and 5 h for CT and non-CT treated samples. Cooling curves after tempering are depicted in (Fig. 5). Again, the relative length change axis is not scaled, because curves were shifted for the purpose of good comparability. During cooling after tempering at 600°C again a martensitic trans-

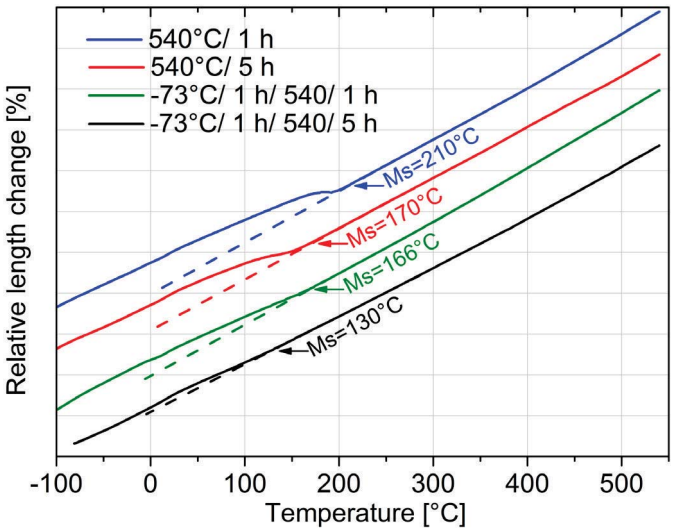

Fig. 4. Dilatometric cooling curves of the CT and non-CT samples after a tempering treatment at 540°C for 1 h and for 5 h. Curves show a martensitic transformation during cooling, which is less intense and starts at lower temperatures with longer holding times and with the application of a previous cryogenic treatment

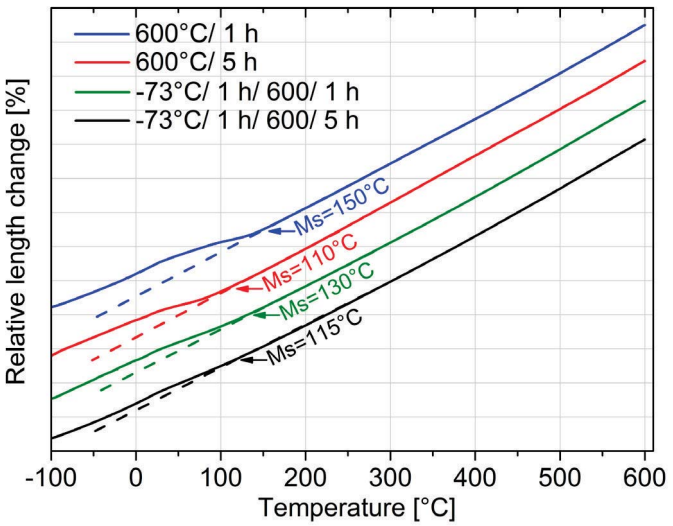

Fig. 5. Dilatometric cooling curves of the CT and non-CT samples after a tempering treatment at 600°C for 1 h and for 5 h. Curves show a martensitic transformation during cooling, which is less intense and starts at lower temperatures with longer holding times and with the application of a previous cryogenic treatment

formation occurs. Also in this case, martensitic transformation of austenite during cooling after tempering at 600°C is weaker for CT samples and for samples which were tempered for 5 h.

The martensite start (Ms) temperature was determined by the first deviation from the linear behavior of relative length change curve during cooling. This was done because the cooling curves behave slightly different when martensitic transformation has started. In (Fig. 4) and (Fig. 5) *Ms* temperatures of all tempering treatments are presented. From the analysis of *Ms* temperatures it can be deduced that *Ms* temperature is lower the higher the tempering temperatures and the longer the tempering times are. Also CT reduces the *Ms* temperatures in most cases, except for tempering at 600°C for 5 h.

3. Discussion

Phase fraction measurements by XRD indicate that the austenite content is 6 wt.% after quenching from austenitizing and 2 wt.% after CT. During subsequent tempering an increase of austenite phase fraction due to formation of reverted austenite was determined by *in-situ* high temperature XRD measurements. After 5 h of tempering the austenite phase fraction is approximately 15 wt.% for the samples tempered at 540°C and 25-30 wt.% for the samples tempered at 600°C.

Microstructural characterization via TEM investigations demonstrated that retained austenite after quenching from 885°C as well as reverted austenite after tempering at 600°C for 5 h is located at martensite lath boundaries. Films of retained austenite exhibit a thickness of about 20 nm, whereas reverted austenite films have grown to a thickness of about 200 nm. From position of occurrence and growth behavior of the austenite films it is suggested that reverted austenite mainly nucleates at retained austenite. Composition of austenitic regions after tempering at 600°C for 5 h shows a clear enrichment of nickel. This is in good correlation with the literature dealing with nickel enrichment in reverted austenite [2,9,16].

Dilatometric investigations of cooling behavior after tempering reveal that martensitic transformation is less intense and occurs at lower temperatures with higher tempering temperatures, longer tempering times and with the application of a cryogenic treatment at –73°C. As the resistance of austenite against its transformation can be correlated with the stability [17], *Ms* temperatures were used to characterize the stability of austenite after different heat treatments. The higher the *Ms* temperature is the lower is the stability of austenite. Therefore, it can be assumed that the austenite stability is higher after longer tempering times, higher tempering temperatures and with the application of a CT. In order to explain these differences due to different tempering treatments, it is necessary to understand the mechanism of austenite stabilization during tempering. Therefore, equilibrium calculations as well as diffusional calculations were carried out with MatCalc [18-20]. As nickel is the element, which stabilizes austenite [5], equilibrium calculations of nickel distribution in austenite and ferrite at 540°C and 600°C were performed for the composition given in (Table 1). Simulations reveal that nickel concentration is higher in austenite compared to ferrite, as nickel concentration in austenite is predicted to be 31.6 wt.% and 25 wt.% for the equilibrium condition at 540°C and 600°C, respectively. Thus, the stability of austenite should be higher at 540°C which does not agree with the experimental results in this work. As a consequence of this, the varying stability of austenite is probably originated by the kinetics of nickel transport at 540°C and 600°C. Also, Schnitzer et al. [9] described that formation of reverted austenite is controlled by the diffusion of Ni to an austenite nuclei. It is assumed that reverted austenite is enriched with nickel from the beginning of its creation, which is also in good agreement with the higher Ni concentration in equilibrium austenite at 540°C and 600°C. According to these findings, it can be followed that reverted austenite is more stable from the beginning of formation due to enrichment of nickel than the retained austenite. However, from a thermodynamic point of view it is suggested that retained austenite also gets enriched in nickel during tempering by diffusion of nickel from the adjacent reverted austenite into the retained austenite. As this stabilization effect is diffusion controlled, *Ms* temperatures versus the diffusion lengths of nickel as defined in Eq. (1) are depicted in (Fig. 6).

Diffusion coefficients of nickel in austenite were calculated at 540°C and 600°C by using MatCalc and the composition in (Table 1). The diffusion lengths x of the various tempering times t were derived from the diffusion coefficients D and the Eq. (1) for the mean diffusion path [21,22].

$$x = \sqrt{4Dt} \tag{1}$$

In (Fig. 6) it is shown that the diffusion length of nickel in austenite increases with higher tempering temperatures and longer tempering times. It is also derived that *Ms* temperature of non-CT as well as of CT samples decreases with increasing diffusion length of nickel in austenite. Consequently, it is argued that stabilization of austenite is controlled by diffusion of nickel in austenite. On the one hand diffusion of nickel into retained austenite leads to stabilization due to nickel enrichment, on the other hand the size of non-stabilized austenite is reduced which also may lead to stabilization. Therefore, it can be summarized that the higher the tempering temperatures and the longer the tempering times are, the higher the stabilization of austenite due to nickel diffusion into austenite is.

Furthermore, the findings from (Fig. 6) can be described with the relationship found in literature [6,23,24], which assumes that the probability of finding a defect that can act as a nucleus for the martensitic transformation is proportional to the volume of the non-stable austenite film. The probability of finding such a defect can be related to the *Ms* temperature because the more nucleation sites are present the higher the probability for martensitic transformation is. A higher probability for martensitic transformation leads to a higher martensite start temperature. The size of the non-stabilized austenite can be correlated with the diffusion length of nickel in austenite.

The longer the diffusion length of nickel in austenite is, the more the retained austenite gets stabilized. It is suggested that stabilized austenite does not participate in martensitic transformation. Hence, thickness of non-stabilized austenite is getting smaller due to stabilization because of Ni diffusion into austenite which results in a lower effective thickness of unstable retained austenite films and a lower probability of finding a defect for martensitic transformation. This leads to a lower *Ms* temperature for thinner unstable austenite films, which is in agreement with the findings in this work.

It is also shown in (Fig. 6) that *Ms* temperature is lower for the CT samples. As the main difference between CT and non-CT samples is the content of retained austenite, it is argued that the less intense martensitic transformations of the CT samples are due to the lower content of non-stabilized retained austenite. Additionally, it is supposed that the average size (mainly the thickness) of retained austenite is smaller due to CT treatment and therefore austenite grains exhibit a higher stability, which may lead to the decrease of martensite start temperature due to CT treatment. It should be noticed that the decrease of *Ms* temperature and the less intense transformations due to cryogenic treatment also supports the assumption that mainly retained austenite is not stable after tempering and needs to be stabilized with nickel during tempering. Additionally, by further comparing the behavior of CT and non-CT samples in (Fig. 6) it is asserted that the slope of the curve for CT samples is smaller compared to the curve for the non-CT samples. Hence, it can be followed that this is also due to the reduced average thickness of retained austenite after cryogenic treatment. Because retained austenite is smaller, stabilization due to tempering is not that pronounced compared to non-CT samples.

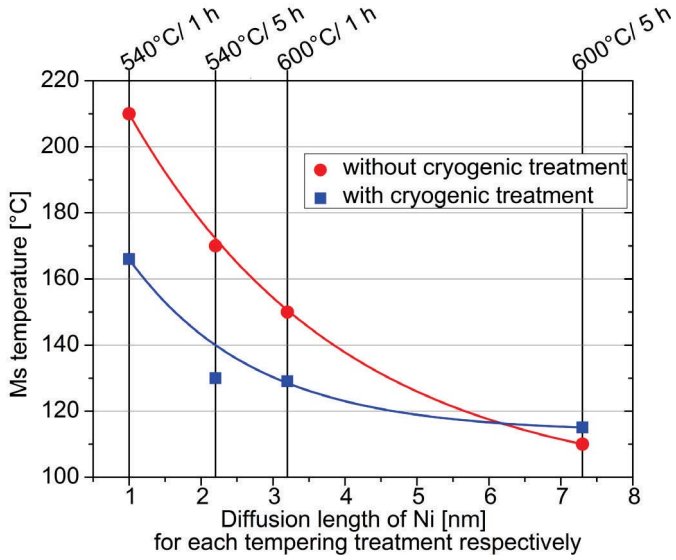

Fig. 6. Martensite start (Ms) temperature as a function of the diffusion length of Ni in austenite for each heat treatment

4. Conclusions

From *in-situ* XRD measurements, dilatometry analyses and TEM investigations the influence of combined heat and cryogenic treatments on the stability of austenite was evaluated and leads to the following conclusions:

- After quenching from austenitizing treatment 6 wt.% austenite remains untransformed. This retained austenite is preferentially located at martensite lath boundaries in form of thin films. Due to subsequent cryogenic treatment austenite phase fraction is reduced to 2 wt.%.
- During tempering at 600°C and 540°C reverted austenite is formed. As reverted austenite is also located at lath boundaries, it is suggested that reverted austenite mainly nucleates at retained austenite.
- From dilatometer investigations it is derived that austenite is more stable after tempering, when tempering was performed at higher temperatures and longer times. Also cryogenic treatment before tempering seems to enhance stability of austenite.
- It is demonstrated by comparing the transformation behavior of CT and non-CT samples that mainly retained austenite transforms during cooling. Retained austenite is stabilized as a result of tempering due to nickel diffusion in austenite from reverted into retained austenite.
- Furthermore, it can be concluded that retained austenite can be stabilized via tempering treatment and stabilization is dependent on the diffusion length of nickel at different temperatures.

REFERENCES

[1] P.M. Novotny G. E. Maurer, Adv. Mater. Process, 37-40 (2007).
[2] R. Ayer, P.M. Machmeier, Metall. Trans. A **24A**, 1943-1955 (1993).
[3] K. Sato. Improving the Toughness of Ultrahigh Strength Steel. PhD thesis, University of California (2002).
[4] M. Gruber. Mikrostruktur und mechanische Eigenschaften der Aermet 100 Legierung. Diploma thesis, University of Leoben (2012).
[5] G. Haidemenopoulos. Dispersed-Phase Transforamtion Toughening in Ultrahigh-Strength Steels. PhD thesis, Massachusetts Institute of Technology (1988).
[6] G. Haidemenopoulos, M. Grujicic, G. Olson, M. Cohen, J. Alloy. Compd. **220**, 142-147 (1995).
[7] J. Wang S. v. d. Zwaag, Metall. Trans. A **32A**, 1527-1539 (2001).
[8] T. Waitz, T. Antretter, F. Fischer H. Karnthaler, Mater. Sci. Technol. **24**, 934-940 (2008).
[9] R. Schnitzer, R. Radis, M. Nöhrer, M. Schober, R. Hochfellner, S. Zinner, E. Povoden-Karadeniz, E. Kozeschnik H. Leitner, Mater. Chem. Phys. **122**, 138-145 (2010).
[10] H.K.D.H. Bhadeshia, D.V. Edmonds, Met. Sci. **17**, 411-419 (1983).

[11] R. Ayer, P. M. Machmeier, Metall. Trans. A **27A**, 2510-2517 (1996).
[12] H.E. Lippard. Microanalytical Investigations of Transformation Toughened Co-Ni Steels. PhD thesis, Northwestern Universitiy, Evanston Illinois (1999).
[13] C.J. Kuehmann. Thermal processing optimation of nickel-cobalt ultrahigh-strength steels. PhD thesis, Northwestern University, Evanston, Illinois (1994).
[14] R.A. Young, The Rietveld Method, Oxford Universitiy Press, New York 2002.
[15] M. Gruber, S. Ploberger, M. Wiessner, S. Marsoner, R. Ebner, Work presented at the International Conference on Martensitic Transformations 2014, Bilbao Spain.
[16] M. Farooque, H. Ayub, A. UlHaq and A. Kahn, J. Mater. Sci. **33**, 2927-2930 (1998).
[17] A. Kokosza, J. Pacyna, Arch. Metall. Mater. **55**, 1001-1006 (2010).
[18] E. Kozeschnik, MatCalc Version 5.61, Vienna University of Technology.
[19] MatCalc, Thermodynamic Database "mc_fe_V2.040", Vienna University of Technology.
[20] MatCalc, Mobility Database "mc_fe_V2.006", Vienna University of Technology.
[21] A. Einstein, Ann. Phys. 549-560 (1905).
[22] H.K.D.H. Bhadeshia, http://www.msm.cam.ac.uk/phase-trans/mphil/MP6-3.pdf.
[23] R. Cech, D. Turnbull, Trans. AIME, 124-132 (1956).
[24] M. Cohen, G. Olson, New aspects of Martensitic Transformation, First Japan Institut of Metals, 93-98 (1976).

Received: 20 April 2015

Publication IV

Characterization of the effect of cryogenic treatment on the tempering behavior of a secondary hardening high Co-Ni steel

Marina Gruber [1], Gerald Ressel [1], Sarah Ploberger [2], Stefan Marsoner [1] and Reinhold Ebner [1]

[1]Materials Center Leoben Forschung GmbH, Roseggerstraße 12, A-8700 Leoben, Austria
[2]Böhler Edelstahl GmbH & Co KG, Mariazeller Straße 25, A-8605 Kapfenberg, Austria

E-mail: marina.gruber@mcl.at

Abstract. For high Co-Ni steels sub-zero treatments are conducted to reduce the retained austenite phase fraction for obtaining excellent fracture toughness properties, but in general, cryogenic treatment has a great impact on the microstructural evolution of steels during tempering. Hence, the aim of this work was to analyze the influence of cryogenic treatments on the microstructural evolution of high Co-Ni steels, including carbide precipitation kinetics and austenite phase fraction evolution, during heating to elevated temperatures. In order to study the formation properties of carbides, the heating processes of cryogenically and non-cryogenically treated specimens were analyzed by dilatometer measurements. Furthermore, for determining the evolution of austenite phase fraction and hardness due to tempering, dilatometer investigations were combined with X-ray diffraction analyses and hardness measurements. It is revealed that sub-zero treated samples exhibit much stronger carbide precipitation signals. This was ascribed to the lower phase fraction of retained austenite, as more carbon is available for carbide precipitation.

1. Introduction

For tool steels, the application of a cryogenic treatment during the heat treatment, i.e. before tempering, has a massive impact on mechanical and microstructural properties such as enhancement of wear resistance and hardness, reduction of retained austenite phase fraction and refinement of carbide structure [1, 2, 3, 4, 5]. Nevertheless, a cryogenic treatment is also applied before tempering of the martensitic high Co-Ni steel Aermet® 100 for obtaining excellent toughness properties. Generally, high Co-Ni steels contain retained austenite, which is present after quenching from austenitization, and reverted austenite, which forms during tempering [6, 7]. As retained austenite in Aermet® 100 would lower toughness values because of its low stability, a sub-zero treatment is conducted to reduce the retained austenite content [6, 7, 8]. However, the effect of cryogenic treatment on carbide precipitation kinetics in high Co-Ni steels has not been precisely characterized so far.

Hence, this work presents experimental results on the influence of sub-zero treatments on the carbide precipitation kinetics and the austenite evolution during tempering of a high Co-Ni steel. The microstructural evolution during heating was characterized by dilatometer investigations on specimens, which were quenched to room temperature or cryogenically treated. Furthermore,

X-ray diffraction (XRD) analyses and hardness measurements in combination with dilatometer investigations were conducted to determine the austenite phase fraction and the hardness after various tempering treatments. It is shown that cryogenically treated samples present a more pronounced carbide precipitation reaction during heating compared to the non-cryogenically treated samples. It could be revealed that the austenite phase fraction affects the precipitation kinetics, causing further microstructural differences between cryogenically and non-cryogenically treated samples.

2. Experimental

The used material in this work was a high Co-Ni steel with 11 wt.% Ni, 13.5 wt.% Co, 2.9 wt.% Cr, 1.2 wt.% Mo and 0.22 wt.% C. The material was forged to round bars with a diameter of 200 mm and austenitized in a vacuum furnace at 885°C for 1 h and cooled to room temperature with 10°C/ min. Half of the samples were cryogenically treated (CT) in a freezing unit at −73°C for 1 h.

Dilatometer investigations were carried out by using a DIL 805A dilatometer from TA Instruments (formerly BAEHR). The samples for dilatometer investigations had a diameter of 4 mm and a length of 10 mm. The differential length change signals from the dilatometer measurements were obtained by deriving the relative length change with respect of time. CT and non-CT samples were heated (1st run) in the dilatometer to a maximum temperature of 620°C with 20°C/ min and immediately cooled to room temperature (20°C/ min) and additionally reheated (2nd run) with the same parameters. Heating parameters were chosen in a way that no significant reverted austenite formation occurs.

Austenite phase fraction and hardness measurements were carried out on CT and non-CT samples with a diameter of 10 mm and a length of 15 mm, which were heated in the dilatometer with 20°C/ min to various temperatures up to 620°C and immediately cooled to room temperature with 100°C/ min. XRD measurements for austenite phase fraction determination were performed by using a D8 Discover diffractometer from Bruker AXS. Cr-K_α radiation with a wavelength of 2.29 Å was used for measurements and for a quantitative determination of phase fractions the Rietveld method was applied [9]. The absolute inaccuracy of phase fraction determination was about 1-2 %. Transmission electron microscopy (TEM) investigations were carried out on a Philips CM12 microscope. Samples were conventionally prepared by grinding to a thickness of 80 μm and a subsequent electro polishing procedure.

3. Results

3.1. Characterization of the evolution of austenite

To study the evolution of austenite content due to tempering, austenite phase fraction measurements were carried out on CT and on non-CT samples before heating and after heating to 200°C, 400°C, 500°C and 580°C and immediately cooling to room temperature. The results are shown in Fig. 1. The austenite content of the non-CT sample without tempering is approximately 6.5 %. By performing a cryogenic treatment the austenite content decreases to 3.5 %. After heating the cryogenically treated samples to different temperatures, the austenite phase fraction does not change significantly, whereas heating of the non-cryogenically treated samples beyond 400°C leads to a marked decrease of austenite content to about 4.5 %. For analyzing this decrease of phase content more precisely, the relative length change curves, obtained from dilatometer experiments, were studied. Fig. 2 depicts the dilatometer cooling curves of the non-cryogenically treated samples after tempering to 400°C, 500°C or 580°C. A distinct phase transformation can be observed for the samples, which were annealed to 500°C and 580°C, as indicated by the volume increase during cooling compared to the sample, which was annealed to 400°C. Since the phase transformation is accompanied with a volume increase, it is attributed to a transformation of austenite into a bcc phase, e.g. martensite. Furthermore, these dilatometer investigations also

reveal that the reduction of austenite content of the non-CT samples occurs during cooling from the tempering treatment.

For characterizing the retained austenite more precisely, TEM investigations were carried out. Fig. 3 shows a TEM bright-field image of the microstructure of the investigated steel. The material exhibits a martensitic matrix after austenitizing and quenching to room temperature. Retained austenite films are present along martensite lath boundaries, as indicated by the arrows. It is estimated that austenite films have a thickness between 3 nm (detection limit) and 40 nm.

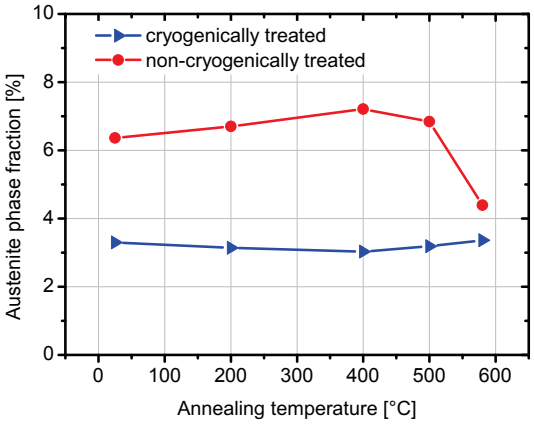

Figure 1. Austenite phase fraction of cryogenically and non-cryogenically treated samples after heating in the dilatometer to various temperatures up to 580°C (heating rate: 20°C/ min) and cooling down to room temperature (cooling rate: 100°C/ min). The non-cryogenically treated samples exhibit a decrease of austenite phase fraction, when tempering is conducted beyond 400°C.

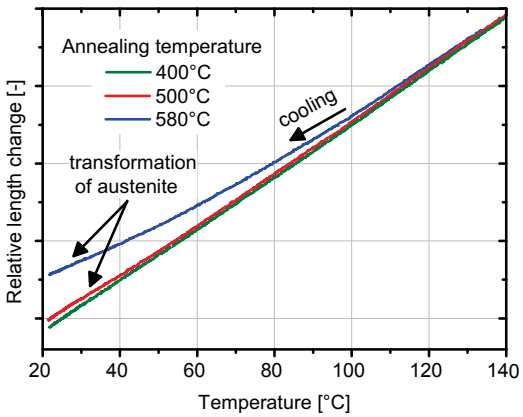

Figure 2. Relative length change of dilatometer cooling curves after heating of non-CT samples to 400°C, 500°C or 580°C and subsequent cooling (100°C/ min). A transformation of austenite occurs during cooling for the non-CT samples, which were annealed to 500°C or 580°C. For a better comparability, the curves were shifted along the y-axis. Therefore, no scaling of the y-axis is shown.

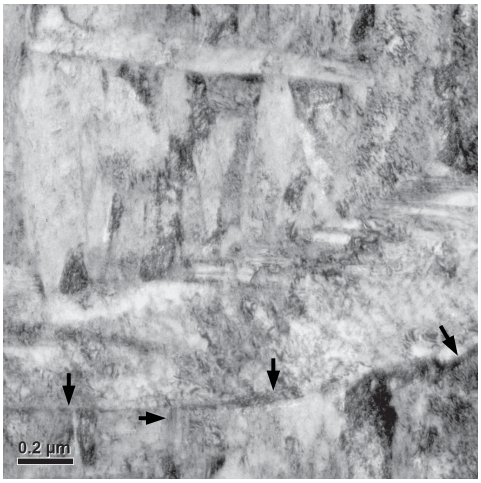

Figure 3. TEM bright-field image of the martensitic microstructure after austenitizing at 885°C for 1 h and quenching to room temperature. Retained austenite is present at martensite lath boundaries, as marked by the arrows.

3.2. Detailed analyses of the tempering behavior

For a detailed characterization of the processes, taking place during tempering of CT and non-CT samples, dilatometer analyses were conducted. In Fig. 4 the relative length change during heating of CT and non-CT samples is plotted as a function of temperature. Generally, the heating curves of both conditions exhibit differences. The most significant difference is observed in the range between 250°C-350°C, as CT samples exhibit a more pronounced deviation from the linear expansion. For a more precise characterization of the phenomena, which occur during heating, the derivatives of the relative length change curves were calculated as depicted in Fig. 5. These curves show three main reactions, which are indicated by the numbers 1 - 3, respectively. The first effect during heating in the range between 100°C and 200°C may be attributed to transition carbide precipitation, as this process generally occurs in the temperature range between 80°C and 200°C and causes a reduction of volume [10, 11, 12]. The second effect, which also causes a reduction of volume, occurs in the temperature regime between 250°C and 400°C and can be assigned to cementite precipitation [10, 11, 12].

There are distinct differences between CT and non-CT samples regarding cementite precipitation properties, as precipitation is more enhanced for CT samples. This is also observed for the processes, which start at temperatures above 450°C - 500°C. These processes are ascribed to secondary hardening carbide precipitation, because the formation of these carbides generally proceeds in this temperature range and would cause an increase of length [6, 10, 13, 14, 15].

The dilatometer curves of both conditions do not show any increase of length in the range between 200°C and 350°C, which is typical for austenite transition into ferrite and carbides or bainite [10, 11, 12, 16, 17]. Hence, it is suggested that austenite stays stable and no austenite transformation occurs during heating. This is also supported by austenite phase fraction measurements, where no reduction of austenite phase fraction occurs up to temperatures of 400°C.

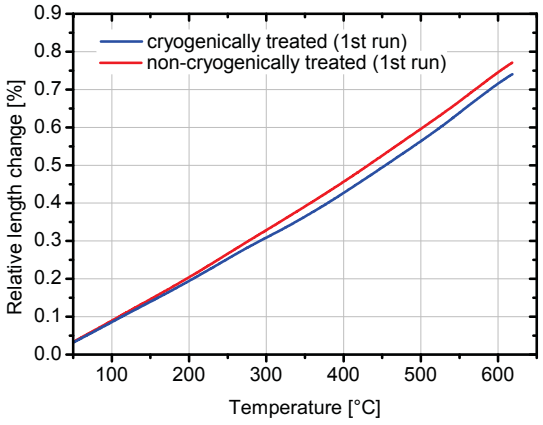

Figure 4. Relative length change curves of dilatometer heating experiments of cryogenically and non-cryogenically treated samples. The heating rate was 20°C/ min. Generally, the curves of CT and non-CT conditions exhibit a different behavior, which is indicated by the lower expansion for CT compared to non-CT samples during heating.

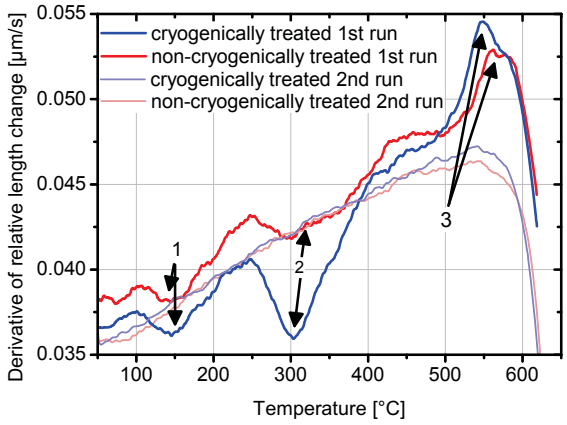

Figure 5. The derivatives of the relative length change curves obtained from dilatometer heating experiments of the 1st and the 2nd run of CT and non-CT samples. The heating rate was 20°C/ min. The effect 1 can be attributed to transition carbide precipitation, the effect 2 to cementite precipitation and the effect 3 is ascribed to secondary hardening carbide formation.

For correlating the results of the dilatometer analyses, hardness measurements were carried out after various tempering treatments. The results are shown in Fig. 6. It is revealed that the hardness of the CT samples is higher compared to the non-CT samples after tempering up to temperatures of 500°C. After tempering beyond temperatures of 500°C the hardness of CT and non-CT conditions is the same. A decrease of hardness values for both conditions can be observed between 200°C and 400°C (process 2, shown in Fig. 6), which corresponds, according to dilatometer analyses, to the region of cementite precipitation. Additionally, the raise of hardness, which occurs for CT and non-CT samples in excess of 400°C can be attributed to secondary hardening carbide formation, which supports the results from dilatometer analyses.

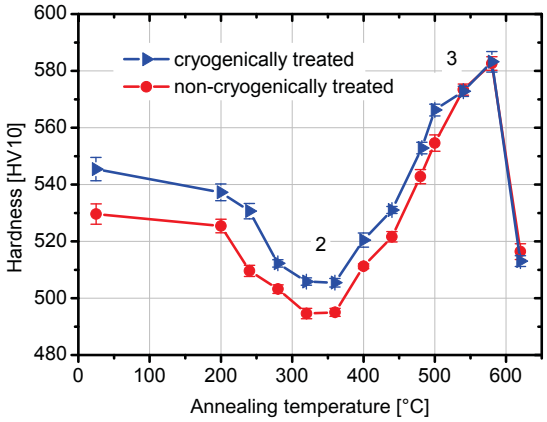

Figure 6. Hardness measurements of the CT and non-CT samples after heating (20°C/ min) to various temperatures up to 620°C and cooling to room temperature (100°C/ min). The reduction of hardness can be related to cementite formation (2). The large increase of hardness (3) is caused by the formation of secondary hardening carbides.

4. Discussion

The influence of cryogenic treatments on the microstructural evolution during heating was analyzed. It is identified that CT compared to non-CT samples exhibit a more intense cementite formation between 250°C and 400°C and more pronounced secondary hardening carbide precipitation above temperatures of 450°C - 500°C.

By XRD measurements, the austenite phase fraction of the cryogenically treated sample without tempering was determined with approximately 3.5 %. Due to tempering, the austenite content of the CT samples does not change significantly. Hence, it is suggested that for the CT samples neither austenite formation nor austenite transition occurs during tempering. This is also in accordance with the dilatometer heating and cooling (not shown here) curves, as they do not show any indication for austenite transformation. Conversely, the austenite phase fraction of the non-CT samples, which is about 3 % higher compared to the CT samples after tempering up to temperatures of 400°C, decreases due to tempering at higher temperatures. This decrease of the austenite phase fraction is identified to occur during cooling by dilatometer investigations. As the transformation of austenite is accompanied with an increase of volume, it is expected that austenite transforms into a bcc phase, e.g. martensite.

The lower hardness values of the non-CT compared to the CT conditions after tempering up to temperatures of 500°C can be ascribed to the higher austenite phase fraction of non-CT samples. Since the austenite of non-CT samples partially transforms upon cooling after tempering above temperatures of 500°C into martensite, the hardness values of the non-CT and CT conditions are comparable, as also the austenite phase fraction is in the same range.

The decrease of hardness between 200°C and 400°C can be attributed to a reduction of carbon content in martensite. This reduction of carbon content is a result of carbon segregation to lattice defects, e.g. dislocations, which is followed by the formation of carbides such as cementite. However, the reduction of carbon in martensite causes a decrease of tetragonality, which is accompanied with a stress relief in martensite. This process causes a reduction of

hardness, whereas the formation of cementite principally produces an increase of hardness. As the increase of hardness produced by cementite formation is to neglect compared to the hardness reduction due to the relief of stresses in martensite, the hardness decreases in the temperature range between 200°C and 400°C.

Furthermore, it is observed that the decrease of hardness in the temperature range between 200°C and 400°C is as high for CT samples as for non-CT samples. As carbon diffusion out of martensite causes this hardness decrease, it is assumed that for CT and non-CT conditions an equal reduction of carbon content in martensite occurs. In contrast to that, it is observed by dilatometer analyses that the cementite precipitation reaction for CT samples is more intense, indicating that more carbon is available for cementite formation in CT samples as in non-CT samples. Since it is suggested that a significant amount of carbon may also diffuse into austenite, the lower austenite phase fraction of CT samples compared to non-CT samples (in the temperature range between 200°C and 400°C) is probably the reason for the higher availability of carbon for cementite precipitation in CT samples. Generally, austenite has a higher solubility for carbon than martensite. Therefore, carbon is eager to diffuse from the supersaturated martensite into austenite. As non-CT samples exhibit two times as much austenite as CT samples in this temperature region, also the amount of carbon which can dissolve in austenite is twice as much. By assuming a maximum carbon enrichment in austenite of 2 wt.% [18, 19, 20], the non-CT samples can dissolve 0.12 wt.%, whereas the CT samples are only able to dissolve 0.06 wt.% of carbon in austenite. Consequently, less carbon is available for forming cementite in the non-CT samples, resulting in a smaller reaction peak for cementite formation.

The increase of hardness beyond temperatures of 400°C is assigned to be a result of secondary hardening carbide precipitation, which may also be influenced by the preceding precipitation processes. Thus, the carbide precipitation reaction in the CT samples is more intense, which was also determined by dilatometer analyses. Alterations in the carbide structure due to cryogenic treatment are also described by Das and Huang et al. [1, 4].

Secondary hardening carbide precipitation near or at the interface between retained austenite and martensite would cause a reduction of carbon content in austenite. Generally, this reduction leads to a decrease of the stability of austenite [21]. Conversely, cryogenic treatment would cause an enhancement of the stability of austenite, as it is explained in the following. It is expected that the thickness of retained austenite particles varies, as estimated by Fig. 3. Waitz et al. [22] reported that larger austenitic particles exhibit a lower stability. As cryogenic treatment causes a partially transformation of retained austenite, it is estimated that due to the cryogenic treatment a transformation of the larger, less stable austenitic regions takes place. As a result, for CT samples the less stable austenitic particles have already transformed during the cryogenic treatment. Hence, no transformation of austenite occurs during cooling of the CT samples after heating to temperatures beyond 400°C. Conversely, during cooling of the non-CT samples some austenite transforms, proving its lower stability. This transformation of austenite into martensite, produces an increase of hardness for the non-CT samples, which overlaps with the increase of hardness due to secondary hardening carbide precipitation. Hence, no comparison between CT and non-CT samples regarding the hardness increase due to formation of secondary carbides can be carried out.

5. Conclusion

The investigations on the effect of cryogenic treatment on the microstructural evolution during tempering of a high Co-Ni steel leads to the following conclusions:

- Cryogenic treatment causes a reduction of austenite phase fraction. This reduction is probably accompanied with a stabilization of austenite, as the less stable austenitic regions transform during the cryogenic treatment. Conversely, tempering causes a destabilization of austenite because of carbon reduction in austenite due to secondary hardening carbide formation. As a result of these opposing processes, the austenite of the CT samples does not transform due to the stabilization of austenite by the cryogenic treatment. In contrast, the austenite of the non-CT samples transforms upon cooling when tempering is conducted beyond 400°C, i.e. in the temperature range of secondary hardening carbide precipitation.
- Due to the higher austenite content of the non-CT samples during tempering in the temperature range between 200°C and 400°C, a higher amount of carbon can be dissolved in austenite. Thus, less carbon is present in martensite, causing a reduction of the intensity of the cementite precipitation reaction compared to the CT samples.
- The precipitation of secondary hardening carbides may also be influenced by the preceding precipitation processes. As a result, the CT samples also exhibit a more pronounced secondary hardening carbide precipitation.

References

[1] Das D, Sarkar R, Dutta A K and Ray K K 2010 *Mat. Sci. Eng. A* **528** 589–603
[2] Zhirafar S, Rezaeian A and Pugh M 2007 *J. Mater. Process. Tech.* **186** 298–303
[3] Molinari A, Pellizzari M, Gialanella S, Straffelini G and Stiasny K H 2001 *J. Mater. Process. Tech.* **118** 350–355
[4] Huang J, Zhu Y, Liao X, Beyerlein I, Bourke M and Mitchell T 2003 *Mat. Sci. Eng. A* **339** 241–244
[5] Stratton P F 2007 *Mat. Sci. Eng. A* **449-451** 809–812
[6] Ayer R and Machmeier P M 1993 *Metall. Trans. A* **24** 1943–1955
[7] Sato K 2002 Ph.D. thesis Universitiy of California, Berkeley
[8] Haidemenopoulos G N 1988 Ph.D. thesis Massachusetts Institute of Technology
[9] Young A 2002 *The Rietveld Method* (Oxford Universitiy Press)
[10] Speich G R and Leslie W C 1972 *Metall. Trans.* **3** 1043–1054
[11] Morra P V, Böttger A J and Mittemeijer E J 2001 *J. Therm. Anal. Calorim.* **64** 905–914
[12] Waterschoot T, Verbeken K and De Cooman, B C 2006 *ISIJ International* **46** 138–146
[13] Bala P, Pacyna J and Krawczyk J 2007 *Archives of Materials Science and Engineering* **28** 517–524
[14] Bala P, Pacyna J and Krawczyk J 2007 *Journal of Achievements in Materials and Manufacturing Engineering* **22** 15–18
[15] Thelning K E 1978 *Steel and its heat treatment* (Butterworth Co Publishers Ltd)
[16] Pacyna J 2011 *Journal of Achievements in Materials and Manufacturing Engineering* **46** 7–17
[17] Cheng L, Brakman C M, Korevaar B M and Mittemeijer E J 1988 *Metall. Trans. A* **19** 2415–2426
[18] Garcia-Mateo C, Caballero F G, Miller M K and Jimenez J A 2012 *J. Mater. Sci.* **47** 1004–1010
[19] Speer J, Matlock D K, De Cooman, B C and Schroth J G 2003 *Acta. Mater.* **51** 2611–2622
[20] Wang J and Van Der Zwaag, Sybrand 2001 *Metall. Trans. A* **32** 1527–1539
[21] Lerchbacher C, Zinner S and Leitner H 2012 *Metall. Mater. Trans. A* **43A** 4989–4998
[22] Waitz T, Antretter T, Fischer F D and Karnthaler H P 2008 *Mater. Sci. Technol.* **24**(8) 934–940

Publication V

Formation and growth kinetics of reverted austenite during tempering of a high Co-Ni steel

M. Gruber[a,], G. Ressel[a], F. Méndez Martín[b], S. Ploberger[c], S. Marsoner[a], R. Ebner[a]*

[a] Materials Center Leoben Forschung GmbH, Roseggerstrasse 12, A-8700 Leoben, Austria
[b] Department Physical Metallurgy and Materials Testing, Montanuniversität Leoben, Roseggerstrasse 12, A-8700 Leoben, Austria
[c] Böhler Edelstahl GmbH & Co KG, Mariazeller Strasse 25, A-8605 Kapfenberg, Austria

**Corresponding author*. Tel.: +43 3842 45922502, E-mail address: marina.gruber@mcl.at.

It is well known that high Co-Ni steels exhibit excellent toughness. Since the good toughness in these steels is supposed to be related to thin layers of austenite between martensite crystals, this work presents an experimental study corroborated with diffusional calculations to characterize the evolution of reverted austenite. Atom probe measurements were conducted for analyzing the element distribution in austenite and martensite during tempering. These results were correlated with crystallographic information, which was obtained by using transmission electron microscopy investigations. Additionally, the experimental findings were compared with kinetic calculations with DICTRA™. The investigations reveal that reverted austenite formation during tempering is connected with a redistribution of Ni, Co, Cr and Mo atoms. The austenite undergoes a Ni and Cr enrichment and a Co depletion, while in the neighboring martensite a zone of Ni and Cr depletion and Co enrichment is formed. The changes in the chemical composition of austenite during tempering affect the stability of the austenite against phase transformation to martensite during plastic deformation and have thus decisive influence on the toughness of the material.
Keywords: atom probe tomography; transmission electron microscopy; reverted austenite; growth kinetics; thermodynamic modeling.

1 Introduction

The combination of material properties such as good strength and hardness on one hand and excellent fracture toughness on the other hand is favorable in many applications, e.g. structural parts in airplanes. A steel class, which perfectly satisfies this property combination, are high Co-Ni secondary hardening steels [1-2]. The excellent toughness properties of these steels are assigned to thin austenite films, which are present preferentially along martensite lath boundaries. Despite different opinions about the toughening mechanism of the austenite films, it is principally asserted that a higher stability, i.e. resistance against phase transformation to martensite, of these films leads to a larger toughness of the material [3-9].
In Aermet® 100, which is the most prominent representative of this steel class, two different types of austenite are present - retained austenite and the so-called reverted austenite [6,7,10]. Retained austenite is the product of an incomplete martensitic transformation after austenitization. Sato [7] found that this type of austenite has a negative influence on fracture

toughness properties because of its low stability and its early transformation to brittle martensite during deformation. Reverted austenite is formed during a subsequent tempering treatment in high Co-Ni steels [11,12]. As it is described by Haidemenopoulos et al. [8], the main difference to retained austenite is that reverted austenite can be altered in composition and size during tempering, which both affects the stability. In literature it is reported that pronounced Ni or Mn enrichments in reverted austenite as well as the nm size of the films lead to an increased stability [13-16]. It was found by Ayer [6] and Haidemenopoulos [3] that reverted austenite in high Co-Ni steels exhibits such properties. However, the influence of carbon, one of the most powerful austenite stabilizers, on the formation as well as the growth mechanism of reverted austenite has not been precisely studied in the literature of high Co-Ni steels until now [3-8].

Thus, in order to obtain more information about the microstructural evolution of high Co-Ni steels, this work concentrates on the behavior of martensite, reverted and retained austenite upon tempering, with focus on the redistribution of elements. To this end, atom probe tomography (APT) measurements were applied to obtain the chemical composition of the phases with a high spatial resolution and transmission electron microscopy (TEM) investigations were conducted to correlate the element distribution with microstructural changes. Additionally, kinetic calculations were carried out by using the software DICTRA™. By corroborating these kinetic calculations with experimental results, a novel and detailed description of the evolution of the microstructure during tempering is introduced, giving a fundamental basis for explaining the excellent combination of strength and toughness of these steels.

2 Methods

The investigated high Co-Ni steel exhibits a chemical composition according to Table 1. Samples studied in this paper were taken from forged round bars with a diameter of 100 mm.

Table 1: Actual chemical composition of the investigated alloy in weight percent (wt.%) and atomic percent (at.%).

	C	**Ni**	**Co**	**Cr**	**Mo**
wt.%	0.22	11	13.5	2.9	1.2
at.%	1.03	10.5	12.9	3.1	0.7

The alloy was austenitized at 885°C for 1 h in a vacuum furnace, cooled down to room temperature with 10°C/ min and subsequently cryogenically treated at -73°C for 1 h. The tempering treatments were carried out in a batch furnace at 482°C for 1 h, 5 h and for 50 h.

Austenite phase fraction measurements were conducted via X-ray diffraction (XRD) using a D8 Discover diffractometer from Bruker AXS. A Cr-K_α radiation was used for measurements and Rietveld analyses were applied for determining the austenite content [17]. TEM investigations were carried out on a FEI Tecnai F20 and on a Philips CM20 STEM with an operation voltage of 200 kV and on a Philips CM12 microscope with 120 kV operation voltage. Samples for TEM analyses were conventionally prepared by grinding and electro polishing. Energy dispersive X-ray spectroscopy (EDS) was performed with an EDAX

detector attached to the TEM. For APT measurements, rods were cut from bulk materials and subsequently conventionally electro polished [18]. The measurements were carried out on a Cameca™ Local Electrode Atom Probe (LEAP) 3000X HR in laser mode at 60 K. The pulse rate was 200 kHz and the laser energy was 200 nJ. For reconstruction the software package IVAS version 3.6.8 was used.
Kinetic calculations were conducted with the software package DICTRA™. For the calculations the thermodynamic database TCFE3 and the mobility database MOB2 were used [19,20]. The setup for calculations consisted of a planar system geometry with two phase regions. A fcc phase was created for austenite and a bcc phase for martensite. The martensitic region had a width of 33 nm and the austenitic region had a width of 3 nm. The used grid was chosen finer near the interface. The initial compositional setting of austenite and martensite was homogenous with a composition for both phases of 11 at.% Ni, 13 at.% Co and 2.5 at.% Cr.

3 Results

3.1 Austenite phase fraction analyses

The austenite contents of the investigated heat treatment conditions as determined by means of XRD measurements are listed in Table 2. After austenitization and cryogenic treatment an austenite content of approximately 3.5 % is present. An subsequent tempering treatment at 482°C causes a raise of austenite phase content up to 10.5 % after 50 h. This increase of austenite content is due to the formation of reverted austenite.

Table 2: Analyses of the austenite contents after different heat treatments. The absolute measuring inaccuracy is about ±1 %.

	Austenite [%]
885°C for 1 h / -73°C for 1 h	3.5
885°C for 1 h / -73°C for 1 h / 482°C for 1 h	3.5
885°C for 1 h / -73°C for 1 h / 482°C for 5 h	4.0
885°C for 1 h / -73°C for 1 h / 482°C for 50 h	10.5

3.2 Microstructural characterization by TEM

For analyzing the microstructure, in particular the distribution and evolution of austenite, TEM investigations of austenitized and cryogenically treated samples as well as of samples tempered at 482°C for 5 h and for 50 h were conducted. The microstructure of the austenitized and cryogenically treated sample is shown in Fig. 1a in a TEM bright-field image. The related dark-field image, which uses an austenite reflection for imaging, is depicted in Fig. 1b. In this condition retained austenite is present in form of thin films along martensite lath boundaries. The thickness of the observed films is in the range of 3 nm to 40 nm. As the films might not be orientated in parallel to the electron beam, geometrical errors might occur when measuring the film thickness.

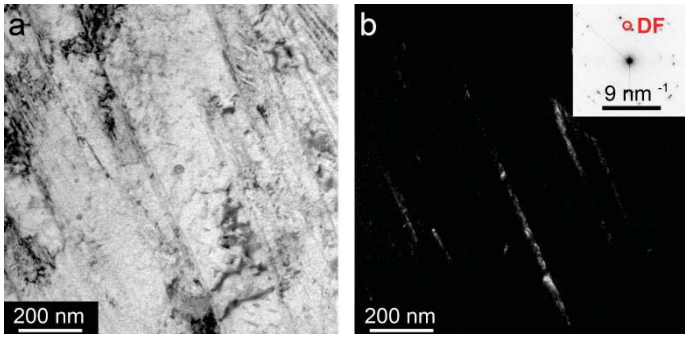

Fig. 1: TEM images of a sample after austenitization and cryogenic treatment. (a) Bright-field image of the microstructure with retained austenite films on lath boundaries. (b) Dark-field (DF) image of austenitic areas (bright areas) by using a 200 reflection.

In Fig. 2 the TEM images of the specimen tempered at 482°C for 5 h are shown. The austenite films are again present along martensite lath boundaries and their thickness is comparable to the films of the untempered condition.

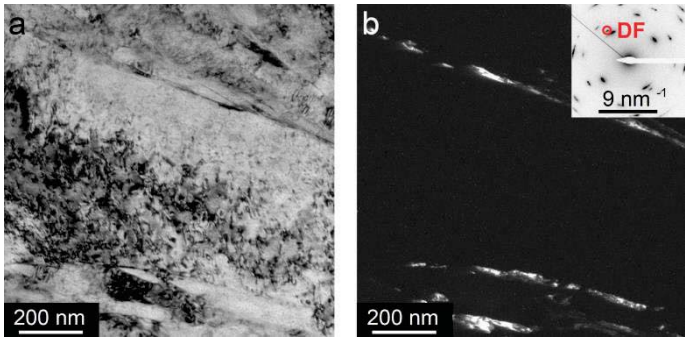

Fig. 2: TEM images from the microstructure of a sample, which was austenitized, cryogenically treated and subsequently tempered at 482°C for 5 h. (a) Bright-field image of the microstructure with austenite on lath boundaries. (b) Dark-field image of austenitic areas (bright areas) by using a 200 reflection.

Austenite films at martensite lath boundaries were also found in the sample after austenitization, cryogenic treatment and tempered at 482°C for 50 h as shown by the TEM images in Fig. 3. The thickness of the austenite layers at both positions is up to ~80 nm and is thus definitively larger than the thickness of the layers in the untempered condition.
An EDS line scan was created across an austenite film on the position marked with the red line in Fig. 3a and b. It is shown by the EDS concentration profile in Fig. 4 that there are austenitic zones, which are enriched in Ni. Since reverted austenite is enriched in Ni in high Co-Ni steels [4,6], these zones can be ascribed to reverted austenite. Within the reverted austenite along martensite lath boundaries, a region with reduced nickel content is present. This region is termed in the following as “interaustenitic layer”.

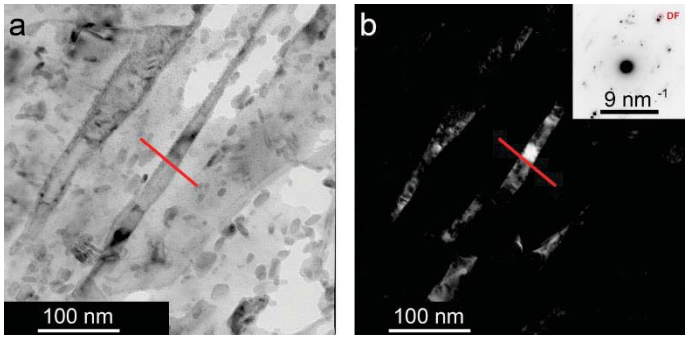

Fig. 3: TEM images of the specimen tempered at 482°C for 50 h. The red line marks the position of the EDS line scan shown in Fig. 4a. (a) Bright-field image. (b) Dark-field image by using the marked austenite reflex (311). The bright areas indicate austenitic regions.

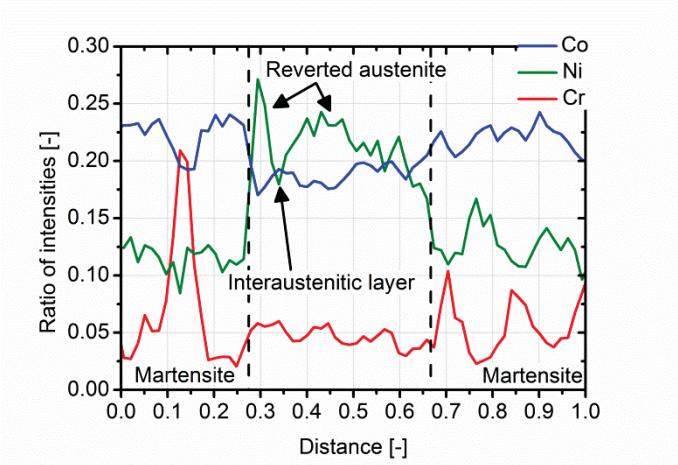

Fig. 4: EDS line scan of an austenite film with an interaustenitic layer from the specimen tempered at 482°C for 50 h. The vertical lines roughly indicate the positions of the interfaces of austenite to martensite. The positions at which nickel is enriched mark the zones of reverted austenite. The nickel depleted zone in the middle of the nickel enriched films is assigned to an interaustenitic layer. Carbides are indicated by the chromium enrichments.

3.3 Microstructural characterization by atom probe tomography (APT)

APT measurements were carried out on specimens tempered at 482°C for 1 h, 5 h and 50 h. The three-dimensional reconstruction of Ni atoms of the sample tempered for 1 h is illustrated in Fig. 5. The regions where carbon, chromium and molybdenum are enriched are ascribed to secondary hardening carbides. These carbides are displayed by violet isoconcentration surfaces for which the summed concentration of carbon and chromium exceeds 11 at.%. Furthermore, also nickel enriched zones can be identified. These zones are attributed to reverted austenite and are represented by using a 20 at.% Ni isoconcentration surface (green). However, due to the inhomogeneous Ni distribution in this sample only the larger Ni-enriched zones are expected to be austenite films. The regions with carbides but without nickel enrichments are assigned to the martensitic matrix. Carbides were also observed adjacent to the reverted austenite film in Fig. 5b. It should be noted that regardless of meaningful values of the Ni isoconcentration surface, the austenite films in this condition seems to consist of several small particles.

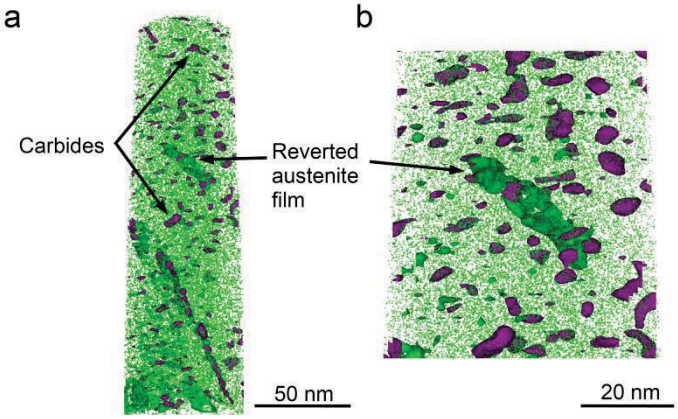

Fig. 5: Three-dimensional APT reconstruction of Ni atoms (green) of a sample tempered at 482°C for 1 h. Carbides are represented as violet isoconcentration surfaces (totaled concentration of Cr and C is 11 at.%) and austenite as green isoconcentration surfaces (20 at.% nickel). (a) Reconstruction of the entire volume of the APT measurement. (b) Magnified image of the marked austenite film.

In Fig. 6a the results from APT investigations of the specimen tempered for 5 h are depicted. The boundary value of the Ni isoconcentration surface was adapted from 20 at.% to 15 at.% for a better reliability of results due to differences in Ni distribution and concentration content in the tips. Fig. 6b and c show a 12 nm thick vertical intersection of Fig. 6a and therefore, they present a detailed insight into the austenite layer marked with arrows. It is found that the nickel content of this austenite layer decreases below 15 at.% in the center of the austenite film, indicating that also after tempering for 5 h an interaustenitic layer exists. Furthermore, it is observed that this interaustenitic layer is completely surrounded with a zone of nickel enrichment of at least 15 at.% to 20 at.%. As a consequence, it is suggested that this interaustenitic layer is enclosed by reverted austenite.

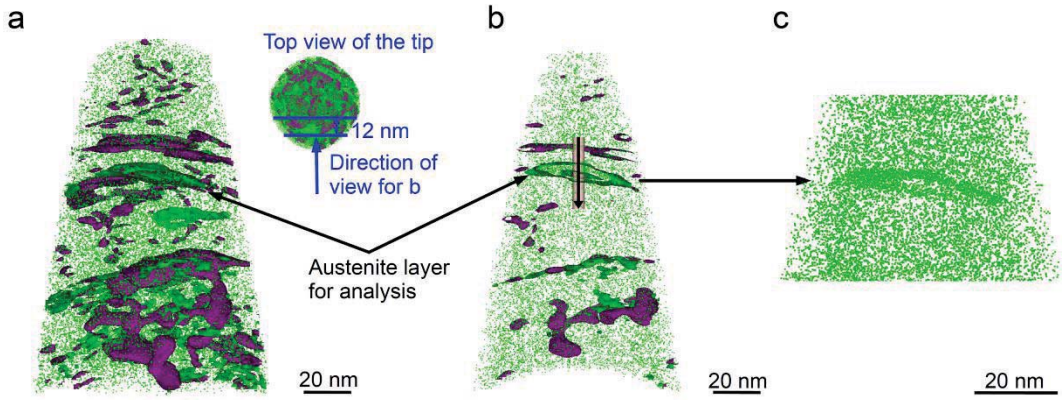

Fig. 6: Three-dimensional APT reconstruction of Ni atoms (green) of a sample tempered at 482°C for 5 h. Carbides are represented as violet isoconcentration surfaces (totaled concentration of Cr and C is 11 at.%) and austenite as green isoconcentration surfaces (15 at.% nickel). (a) Reconstruction of the entire volume of the APT measurement. The arrows indicate the austenite layer for further analysis. (b) Detail of a 12 nm thick vertical intersection of the atom probe data, as presented in Fig. 6a. The small insert shown in the upper right of Fig. 6a indicates the direction of view. The cylinder marks the volume used for creating a one-dimensional line profile. (c) Magnified image of the austenite layer (marked in a and b).

For characterizing the interaustenitic layer in the middle of the reverted austenite layer, a one-dimensional concentration profile (Fig. 7) was created through these zones, as indicated in Fig. 6b by the vertical cylinder with the downward orientated arrow. The profile shows two reverted austenite films, which are enriched in nickel but depleted in cobalt. The thickness of the reverted austenite films is in the range of 1-3 nm. In the region of the interaustenitic layer the nickel content is reduced and the cobalt content is enhanced compared to reverted austenite. Furthermore, it was found that the concentration of elements in the interaustenitic layer is rather comparable to the composition of martensite, which is the matrix of the steel.

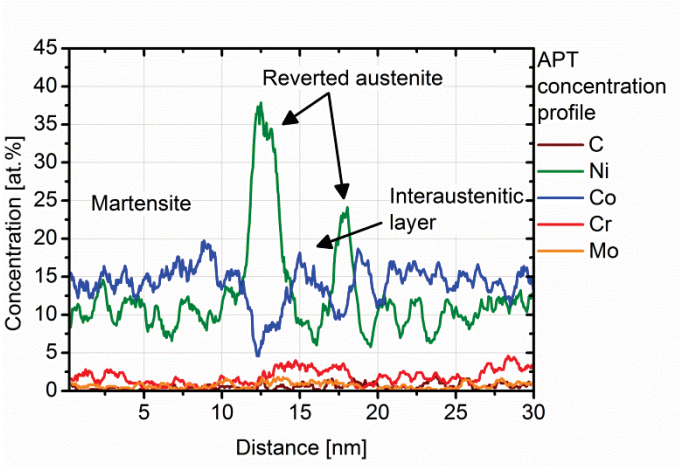

Fig. 7: One-dimensional concentration profile of carbon, nickel, cobalt, chromium and molybdenum of the specimen tempered at 482°C for 5 h. The analyzed volume is marked by the cylinder with the arrow in Fig. 6b. Regions with high nickel contents correspond to reverted austenite. The region between the reverted austenite layers is denoted as interaustenitic layer.

In Fig. 8a the three-dimensional APT reconstruction of the specimen tempered at 482°C for 50 h is shown. Carbides are identified in this sample in martensite as well as in reverted austenite. Also in this heat treatment condition a reverted austenite film is present, which surrounds an interaustenitic layer. This interaustenitic layer exhibits almost the same chemical composition than the interaustenitic layer found in the sample tempered for 5 h. This is demonstrated by the one-dimensional concentration profile across the austenitic region, which is shown in Fig. 8b. The position of the concentration profile was chosen in a way that carbides are not included and that it is nearly perpendicular to the 20 at.% Ni isoconcentration surfaces. The reverted austenite film in this condition has a thickness of 3-10 nm. The nickel concentration in austenite is increased to a maximum of approximately 40 at.%, whereas cobalt content is reduced at the same position to about 4 at.%. In reverted austenite also the concentrations of chromium, molybdenum and carbon are enhanced compared to martensite, as also shown in Table 3, which presents the chemical composition of the phases. However, the carbon content is only slightly higher in reverted austenite as carbon is predominately bound in carbides.

Furthermore, it was identified that the composition of the interaustenitic layer significantly differs from the martensite as well as from the reverted austenite. It was determined that the

layer presents a concentration of substitutional elements, which is comparable to the overall composition of the steel, as shown by Fig. 8b and Table 3.

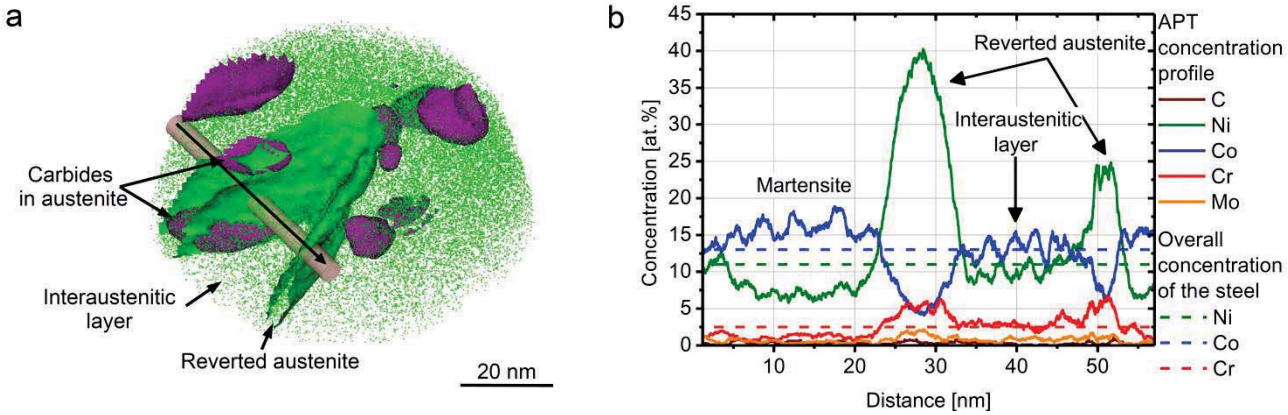

Fig. 8: (a) Three-dimensional reconstruction of the APT tip of the sample tempered at 482°C for 50 h showing Ni atoms (green). Carbides are represented by 11 at.% chromium plus carbon isoconcentration surfaces (violet) and austenite is represented by a 20 at.% nickel isoconcentration surface (green). (b) One-dimensional concentration profile of Ni, Co, Cr, Mo and C atoms through the austenite layer. The volume for analyzing is indicated in (a) by the cylinder with the arrow that indicates the direction of the distance in the diagram. The reverted austenite is markedly enriched in nickel, whereas the composition of the interaustenitic layer within the reverted austenite is comparable to the overall concentration of Ni, Co and Cr in the steel (dashed lines).

Table 3: Compositions of the phases evaluated from the APT data of a sample tempered at 482°C for 50 h. The compositions are obtained by creating a 20 at.% nickel isoconcentration surface and a 11 at% chromium plus carbon isoconcentration surface.

	Chemical composition in [at.%]					
Averaged composition of:	**C**	**Co**	**Ni**	**Cr**	**Mo**	**Fe**
Martensite	0.36	13.6	8.8	1.9	0.2	75.2
Reverted austenite	0.52	7.3	29.7	5.9	1.0	55.6
Interaustenitic layer	0.35	13.0	10.7	3.4	0.8	71.7
Carbides	13.17	6.0	6.4	24.3	9.4	40.6
Averaged overall composition of the steel (Table 1)	1.03	12.9	10.5	3.1	0.7	71.8

3.4 Study of element redistribution in austenite and martensite during tempering

For a detailed characterization of the chemical changes of martensite, reverted austenite and the interaustenitic layer due to tempering at 482°C for 50 h the elemental distribution behavior near the reverted austenite interfaces was analyzed. Therefore, proximity histograms [21] were created using a 20 at.% nickel isoconcentration surface. The data of carbides were removed from the characterized volume prior to analyzing by using an 11 at.% chromium-carbon isoconcentration surface. The volumes, which were used for studying the elemental distribution at the reverted austenite-martensite boundary and at the reverted austenite-interaustenitic layer boundary are marked by the boxes in Fig. 9a and b. These volumes were selected in a way that either martensite and reverted austenite or reverted austenite and the interaustenitic layer are present for analysis.

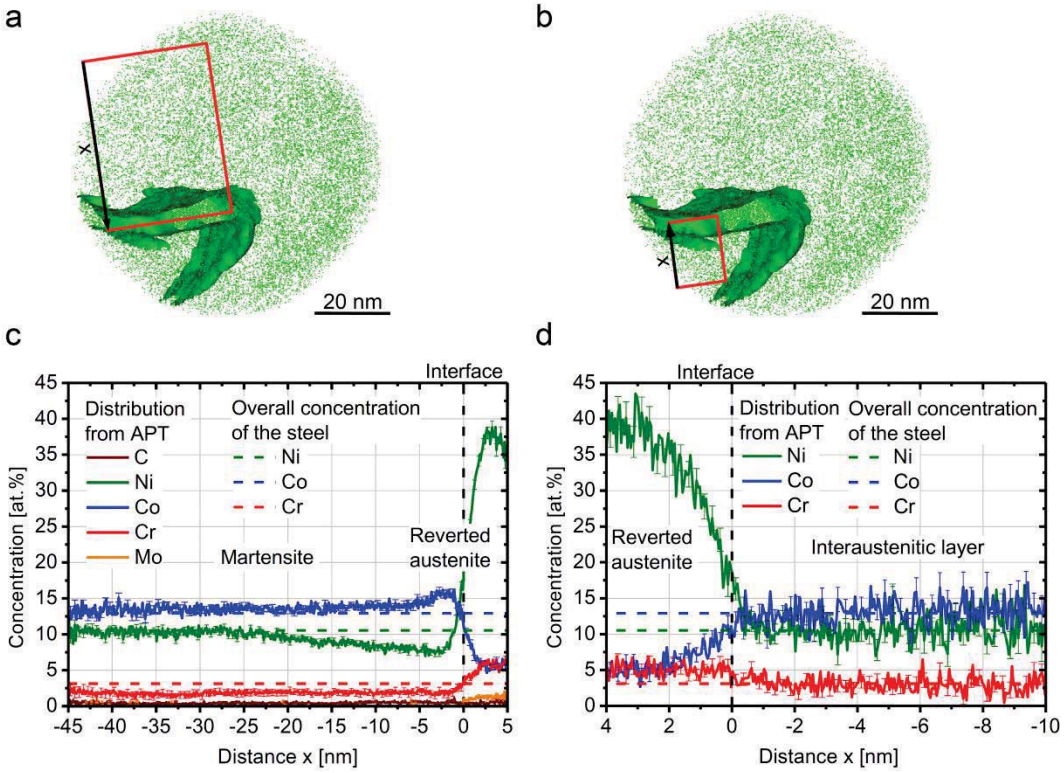

Fig. 9: Elemental distribution in the region of the reverted austenite film after tempering at 482°C for 50 h by using a proximity histogram. (a), (b) Three-dimensional reconstructions of Ni atoms with 20 at.% Ni isoconcentration surfaces. By the boxes the volumes used for evaluating the element distribution are indicated. The arrows indicate the directions of the x-axes for the analyses. (c) Elemental distribution in reverted austenite and martensite. The volume used for analyzing is marked in (a). (d) Elemental distribution in reverted austenite and the interaustenitic layer. The volume used for analyzing is marked in (b). The horizontal dashed lines indicate the overall concentration of Cr, Ni or Co atoms in the steel, respectively. The vertical dashed lines represent the positions of the interface of reverted austenite to martensite and of interface of reverted austenite to the interaustenitic layer.

Fig. 9c and d show the proximity histograms of the chemical composition near the martensite-reverted austenite (Fig. 9c) and near the reverted austenite-interaustenitic layer (Fig. 9d) interface region. The reverted austenite film is characterized in both profiles by the nickel enrichment. In Fig. 9c martensite is present outside the austenite. In the martensite a zone of nickel depletion with a width of 22 nm and a minimum of 8 at.%. occurs near to the austenitic region. The nickel content far away from the reverted austenite layer is about 11 at.%, which is the averaged Ni content of the material. Conversely, in austenite a depletion of cobalt to about 5 at.% occurs, whereas in martensite near the austenite interface the cobalt accumulates to a maximum content of about 16 at.%. An area of a slight depletion is also observed for chromium atoms in martensite and in addition chromium is enriched in austenite to about 6 at.%. The lower chromium content in martensite compared to the overall composition of the steel might be a result of carbide precipitation. It is to note that the contents of carbon and molybdenum in the investigated steel grade were too low for a reliable statement of the element distribution behavior near the reverted austenite-martensite interface.

In Fig. 9b the transition from reverted austenite (left side) to the interaustenitic layer (right side) is illustrated. While reverted austenite shows the properties as described in the previous paragraph, in the region of the interaustenitic layer no distinct variation of elemental concentration can be observed. Nickel, cobalt and chromium concentrations show similar values compared to the overall Ni, Co, Cr concentrations of the material (Table 1).

4 Discussion

4.1 Nucleation and growth mechanism of reverted austenite

To understand the formation behavior of reverted austenite a detailed evaluation of the microstructural evolution during tempering is essential. Hence, the development of phases and the distribution of elements were studied by the aid of phase fraction analyses, TEM and APT measurements.

TEM analyses revealed that retained austenite is present in form of thin films on martensite lath boundaries after austenitization and cryogenic treatment. These austenite films have a thickness of approx. 3-40 nm and the austenite phase fraction is about 3.5 % in this heat treatment condition. During tempering at 482°C reverted austenite is formed, which is as well located at martensite lath boundaries. Tempering for 5 h leads to a thickness of austenite films in TEM images akin to the size before tempering. This is expected to be a result of the slow reverted austenite formation because of tempering at 482°C. It was determined by APT measurements that in this condition small reverted austenite films are present with a thickness of approx. 1-3 nm. After 50 h of tempering, the austenitic regions found by TEM have significantly grown in to a maximum size of about 80 nm. The reverted austenite films characterized by APT after 50 h of tempering exhibit a size of approx. 3-10 nm and as a result of that indicate that reverted austenite films grow in thickness during tempering. Additionally, interaustenitic layers with a composition similar to the overall composition of the material are found within the reverted austenite films along the martensite laths in the samples tempered at 482°C for times of 5 h and 50 h.

In contrast to the present work, no retained austenite was found after cryogenic treatment in some prior investigations for a similar steel grade [5,6,12]. As a result, the impact of retained austenite on phase evolution was not considered. In order to understand and to describe the microstructural changes during tempering at 482°C for 50 h quantitatively, the martensitic microstructure with small amounts of retained austenite, as experimentally found in the austenitized and cryogenically treated condition, was taken as the initial microstructure for calculations with DICTRA™. Thus, for the calculations, a bcc phase (martensite) and a fcc phase (retained austenite) at the martensite boundary was defined. The initial composition of the fcc and bcc phase was obtained from the APT sample tempered for 50 h by averaging the compositions of martensite, reverted austenite and the interaustenitic layer, listed in Table 4.

Table 4: Initial chemical composition in at.%, which was used for calculating the elemental redistribution during tempering with DICTRA™. The elemental concentrations were obtained from the composition of the APT tip after tempering at 482°C for 50 h by averaging the compositions of martensite, reverted austenite and the interaustenitic layer.

Ni [at.%]	Co [at.%]	Cr [at.%]	Fe [at.%]
11	13	2.5	Bal.

The results of the calculations are depicted in Fig. 10. Before calculating the tempering step, the concentrations of Cr, Co and Ni atoms are equal in retained austenite and in martensite as marked by the horizontal dashed lines. Retained austenite and martensite are separated by the original interface at the time t=0 h. Due to the tempering treatment at 482°C for 50 h, the phase boundary between the fcc phase and martensite was shifted towards the martensite phase. As a result, a new fcc phase is created, which is referred to reverted austenite as it is formed during tempering. The reverted austenite has a thickness of about 2 nm and is, such as the reverted austenite found by experiments, enriched in nickel (up to 40 at.%) and chromium, but depleted in cobalt (4 at.%). As also found in the experiments, zones of Ni and Cr depletion and Co enrichment evolve in the martensite next to retained austenite. The widths of the reverted austenite and the elemental accumulation or depletion zones agree also quite well with the experimental results. Additionally, the calculations demonstrate that in retained austenite the concentration of elements remains more or less constant during tempering, except for the small margin zone to the reverted austenite. Consequently, the retained austenite shows a composition similar to the one before tempering, i.e. the overall composition of the material in the austenitized and cryogenically treated condition. Such a composition and almost no elemental redistribution were also identified in the interaustenitic layers found by APT measurements. Furthermore, as it was found by TEM investigations, that the interaustenitic layers and the retained austenite are both present along martensite boundaries, it is expected that the interaustenitic layer is originally retained austenite. Therefore, it is suggested that reverted austenite grows by nucleating along retained austenite boundaries and is producing a phase arrangement as observed by DICTRA™ calculations and experimental results by APT (Fig. 6, Fig. 10).

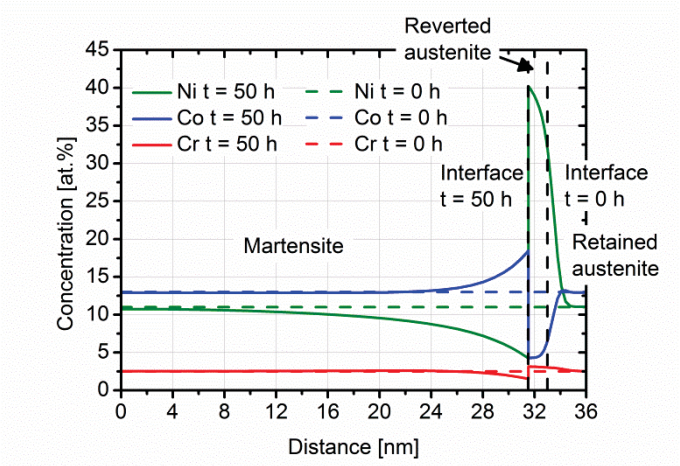

Fig. 10: DICTRA™ (MOB2 and TCFE3) calculations of the Ni, Co and Cr distribution in martensite and austenite due to tempering at 482°C for 50 h. The dashed horizontal lines indicate the overall concentration of Cr, Ni or Co atoms in the steel before tempering. The vertical dashed lines show the original position of the martensite-austenite interface (t=0 h) and after tempering for 50h.

Also Dmitrieva et al. [22] proposed that reverted austenite grows after nucleating at retained austenite layers during tempering. Predictions presented in previous papers of Gruber et al. [10,23], Dmitrieva et al. [22] and Raabe et al. [24] point out a low diffusivity of substitutional elements in austenite compared to martensite. Accordingly, APT measurements and calculations of specimens tempered at 482°C revealed that in retained austenite no chemical alterations occur. Furthermore, the element diffusion for the formation of the highly Ni-enriched reverted austenite has to proceed in martensite. As a result, in martensite large zones of element redistribution evolve as determined by APT. Hence, it is suggested that the growth of reverted austenite is dominated by the diffusion of Ni from martensite to the austenite-martensite phase boundary. A diffusion controlled formation of reverted austenite was also identified by Schnitzer et al. [25]. Additionally, the formation mechanism of reverted austenite is reported to be diffusion controlled but coupled with shear processes by Shiang et al. [26], Li et al. [27] and Farooque et al. [28].

Furthermore, the effects of Cr, Mo and Co redistribution during tempering were also analyzed. It was identified that chromium and molybdenum accumulate in reverted austenite but cobalt atoms are depleted in reverted austenite. As a result of this elemental redistribution, the composition of reverted austenite is comparable to the equilibrium concentration of elements in austenite at 482°C, which is listed in Table 5. Thus, it is expected that reverted austenite forms when the chemical composition required for formation of austenite approaches the equilibrium composition. Consequently, the formation of reverted austenite should not only be dominated by the diffusion of Ni but may also be controlled by the diffusion of the other elements present in the material.

Table 5: Equilibrium concentration of alloying elements in austenite for the investigated steel grade. The calculations were performed with Thermo-Calc (TCFE3) at 482°C.

Ni [at.%]	Co [at.%]	Cr [at.%]	Mo [at.%]	C [at.%]
40.3	3.5	1.1	0.2	$7*10^{-4}$

It should be noted that the DICTRA™ simulations also suggest a small zone (<2 nm) of Ni accumulation and Co rejection located in the retained austenite near the reverted austenite. This indicates that the composition of retained austenite also tends to change towards the composition of reverted austenite but is hindered by the diffusional inability of austenite. However, as a result of the low diffusion coefficient of the fcc phase, the retained austenite cannot be enriched in nickel due to tempering at 482°C for 50 h and thus exhibits a low stability as also indicated by Gruber et al. [10].

4.2 Influence of carbon on the precipitation of reverted austenite

Carbon is one of the most powerful austenite stabilizers and has a much higher solubility in austenite than in martensite. Nonetheless, in prior investigations of high Co-Ni steels the effect of carbon and its redistribution during tempering was not considered [4-7,12]. For the investigated steel grade, it was determined by APT measurements that concentration of carbon is only slightly higher in austenite than in martensite after tempering. In steel grades that exploiting a highly stable retained austenite, high amounts of carbon (2 wt.%) were found in this phase [29-31]. Nevertheless, in most of these steels the formation of carbides, e.g. cementite, is weak or suppressed by alloying [14,31]. In contrast, in the investigated steel grade of this work nm-sized carbides are present after tempering at 482°C for 1 h. Thus, the low carbon content in austenite should be a result of the formation of carbides. Additionally, in the APT measurements in general lower carbon contents are detectable as a consequence of the higher field evaporation for carbon compared to the substitutional elements [18]. Also equilibrium calculations at 482°C, as shown in Table 5, suggest for the investigated steel grade low carbon contents in austenite.

Furthermore, it is indicated by Fig. 5 that carbides are precipitated after tempering for 1 h in the martensite and at the martensite-austenite interface. Furthermore, carbides were also found in reverted austenite after tempering for 50 h. Therefore, it is thus suggested that carbides, which consume carbon are formed mainly prior to the formation of reverted austenite. When the reverted austenite grows and its phase boundary reaches the carbides the boundary moves across these carbides but they are not dissolved due to this process. Based on these results, it is expected that carbon may indeed promote the formation of reverted austenite but is more eager to form carbides than reverted austenite.

5 Conclusions

The microstructural evolution and the redistribution of alloying elements during tempering were analyzed by means of X-ray diffraction, APT and TEM measurements as well as by kinetic calculations with DICTRA™. The findings lead to the following conclusions:

- After austenitization and subsequent cryogenic treatment about 3.5 % retained austenite are present. This retained austenite is located along martensite lath boundaries in form of thin films with thicknesses of about typically 3 up to 40 nm. Due to tempering at 482°C reverted austenite precipitates.
- As reverted austenite is also located at martensite lath boundaries it is expected that it nucleates at retained austenite. Thus, retained austenite is present within the Ni-enriched reverted austenite, as found by APT.
- Since the diffusion of substitutional elements is slowly in austenite at 482°C, it is assumed that in retained and reverted austenite almost no diffusion occurs. Thus, most of the retained austenite exhibits a composition, which is comparable to the composition of an as-quenched retained austenite.
- Reverted austenite was found by APT to be enriched in Ni, Cr and Mo and depleted in Co. As a result of these chemical alterations to the matrix of the steel, diffusion in the martensite is required to form reverted austenite. Accordingly, large zones of elemental redistribution were identified by APT in martensite.
- Furthermore, it was determined that the growth of reverted austenite during tempering is controlled by the diffusion of substitutional elements, predominately Ni, to the austenite-martensite interface. As reverted austenite exhibits a chemical composition similar to the equilibrium composition at 482°C, it is suggested that reverted austenite forms when the compositional conditions are reached, e.g. when the local equilibrium composition is achieved. Consequently, also the diffusion of Co, Cr and Mo atoms during tempering contributes to the reverted austenite formation.
- Although carbon is a powerful austenite stabilizer, it is more eager to accumulate in carbides than in austenite. Thus, it is suggested that the formation of reverted austenite is influenced by carbon but not controlled.

6 Achnowledgement

Financial support for part of the work by the Austrian Federal Government (in particular from Bundesministerium für Verkehr, Innovation und Technologie and Bundesministerium für Wissenschaft, Forschung und Wirtschaft) represented by Österreichische Forschungsförderungsgesellschaft mbH and the Styrian and the Tyrolean Provincial Government, represented by Steirische Wirtschaftsförderungsgesellschaft mbH and Standortagentur Tirol, within the framework of the COMET Funding Programme is gratefully acknowledged.

The Authors thank also Krystina Spiradek-Hahn for the support regarding TEM investigations.

7 References

[1] K. Cho, J. Choi, H. Kang, S. Kim, K. Lee, H. Yang, H. Kwon, Influence of rolling temperature on the microstructure and mechanical properties of secondary hardening high Co–Ni steel bearing 0.28 wt% C, Mater. Sci. Eng. A, 527 (2010) 7286-7293.

[2] P. M. Novotny, G. E. Maurer, Ultra-High-Strength Steels vs. Titanium Alloys, Adv. Mater. & Process. (2007) 37-40.

[3] G. Haidemenopoulos, Dispersed-Phase Transformation Toughening in Ultrahigh-Strength Steels, PhD Thesis, Massachusetts Institute of Technology, 1988.

[4] H. E. Lippard, Microanalytical Investigations of Transformation Toughened Co-Ni Steels, PhD Thesis, Northwestern University, Evanston Illinois, 1999.

[5] C. J. Kuehmann, Thermal processing optimation of nickel-cobalt ultrahigh-strength steels, PhD Thesis, Northwestern University, Evanston, Illinois, 1994.

[6] R. Ayer, P. Machmeier, Transmission Electron Microscopy Examination of Hardening and Toughening Phenomena in Aermet 100, Metall. Trans. 24A (1993) 1943-1955.

[7] K. Sato, Improving the Toughness of Ultrahigh Strength Steel, PhD Thesis, University of California, Berkeley, 2002.

[8] G. Haidemenopoulos, M. Grujicic, G. Olson, M. Cohen, Thermodynamics-based alloy design criteria for austenite stabilisation and transformation toughening in Fe-Ni-Co system, J. Alloy. Compd. 220 (1995) 142-147.

[9] H. E. Leal, Transformation toughening of metastable austenitic steels, PhD Thesis, Massachusetts Institute of Technology, 1984.

[10] M. Gruber, S. Ploberger, G. Ressel, M. Wiessner, M. Hausbauer, S. Marsoner, R. Ebner, Effects of the combined heat and cryogenic treatment on the stability of austenite in a high Co-Ni steel, Arch. Metall. Mater. 60 (2015) 2131-2137.

[11] R. Ayer, P. M. Machmeier, Microstructural Basis for the Effect of Chromium on the Strength and Toughness of AF1410- Based High Performance Steels, Metall. Mater. Trans. 27A (1996) 2510-2517.

[12] C. H. Yoo, H. M. Lee, J. W. Chan, J. W. Morris, M_2C Precipitates in Isothermal Tempering of High Co-Ni Secondary Hardening Steel, Metall. Mater. Trans. 27A, (1996) 3466-3472.

[13] T. Waitz, T. Antretter, F. Fischer, H. Karnthaler, Size effects on martensitic phase transformations in nanocrystalline NiTi shape memory alloys, Mater. Sci. Technol. 24 (2008) 934-940.

[14] H. K. D. H. Bhadeshia, D. V. Edmonds, Bainite in silicon steels: new composition-property approach Part 1, Metal Sci. 17 (1983) 411-419.

[15] V. Raghaven, Effect of Manganese on the Stability of Austenite in Fe-Cr-Ni Alloys, Metall. Mater. Trans. 26A (1995) 237-242.

[16] R. L. Klueh, P. J. Maziasz, E. H. Lee, Manganese as an Austenite Stabilizer in Fe-Cr-Mn-C Steels, Mater. Sci. Eng. A 102 (1988) 115-124.

[17] A. Young, The Rietveld Method, Oxford University Press, 2002.

[18] M. K. Miller, A. Cerezo, M. G. Hetherington, G. D. W. Smith, Atom Probe Field Ion Microscopy, New York, Oxford University Press Inc., 1996.

[19] MOB2-TCS Alloy Mobility Database, DICTRA version 24, Foundation for Computational Thermodynamics Stockholm.

[20] TCFE3-TCS Steels/Fe-alloys Database, Thermo-Calc version R, Foundation of Computational Thermodynamics Stockholm.
[21] O. C. Hellman, J. A. Vandenbroucke, J. Rüsing, D. Isheim, D. N. Seidman, Analysis of Three-dimensional Atom-probe Data by the Proximity Histogram, Microsc. Microanal. 6 (2000) 437-444.
[22] O. Dmitrieva, D. Ponge, G. Inden, J. Millan, P. Choi, j. Sietsma, D. Raabe, Chemical gradients across phase boundaries between martensite and austenite in steel studied by atom probe tomography and simulation, Acta Mater. 59 (2011) 364-374.
[23] M. Gruber, S. Ploberger, M. Wiessner, S. Marsoner and R. Ebner, Influence of heat treatment on the stability of austenite in a high Co-Ni secondary hardening steel, Proceedings of the International Conference on Solid-Solid Phase Transformations in Inorganic Materials, Whistler (2015) 115-122.
[24] D. Raabe, S. Sandlöbes, J. Millan, D. Ponge, H. Assadi, M. Herbig, P. Choi, Segregation engineering enables nanoscale martensite to austenite phase transformation at grain boundaries: A pathway to ductile martensite, Acta Mater. (2013) 6132-6152.
[25] R. Schnitzer, R. Radis, M. Nöhrer, M. Schober, R. Hochfellner, S. Zinner, E. Povoden-Karadeniz, E. Kozeschnik, H. Leitner, Reverted austenite in PH 13-8 Mo maraging steels, Mater. Chem. Phys. 122 (2010) 138-145.
[26] L. T. Shiang, C. M. Wayman, Maraging Beahvior of an Fe-19.5Ni-5Mn Alloy, II: Evolution of Reverse-Transformed Austenite During Overaging, Metallogr. 21 (1988) 425-451.
[27] X. Li, Z. Yin, Reverted austenite during aging in 18Ni(350) maraging steel, Materials Letters 24 (1995) 239-242.
[28] M. Farooque, H. Ayub, A. U. Haq and A. Khan, The formation of reverted austenite 18% Ni 350 grade maraging steel, J. Mater. Sci. 33 (1998) 2927-2930.
[29] J. Wang, S. van der Zwaag, Stabilization Mechanisms of Retained Austenite in Transformation-Induced Plasticity Steel, Metall. Mater. Trans. 32A,(2001) 1527-1539.
[30] C. Garcia-Mateo, F. G. Caballero, M. K. Miller, J. A. Jimenez, On measurement of carbon content in retained austenite in a nanostructured bainitic steel, J. Mater. Sci. 47 (2012) 1004-1010.
[31] J. Speer, D. K. Matlock, B. C. De. Cooman, J. G. Schroth, Carbon partitioning into austenite after martensite transformation, Acta Mater. 51 (2003) 2611-2622.